MIOMD 2023 Program Overview

Room /Time	Lecture Hall, Nielsen Hall	Great Hall, Sam Noble Museum
MoM	MIOMD-MoM1: Frequency Combs MIOMD-MoM2: Interband Cascade and Diode Lasers	
MoA	MIOMD-MoA1: THz Sources and Detectors MIOMD-MoA2: Quantum and Interband Cascade Lasers	
TuM	MIOMD-TuM1: Plenary Lecture & Integrated Photonics MIOMD-TuM2: Silicon Photonics	
TuA	MIOMD-TuA1: ICLs and LEDs MIOMD-TuA2: Mid-IR Plasmonics	
TuP		POSTER SESSIONS
WeM	MIOMD-WeM1: Plenary Lecture & Applications of Mid-Infrared MIOMD-WeM2: Sensing	
ThM	MIOMD-ThM1: Detectors I MIOMD-ThM2: Detectors II	
ThA	MIOMD-ThA1: Materials for Mid-Infrared MIOMD-ThA2: Metamaterials and Polaritons	

Monday Morning, August 7, 2023

	Room Lecture Hall, Nielsen Hall	
8:20am	**Welcome and Opening Remarks**	**Mid-IR Optoelectronics: Materials and Devices** **Session MIOMD-MoM1** **Frequency Combs** **Moderator:** **David Burghoff**, University of Texas at Austin
8:30am	**INVITED: MIOMD-MoM1-2** Mid-Infrared Semiconductor Laser Frequency Combs: From FM-Combs to Nozaki-Bekki Solitons, *N. Opacak,* TU Wien, Austria*; D. Kazakov,* Harvard University*; L. Columbo,* Politecnico di Torino, Italy*; S. Dal Cin, M. Beiser, F. Pilat,* TU Wien, Austria*; T. Letsou,* Harvard University*; M. Brambilla,* Universit`a e Politecnico di Bari, Italy*; F. Prati,* Universit`a dell'Insubria, Italy*; M. Piccardo,* Universidade de Lisboa, Portugal*; F. Capasso,* Harvard University*;* ***Benedikt Schwarz****,* TU Wien, Austria	
8:40am		
8:50am		
9:00am	**MIOMD-MoM1-5** Temporal Solitons in Coherently-Driven Ring Lasers*,* ***Theodore Letsou****, D. Kazakov,* Harvard University*; M. Piccardo,* Universidade de Lisboa, Portugal*; L. Columbo,* Politecnico di Torino, Italy*; M. Brambilla,* Politecnico di Bari, Italy*; F. Prati,* Università dell'Insubria, Italy*; S. Dal Cin, M. Beiser, N. Opačak,* TU Wien, Austria*; M. Pushkarsky, D. Caffey, T. Day,* DRS Daylight Solutions*; L. Lugiato,* Università dell'Insubria, Italy*; B. Schwarz,* TU Wien, Austria*; F. Capasso,* Harvard University	
9:10am		
9:20am	**MIOMD-MoM1-7** Full-Band Modeling of AM and FM Interband Cascade Laser Frequency Combs*,* ***Michael Povolotskyi****,* Jacobs*; I. Vurgaftman,* Naval Research Laboratory, USA	
9:30am		
9:40am	**BREAK**	
9:50am		
10:00am		
10:10am		
10:20am		
10:30am	**INVITED: MIOMD-MoM2-14** Recent Advances in Interband Cascade Lasers for Mid-Wave Infrared Free-Space Optical Communications*,* ***Frederic Grillot****,* Telecom Paris, France	**Mid-IR Optoelectronics: Materials and Devices** **Session MIOMD-MoM2** **Interband Cascade and Diode Lasers** **Moderator:** **Benedikt Schwarz**, TU Wien, Austria
10:40am		
10:50am		
11:00am	**INVITED: MIOMD-MoM2-17** Continuous Wave Room Temperature Operation of the Epitaxially Regrown GaSb-Based Diode PCSELs*,* ***Leon Shterengas****,* Stony Brook University	
11:10am		
11:20am		
11:30am	**MIOMD-MoM2-20** Single-Mode Tunable Interband Cascade Lasers with a Wide Tuning Range*, J. Gong, Z. Wang, J. He,* Zhejiang University, China*;* ***Rui Yang****,* University of Oklahoma	
11:40am		
11:50am	**MIOMD-MoM2-22** Expanding the Frontiers of Long Wavelength Interband Cascade Lasers using Innovative Quantum Well Active Regions*,* ***Yixuan Shen****, J. Massengale, R. Yang,* University of Oklahoma*; S. Hawkins, A. Muhowski,* Sandia National Laboratories, USA	
12:00pm		

Monday Afternoon, August 7, 2023

	Room Lecture Hall, Nielsen Hall	
1:30pm	**MIOMD-MoA1-1** Stabilization of Terahertz Quantum-Cascade VECSELs, *C. Curwen, J. Kawamura, D. Hayton,* Jet Propulsion Laboratory, California Institute of Technology*; S. Addamane, J. Reno,* Center for Integrated Nanotechnologies at Sandia National Laboratories*; B. Karasik,* Jet Propulsion Laboratory, California Institute of Technology*;* ***Benjamin S. Williams****,* University of California Los Angeles	**Mid-IR Optoelectronics: Materials and Devices** **Session MIOMD-MoA1** **THz Sources and Detectors** **Moderator:** **Daniel Wasserman**, University of Texas at Austin
1:40pm		
1:50pm		
2:00pm		
2:10pm	**MIOMD-MoA1-5** RF Injection Locking of THz Metasurface Quantum-Cascade-VECSEL: Effect of Cavity Length Variation, ***Yu Wu****,* University of California, Los Angeles*; C. Curwen,* Jet Propulsion Laboratory*; J. Reno,* Sandia National Laboratories*; B. Williams,* University of California, Los Angeles	
2:20pm		
2:30pm	**MIOMD-MoA1-7** THz Quantum Photodetector Based on LO-Phonon Scattering-Assisted Extraction, ***Joel Pérez Urquizo****,* Laboratoire de Physique de l'École Normale Supérieure, France	
2:40pm		
2:50pm	**MIOMD-MoA1-9** Multi-Octave THz Wave Generation in PNPA crystal at MHz Repetition Rates, ***Lukasz Sterczewski****, J. Mnich, J. Sotor,* Wroclaw University of Science and Technology, Poland	
3:00pm		
3:10pm	**BREAK**	
3:20pm		
3:30pm		
3:40pm	**MIOMD-MoA2-14** Low Threshold Long Wavelength Interband Cascade Lasers, ***Jeremy Massengale****, Y. Shen, R. Yang,* University of Oklahoma*; S. Hawkins, A. Muhowski,* Sandia National Laboratories, USA	**Mid-IR Optoelectronics: Materials and Devices** **Session MIOMD-MoA2** **Quantum and Interband Cascade Lasers** **Moderator:** **Benjamin S. Williams**, University of California Los Angeles
3:50pm		
4:00pm	**MIOMD-MoA2-16** Progress in Terahertz Quantum Cascade Lasers Supporting Clean N-Level Systems, ***Asaf Albo****,* Bar-Ilan University, Israel	
4:10pm		
4:20pm	**MIOMD-MoA2-18** Improving Transverse Mode Quality of QCLs with Novel Waveguides, ***Matthew Suttinger****, R. Go, A. Lu,* Air Force Research Laboratory	
4:30pm		
4:40pm	**MIOMD-MoA2-20** Broadly Tunable Single Spatial Mode Quantum Cascade Lasers in an External Cavity, ***B. Knipfer****, D. Ruiz, S. Ruder, K. Oresick, M. Klaus, M. Dwyer, C. Galstad, T. Earles,* DRS Daylight Solutions	
4:50pm		

Tuesday Morning, August 8, 2023

	Room Lecture Hall, Nielsen Hall	
8:20am		**Mid-IR Optoelectronics: Materials and Devices** **Session MIOMD-TuM1** **Plenary Lecture & Integrated Photonics** **Moderator:** **Fisher Yu**, University of Arkansas
8:30am	**INVITED: MIOMD-TuM1-2** Plenary Lecture: Hybrid Passive Photonics in the Longwave-Infrared, ***David Burghoff***, University of Texas at Austin	
8:40am		
8:50am		
9:00am		
9:10am	**MIOMD-TuM1-6** Modeling of GaSb-Based Monolithically Integrated Passive Photonic Devices at λ > 2 µm, ***Md Saiful Islam Sumon***, The Ohio State University; *S. Sankar, S. Nikor,* Ohio State University; *I. Faruque,* university of Bristol, UK; *S. Dwivedi,*	
9:20am		
9:30am		
9:40am	**BREAK**	
9:50am		
10:00am		
10:10am		
10:20am		
10:30am	**INVITED: MIOMD-TuM2-14** GaSb-Based ICLs Grown on GaSb, GaAs and Si Substrates, *M. Fagot, D. Díaz-Thomaz, A. Gilbert, G. Kombila N'Dmengoye, Y. Rouillard, A. Baranov, J. Rodriguez, E. Tournié,* ***Laurent Cerutti***, IES - University Montpellier, France	**Mid-IR Optoelectronics: Materials and Devices** **Session MIOMD-TuM2** **Silicon Photonics** **Moderator:** **Daniel Wasserman**, University of Texas at Austin
10:40am		
10:50am		
11:00am	**MIOMD-TuM2-17** Electrically Injected GeSn Laser on Si Substrate Operating Up to 130 K, ***Sudip Acharya***, *S. Yu,* University of Arkansas	
11:10am		
11:20am	**MIOMD-TuM2-19** Temperature and Band Structure Dependent Properties of GeSn Double Heterostructure Lasers, ***Aneirin Ellis***, University of Glasgow, UK	
11:30am		
11:40am	**MIOMD-TuM2-21** Integrating GaSb-Based Infrared Detectors with Si Substrates via Interfacial Misfit Arrays, ***Trent Garrett***, *J. Tenorio, M. Drake,* Boise State University; *P. Reddy, K. Mukherjee,* Stanford University; *K. Grossklaus,* Tufts University; *S. Miamon,* NetzVision LLC; *P. Simmonds,* Boise State University	
11:50am		

Tuesday Afternoon, August 8, 2023

	Room Lecture Hall, Nielsen Hall	
1:30pm	**INVITED: MIOMD-TuA1-1** Interband Cascade Technology for Long Wavelength GaSb based Lasers and LEDs, ***Robert Weih***, *J. Nauschütz,* nanoplus Advanced Photonics Gerbrunn GmbH, Germany*; H. Knötig,* TU Wien, Austria*; N. Schäfer,* nanoplus Advanced Photonics Gerbrunn GmbH, Germany*; B. Schwarz,* TU Wien, Austria*; J. Koeth,* nanoplus Advanced Photonics Gerbrunn GmbH, Germany	**Mid-IR Optoelectronics: Materials and Devices** **Session MIOMD-TuA1** **ICLs and LEDs** **Moderator:** **Jerry Meyer**, Naval Research Laboratory
1:40pm		
1:50pm		
2:00pm	**MIOMD-TuA1-4** Metamorphic Growth of MWIR ICLED on Silicon, ***Fatih Furkan Ince***, *T. Rotter, M. Frost, G. Balakrishnan,* University of New Mexico*; M. McCartney, D. Smith,* Arizona State University*; C. Canedy, W. Bewley, S. Tomasulo, C. Kim,* U.S. Naval Research Laboratory*; M. Kim,* Jacobs Corporation*; I. Vurgaftman, J. Meyer,* U.S. Naval Research Laboratory	
2:10pm		
2:20pm	**MIOMD-TuA1-6** Production MBE Growth of QuiC SLED with Emission in the Longwave Infrared for Custom Gas Sensing Solutions, ***Everett Fraser***, *J. Shao, B. Barnes, P. Frensley, P. Pinsukanjana, Y. Kao,* Intelligent Epitaxy Technology, Inc.*; M. Miller,* Terahertz Device Corporation	
2:30pm		
2:40pm	**MIOMD-TuA1-8** Interband Cascade Laser on Silicon for High-Speed Applications in the Mid-Infrared Domain, ***Sara Zaminga***, Mines-ParisTech, France	
2:50pm		
3:00pm	**BREAK**	
3:10pm		
3:20pm		
3:30pm	**INVITED: MIOMD-TuA2-13** All-Epitaxial Nanophotonic Architectures for Mid-Infrared Optoelectronics, *L. Nordin,* University of Texas at Austin*; A. Kamboj,* University of Delaware*; P. Petluru, M. Bergthold, Y. Wang, A. Muhowski,* ***Daniel Wasserman***, University of Texas at Austin	**Mid-IR Optoelectronics: Materials and Devices** **Session MIOMD-TuA2** **Mid-IR Plasmonics** **Moderator:** **Qijie Wang**, Nanyang Technology University, Singapore
3:40pm		
3:50pm		
4:00pm	**INVITED: MIOMD-TuA2-16** Strategies for Electrical Tuning of Thermal Emissivity in Metamaterials, *B. Shrewsbury, A. Ghanekar, R. Audhkhasi, M. Sakib,* ***Michelle Lynn Povinelli***, University of Southern California	
4:10pm		
4:20pm		
4:30pm	**MIOMD-TuA2-19** Nonlocal Effects in Heavily Doped Semiconductor*, P. Loren,* University of Montpellier, France*; E. Sakat,* Université Paris-Saclay, CNRS, C2N, 91120 Palaiseau, France*; J. Hugonin,* Université Paris-Saclay, CNRS, Laboratoire Charles Fabry, 91127 Palaiseau, France*; L. Cerutti, F. Gonzalez-Posada,* IES, Univ Montpellier, UMR CNRS 5214, Montpellier, France*; A. Moreau,* Université Clermont Auvergne, CNRS, SIGMA Clermont, Institut Pascal, F-63000 Clermont-Ferrand, France*;* ***Thierry Taliercio***, IES, Univ Montpellier, UMR CNRS 5214, Montpellier, France	
4:40pm		
4:50pm	**MIOMD-TuA2-21** Low Doping Level and Carrier Lifetime Measurements in InAs with a Novel THz Characterization Technique, ***Julien Guise***, *S. Blin, T. Taliercio,* Univ. of Montpellier, Montpellier, France	
5:00pm		
5:10pm		
5:20pm		

Mid-IR Optoelectronics: Materials and Devices
Room Great Hall, Sam Noble Museum - Session MIOMD-TuP
Mid-IR Optoelectronics: Materials and Devices Poster Session
5:30 – 7:00 pm

MIOMD-TuP-1 Temperature Dependence of the Infrared Dielectric Function and the Direct Band Gap of InSb from 25 to 800 K, ***Sonam Yadav***, New Mexico State University

MIOMD-TuP-3 Sb-based Mid-Wave Infrared Laser Arrays, ***Rowel Go***, *A. Lu, M. Suttinger,* Air Force Research Laboratory

MIOMD-TuP-5 Carrier Concentration-Dependent Optical Properties of Narrow Gap Semiconductors, ***Yixuan Shen***, *R. Yang, M. Santos,* University of Oklahoma

MIOMD-TuP-7 Tuning the Plasmonic Response of Heavily-Doped Semiconductors in Epsilon-Near-Zero Regime, *P. Fehlen,* French-german research institute of Saint-Louis, France; *J. Guise,* University of Montpellier, France; *G. Thomas,* French-german research institute of Saint-Louis, France; *F. Gonzalez-Posada, J. Rodriguez, L. Cerutti,* University of Montpellier, France; *D. Spitzer,* French-german research institute of Saint-Louis, France; ***Thierry Taliercio,*** University of Montpellier, France

MIOMD-TuP-9 Interfacial Misfit Dislocation Array Assisted MBE Growth of InSb Quantum well on InAs using AlInSb Buffer Layer, ***Fatih Furkan Ince***, *A. Newell, T. Rotter, G. Balakrishnan,* University of New Mexico; *M. McCartney, D. Smith,* Arizona State University

MIOMD-TuP-11 High Efficiency Room Temperature HgTe Colloidal Quantum Dot Photodiodes, ***John Peterson***, *P. Guyot-Sionnest,* The University of Chicago

MIOMD-TuP-13 Experimental Study of Band Offsets at the GeSn/SiGeSn Interface by Internal Photon Emission, ***Justin Rudie***, *H. Tran, S. Amoah, S. Ojo,* University of Arkansas; *M. Shah,* University of Arkansas at Pine Bluff; *S. Yu,* University of Arkansas

MIOMD-TuP-15 A Comparative Study of Ion-Implantation of As and B in GeSn Epilayers Grown on Si (001) by Chemical Vapor Deposition, ***Amoah Sylvester***, *H. Stanchu, F. Yu,* University of Arkansas

MIOMD-TuP-17 Snowflakes Patterns Formation Enhances Performance of Nanostructure-based MWIR PbSe Photoconductive Detector, ***Richard Kim***, *R. Dahl, J. Park,* OPTODIDOE/ITW Research and Development

MIOMD-TuP-19 GaSb-based Interband Cascade Lasers with Hybrid Cladding Layers Operating in the 3-4 µm Wavelength Region, *Y. Shen,* ***Jeremy Massengale***, *R. Yang, T. Mishima, M. Santos,* University of Oklahoma

MIOMD-TuP-21 Halide Perovskite Material Development, Growth, and Characterization for Infrared Optoelectronics, ***Yash Mirchandani***, Syrnatec

MIOMD-TuP-23 Infrared Endovascular Navigation for Enhanced Sensing and Treatment, *D. DeVries, M. Salter, S. Balzora,* ***Linda Olafsen***, *J. Olafsen, K. Schubert,* Baylor University; *S. Dayawansa, J. Huang,* Baylor Scott & White Health System

MIOMD-TuP-25 Residual Gas Analysis of Reactions between Germane and Tin Tetrachloride for the Optimization (Si)GeSn CVD Growth, ***Joshua M. Grant***, *E. Yang, A. Golden, W. Du,* University of Arkansas; *B. Li,* Arktonics LLC; *S. Yu,* University of Arkansas

MIOMD-TuP-27 Low Temperature Plasma Enhanced Growth of $Si_{1-x}Sn_x$ by Chemical Vapor Deposition, ***Alexander Golden***, *J. Grant, E. Yang, S. Acharya, S. Yu,* University of Arkansas

MIOMD-TuP-29 Long Wavelength Distributed Feedback Tapered Quantum Cascade Lasers, *D. Pinto, B. Lendl,* TU Wien, Austria; *A. Baranov,* ***Kinjalk Kumar***, Université de Montpellier, France

MIOMD-TuP-31 Low-Loss Plasmonic Resonances in Heavily Doped InAs for Infrared Optoelectronic Integration, ***Ethan Caudill***, *C. Cailide,* University of Oklahoma; *M. Lloyd, J. Murphy,* Naval Research Laboratory; *K. Arledge, T. Mishima,* University of Oklahoma; *J. Nolde, J. Frantz, C. Ellis,* Naval Research Laboratory; *P. Weerasinghe, T. Golding,* Amethyst Research Inc.; *M. Santos, J. Tischler,* University of Oklahoma

MIOMD-TuP-33 Advancing Precise Control of Electromagnetic Radiation: An Innovative Nanophotonic Multilayer Structure for Mid-Infrared Applications, ***Masoumeh Nazari***, *M. Banad, S. Sharif,* University of Oklahoma

Wednesday Morning, August 9, 2023

	Room Lecture Hall, Nielsen Hall	
8:20am		**Mid-IR Optoelectronics: Materials and Devices** **Session MIOMD-WeM1** **Plenary Lecture & Applications of Mid-Infrared** **Moderator:** **Rui Yang**, University of Oklahoma
8:30am	**INVITED: MIOMD-WeM1-2** Plenary Lecture: Coherent Control of Quantum Cascade Laser Frequency Combs via Optical- and RF-Injection, ***Gerard Wysocki,*** Princeton University	
8:40am		
8:50am		
9:00am		
9:10am	**INVITED: MIOMD-WeM1-6** Compact QCL-Based Coherent Lidar in the Mid-Infrared, ***Bruno Martin,*** Thales / Laboratoire de physique de l'Ecole normale supérieure, France*; P. Feneyrou,* Thales research and technology, France*; N. Berthou,* Thales SIX, France*; D. Gacemi,* Laboratoire de physique de l'Ecole normale supérieure, France*; A. Martin,* Thales Research and Technology, France*; C. Sirtori,* Laboratoire de physique de l'Ecole normale supérieure, France	
9:20am		
9:30am		
9:40am	**MIOMD-WeM1-9** A Markov Chain Approach for Modeling Polarized Infrared Radiative Transfer in Optically Anisotropic Media, ***Feng Xu,*** University of Oklahoma*; W. Espinosa,* NASA Goddard Space Flight Center*; O. Kalashnikova, A. Davis, D. Diner, M. Garay,* Jet Propulsion Laboratory (NASA/JPL)*; J. Gong,* NASA Goddard Space Flight Center*; B. Chen, L. Gao, J. Redemann,* University of Oklahoma*; Z. Zeng,* California Institute of Technology, China	
9:50am		
10:00am	**BREAK**	
10:10am		
10:20am		
10:30am	**INVITED: MIOMD-WeM2-14** Mid-Infrared Trace Gas Detection Enhanced by Tuning Fork, Optical Cavity and Hollow-Core Fiber, ***Wei Ren,*** The Chinese University of Hong Kong	**Mid-IR Optoelectronics: Materials and Devices** **Session MIOMD-WeM2** **Sensing** **Moderator:** **Gerard Wysocki**, Princeton University
10:40am		
10:50am		
11:00am	**MIOMD-WeM2-17** Highly Selective Toluene Detection using Quartz Enhanced Photoacoustic Spectroscopy at λ = 13.71 µm, ***Kumar Kinjalk,*** IES, University of Montpellier, CNRS, France*; G. Menduni, A. Zifarelli, M. Giglio,* PolySense Lab, Dipartimento Interateneo di Fisica, University and Politecnico of Bari, Italy*; R. Teissier,* MirSense, France*; A. N. Baranov,* IES, University of Montpellier, CNRS, France*; A. Sampaolo,* PolySense Lab, Dipartimento Interateneo di Fisica, University and Politecnico of Bari, Italy	
11:10am		
11:20am	**MIOMD-WeM2-19** Quartz Enhanced Photoacoustic Spectroscopy Exploiting Beat Frequency Approach for Environmental Monitoring of Pollutants, ***Giansergio Menduni,*** PolySense Lab - Dipartimento Interateneo di Fisica, University and Politecnico of	
11:30am		
11:40am		
11:50am		

Thursday Morning, August 10, 2023

	Room Lecture Hall, Nielsen Hall	
8:20am	**INVITED: MIOMD-ThM1-1** Progress in Antimonide Unipolar Barrier Infrared Detectors, ***David Ting***, *S. Rafol, C. Hill, A. Khoshakhlagh, B. Pepper, A. Soibel, A. Fisher, S. Keo, Y. Maruyama, t. wenger, S. Gunapala,* NASA Jet Propulsion Laboratory	**Mid-IR Optoelectronics: Materials and Devices** **Session MIOMD-ThM1** **Detectors I** **Moderator:** **Robert Weih**, nanoplus Advanced Photonics Gerbrunn GmbH, Germany
8:30am		
8:40am		
8:50am	**MIOMD-ThM1-4** MWIR Resonant Cavity Infrared Detectors (RCIDs) with High Quantum Efficiency and High Frequency Response, *C. Canedy, E. Jackson, R. Espinola, C. Kim, E. Aifer, I. Vurgaftman,* Naval Research Laboratory*; V. Jayaraman, B. Kolasa,* Praevium Research*; R. Marsland, B. Knipfer,* Intraband, LLC*; M. Turville-Heitz, J. Ryu, L. Mawst, D. Botez,* University of Wisconsin*;* ***Jerry Meyer****,* Naval Research Laboratory	
9:00am		
9:10am	**MIOMD-ThM1-6** Growth and Development of Antimony-Based III-V Detector Materials for the Regime from eSWIR to LWIR, ***Volker Daumer****, L. Kirste, R. Müller, J. Niemasz, M. Wobrock, A. Wörl, Q. Yang, R. Rehm,* Fraunhofer Institute for Applied Solid State Physics IAF, Germany	
9:20am		
9:30am	**MIOMD-ThM1-8** Optically-Addressed Monolithically-Integrated Triple-Band Photodetectors Using Type-II Superlattice Materials, *Z. Ju,* ***Allison McMinn****, X. Qi,* Arizona State University*; S. Schaefer,* National Renewable Energy Laboratory*; T. McCarthy, Y. Zhang,* Arizona State University	
9:40am		
9:50am	**MIOMD-ThM1-10** Optimizing the Design of Type-II InAs/InAsSb Superlattices for the Incorporation of Unintentional Sb in the Tensile Electron Well, ***Marko Milosavljevic****,* Arizona State University*; P. Webster,* Air Force Research Laboratory, USA*; S. Johnson,* Arizona State University	
10:00am		
10:10am	**BREAK**	
10:20am		
10:30am	**MIOMD-ThM2-14** Top-Illuminated Mid-IR HgTe Colloidal Quantum Dot Photodiodes, ***John Peterson****, P. Guyot-Sionnest,* The University of Chicago	**Mid-IR Optoelectronics: Materials and Devices** **Session MIOMD-ThM2** **Detectors II** **Moderator:** **David Ting**, NASA Jet Propulsion Laboratory
10:40am		
10:50am	**MIOMD-ThM2-16** Synthesis of HgTe Colloidal Quantum Dots and Processing of Films to Maximize Photodetector Performance, ***Philippe Guyot-Sionnest****,* University of Chicago	
11:00am		
11:10am	**MIOMD-ThM2-18** Exploring Quantum Dots/Graphene van der Waals Heterostructures for Uncooled SWIR-MWIR Detection, ***Judy Wu****,* University of Kansas	
11:20am		
11:30am	**MIOMD-ThM2-20** Core-Shell Pbse/CdSe Quantum Dot Mid-Infrared Photoconductor, ***Milad Rastkar Mirzaei****, Z. Shi,* University of Oklahoma	
11:40am		

Thursday Afternoon, August 10, 2023

	Room Lecture Hall, Nielsen Hall	
1:30pm	**MIOMD-ThA1-1** Tensile-Strained InGaAs Quantum Dots with Interband Emission in the Mid-Infrared, *K. Vallejo,* ***Trent Garrett,*** Boise State University; *C. Cabrera-Perdomo,* Universidad Autónoma de Zacatecas, Mexico; *M. Drake,* Boise State University; *B. Liang,* UCLA; *K. Grossklaus,* Tufts University; *P. Simmonds,* Boise State University	**Mid-IR Optoelectronics: Materials and Devices** **Session MIOMD-ThA1** **Materials for Mid-Infrared** **Moderator:** **Benjamin S. Williams**, University of California Los Angeles
1:40pm		
1:50pm	**INVITED: MIOMD-ThA1-3** Broadband Room-Temperature Mid-Infrared Detection with Nanoparticles, *C. Wang,* Nanyang Technology University, Singapore; *L. Liang,* Nanyang Technological University, Singapore; *J. Chen, X. Liu,* National University of Singapore; ***Qijie Wang,*** Nanyang Technology University, Singapore	
2:00pm		
2:10pm		
2:20pm	**MIOMD-ThA1-6** Bi-Layered Silicon with Strain-Induced Tunable Optical Properties for IR Applications, *K. Vishal,* Wright State University; ***Yan Zhuang,*** Wright State University	
2:30pm		
2:40pm	**MIOMD-ThA1-8** Growth and Optical Properties of InGaAs QW on c-plane Sapphire for Laser Development, ***Subhashis Das,*** *R. Kumar, F. Maia de Oliveira, Y. Mazur, W. Du, S. Yu, G. Salamo,* University of Arkansas	
2:50pm		
3:00pm	**MIOMD-ThA1-10** Low-Loss Infrared Ultrawide Type II Hyperbolic Metamaterials based on III-V Semiconductors, ***Weerasinghe Priyantha,*** Amethyst Research Incorporated; *E. Caudill, C. Cailide,* University of Oklahoma; *M. Lloyd, J. Murphy,* NRL; *K. Arledge, T. Mishima,* University of Oklahoma; *J. Nolde, J. Frantz, C. Ellis,* NRL; *T. Golding,* Amethyst Research Incorporated; *M. Santos, J. Tischler,* University of Oklahoma	
3:10pm		
3:20pm	**BREAK**	
3:30pm		
3:40pm		**Mid-IR Optoelectronics: Materials and Devices** **Session MIOMD-ThA2** **Metamaterials and Polaritons** **Moderator:** **Lukasz Sterczewski,** Wroclaw University of Science and Technology, Poland
3:50pm	**MIOMD-ThA2-15** A 231 GHz Generation in High-Power Long-Wavelength Quantum Cascade Laser Operating at Room Temperature, ***Shohei Hayashi,*** *A. Ito, T. Dougakiuchi, M. Hitaka, A. Nakanishi, K. Fujita,* Hamamatsu Photonics K.K., Japan	
4:00pm		
4:10pm	**MIOMD-ThA2-17** Mapping Surface Phonon Polaritons with Near-IR Light, ***Kiernan Arledge,*** The University of Oklahoma; *M. Meeker,* U.S. Naval Research Laboratory; *C. Ellis,* U.S. Naval Research Lab; *N. Sarabi, V. Whiteside,* The University of Oklahoma; *C. Kim, M. Kim, D. Ratchford, B. Weng,* U.S. Naval Research Laboratory; *J. Tischler,* The University of	
4:20pm		
4:30pm	**MIOMD-ThA2-19** Surface Phonon Polariton Coupling to 4H SiC Triangular Gratings Produced by Two-Photon Polymerization, ***Nazli Rasouli Sarabi,*** *V. Whiteside,* University of Oklahoma; *E. Cleveland, E. Seabron, C. Ellis,* Naval Research Laboratory; *J. Tischler,* University of Oklahoma	
4:40pm		
4:50pm	**MIOMD-ThA2-21** Dielectric Resonances in Hexagonal Boron Nitride Nanodisks, ***Milad Nourbakhsh,*** University of Oklahoma; *H. Ling,* University of California at Los Angeles; *V. Whiteside,* University of Oklahoma; *A. Davoyan,* University of California at Los Angeles; *J. Tischler,* University of Oklahoma	
5:00pm		
5:10pm	**Closing Remarks**	

Author Index

Bold page numbers indicate presenter

Author Index

— N —

— O —

— P —

— Q —

— R —

— S —

— T —

— V —

— W —

— X —

— Y —

— Z —

Author Index

Mid-infrared semiconductor laser frequency combs: From FM-combs to Nozaki-Bekki solitons

N. Opačak[1,2], D. Kazakov[2], L. Columbo[3], S. Dal Cin[1], M. Beiser[1], F. Pilat[1], Theodore P. Letsou[2,4], M. Brambilla[5], F.Prati[6], M. Piccardo[2,7], F. Capasso[2], and B. Schwarz[1, 2 +]

[1] Institute of Solid State Electronics, TU Wien, Vienna, Austria
[2] John A. Paulson School of Engineering and Applied Sciences, Harvard University, Cambridge, MA, USA
[3] Dipartimento di Elettronica e Telecomunicazioni, Politecnico di Torino, Torino, Italy
[4] Department of Electrical Engineering and Computer Science, Massachusetts Institute of Technology, Cambridge, MA, USA
[5] Dipartimento di Fisica Interateneo and CNR-IFN, Universitá e Politecnico di Bari, Italy
[6] Dipartimento di Scienza e Alta Tecnologia, Universitá dell'Insubria, Como, Italy
[7] Department of Physics, Instituto Superior T´ecnico, Universidade de Lisboa, Portugal

Optical frequency combs (OFCs) stand as the cornerstone of modern optics, with applications ranging from fundamental science to sensing and spectroscopy. Generation of short optical soliton pulses in passive media such as optical fibers and microresonators has been an established technique for stable OFC formation with a broad optical spectrum – however these platforms are driven by an external optical signal and often rely on additional bulky elements that increase the complexity of the system.

Here, we aim to overcome these difficulties by direct OFC generation in mid-infrared semiconductor lasers, such as quantum and interband cascade lasers. After a general introduction to such combs and their nonlinear dynamics, the soliton concept from microresonator Kerr combs will be generalized to active media that are electrically-driven and a new type of solitons in free-running semiconductor laser integrated on a chip will be demonstrated.

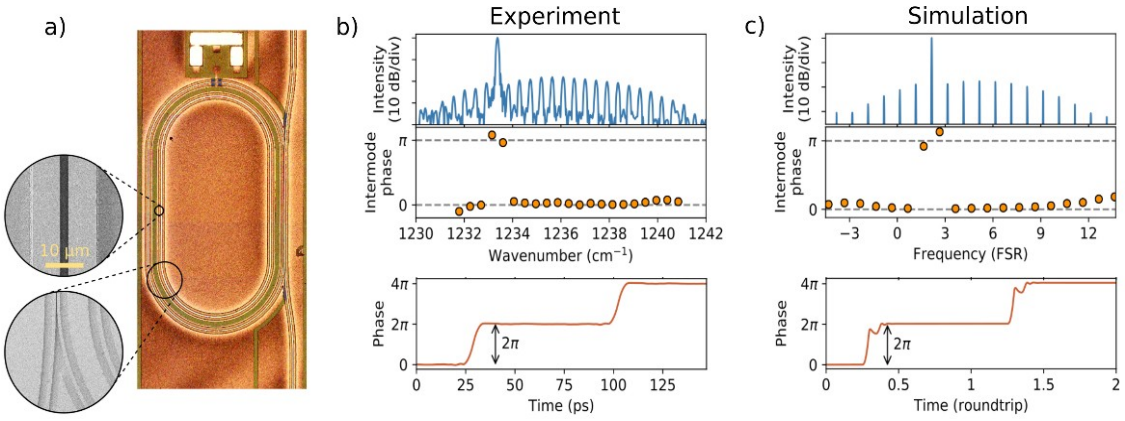

Figure 1 a) Ring laser device with the active coupler waveguide. b) Experimental and simulated c) free-running soliton. The soliton spectrum is displayed in the top, showing a strong mode surrounded by a smooth spectral envelope comprised of weaker sidemodes. The corresponding intermodal phases, given below, indicate a π jump between the sidemodes and the strong mode. The temporal phase profile is plotted in the bottom.

[1] D. Kazakov, et al., arXiv:2206.03379 (2022).
[2] N. Opačak, et al., Phys. Rev. Lett. 127, 093902 (2021).
[3] M. Piccardo et al., Nature 582, 360 (2020).
[+] Author for correspondence: benedikt.schwarz@tuwien.ac.at

Temporal Solitons in Coherently-Driven Ring Lasers

T. P. Letsou,[1, 2, +] D. Kazakov,[1] M. Piccardo[1, 3], L. L. Columbo[4, 5], M. Brambilla[6, 5], F. Prati[7], S. Dal Cin[8], M. Beiser[8], N. Opačak[8], M. Pushkarsky[9], D. Caffey[9], T. Day[9], L. A. Lugiato[7], B. Schwarz[1, 8], F. Capasso[1]

[1] Harvard John A. Paulson School of Engineering and Applied Sciences, Harvard University, Cambridge, MA 02138, USA

[2] Department of Electrical Engineering and Computer Science, Massachusetts Institute of Technology, Cambridge, MA 02142, USA

[3]Department of Physics, Instituto Superior Técnico, Universidade de Lisboa, 1049-001 Lisbon, Portugal

[4]Dipartimento di Elettronica e Telecomunicazioni, Politecnico di Torino, 10129 Torino, Italy

[5]CNR-Istituto di Fotonica e Nanotecnologie, 70126 Bari, Italy

[6]Dipartimento di Fisica Interateneo and CNR-IFN, Università e Politecnico di Bari, 70125 Bari, Italy

[7]Dipartimento di Scienza e Alta Tecnologia, Università dell'Insubria, 22100 Como, Italy

[8]Institute of Solid State Electronics, TU Wien, 1040 Vienna, Austria

[9]DRS Daylight Solutions, San Diego, CA 92127, USA

Pulsed lasers have been the workhorse of ultrafast optics since their advent and rapid development throughout the 20th century, revolutionizing a wide variety of fields from spectroscopy to tattoo removal. Over the past twenty years, pulsed laser sources have shrunk from tabletop laboratory setups down to micron-sized chips, making them ideal components for integrated photonic devices. Despite this miniaturization, chip-scale pulsed laser sources have eluded the mid infrared (IR) spectral region. Active mode-locking of mid IR semiconductor lasers—such as quantum cascade lasers (QCLs)—has produced pulse widths on the order of 6 picoseconds [1]. Pulse compression techniques can be utilized to shrink these pulses to hundreds of femtoseconds [2], but rely on large optical setups that cannot be scaled down. Here, we present a fundamentally new way to produce bright pulses of mid IR light by optically pumping ring QCLs. This technique unifies the physics of passive, Kerr microresonator combs and ring QCLs [3]. Using a modified racetrack QCL with an integrated directional coupler, we injection-lock the unidirectional laser field circulating in the racetrack to a commercial external cavity QCL. Much like in Kerr microresonator combs, when the injection-locked field is detuned from its natural cavity resonance, the resonance becomes bistable, with its unstable branch supporting bright solitons with pulse widths of ~1 picosecond at a center wavelength of 8 μm. This method of pulse formation is well-suited for lasers with fast gain dynamics, which encompasses the entire family of QCLs, spanning from 3 μm to 300 μm. Furthermore, the optical drive can, in principle, be integrated with the racetrack, providing a route for on-chip, ultrashort pulse formation throughout the entire mid-IR.

[1] J. Hillbrand, *et. al.*, Nat. Commun. **11**, 5788(2020).
[2] P. Täschler, *et. al.*, Nat. Photon. **15**, 919-924(2021).
[3] L. Columbo, M. Piccardo, *et. al.*, Phys. Rev. Lett. **126**, 173903(2021).
[+] Author for correspondence: tletsou@g.harvard.edu

Supplementary Pages

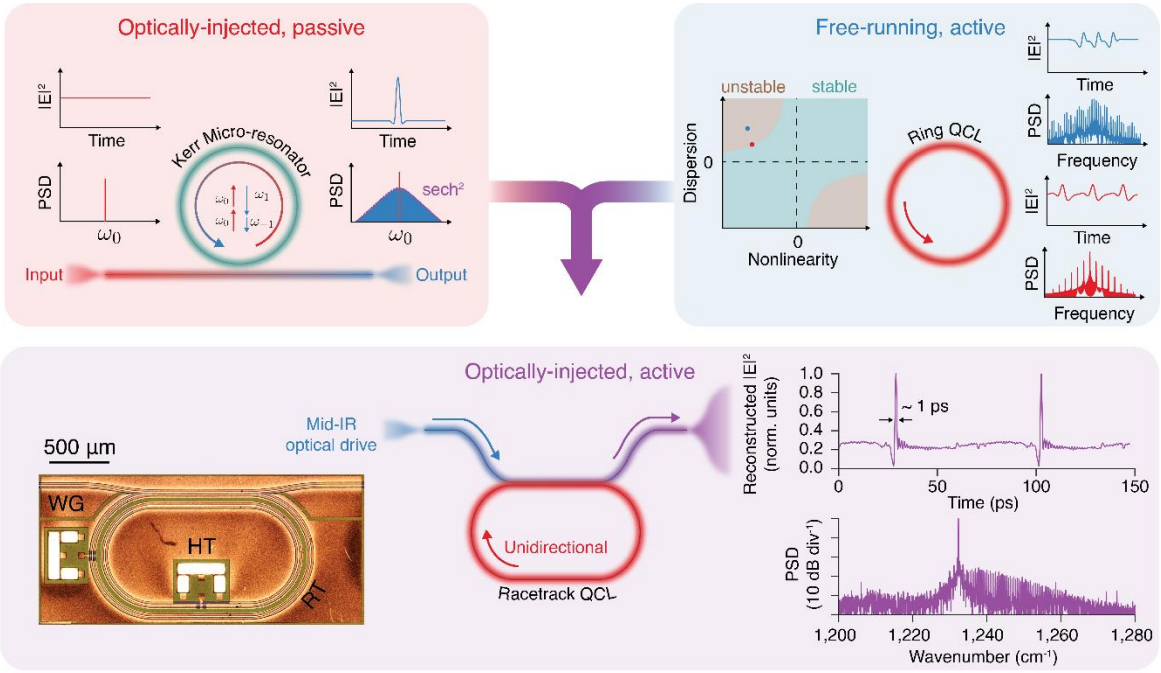

Figure 1: Unifying Kerr Microresonators and Ring Quantum Cascade Lasers (QCLs). Kerr microcombs form by coupling continuous-wave (CW) optical fields to passive microresonators. The resonator's strong non-linearity promotes the production of parametric sidebands which phase-lock via four-wave mixing. Ring QCLs can either operate as stable, single-mode lasers, or as multimode frequency combs depending on their dispersion and non-linearity. In free-running ring QCLs, pulse formation is prevented by fast gain recovery times. This limitation can be bypassed if the ring QCL is coherently-driven with an external laser source. To couple the external optical drive to the ring QCL, we utilize a racetrack (RT) geometry, where light is coupled to the RT using a waveguide directional coupler (WG). We use an integrated heater (HT) to finely tune the cavity resonance of the RT. When the field circulating in the RT is locked to the external laser, the resonance becomes bistable, with its unstable branch supporting bright solitons with pulse widths of ~1 picosecond at a center wavelength of 8 µm.

Dissipative cavity solitons are stable, single-peaked waveforms that maintain their shape while propagating through a nonlinear and dispersive medium at constant velocity. In the frequency domain, optical solitons constitute frequency combs, where the spacing between frequency components is locked down to one part in 10^{12}. Dissipative solitons form through the delicate balance of both dispersion and nonlinearity, as well as gain and loss. One way to form bright solitons is to pump a high-quality (Q) factor, passive microresonator possessing anomalous dispersion with a strong, continuous-wave (CW) optical field. Upon sweeping the field frequency through the cavity resonance, the input field undergoes a modulational instability and may form a bright soliton once it is effectively red detuned from the cold cavity resonance. These so-called 'Kerr soliton microcombs' can span across the visible to the near-infrared, often covering a full spectral

Full-band modeling of AM and FM interband cascade laser frequency combs

M. Povolotskyi,[1] I. Vurgaftman[2]
[1] *Jacobs, Hanover, MD 21076, USA*
[2] *Code 5613, Naval Research Laboratory, Washington, DC 20375, USA*

Compact and efficient mid-infrared (MIR) frequency combs are expected to find widespread use in chemical sensing applications, such as on-chip spectroscopy of toxic substances [1]. While most of the experimental MIR laser comb work has involved quantum cascade lasers (QCLs), interband cascade lasers (ICLs) operate cw at room temperature in the 3-4 μm spectral range, which remains difficult for QCLs, and also promise significant reductions in the operating power throughout the MIR spectral range. Furthermore, owing to the long carrier lifetime in an ICL, both passive mode-locking with short pulses (AM) and quasi-cw (FM) comb generation should be possible.

In spite of these promising characteristics, only FM combs based on ICLs have been demonstrated to date. In order to clarify the physical requirements for both AM and FM operation, we have developed a multiscale numerical model that efficiently solves the Maxwell-Bloch equations for the full subband dispersion in the ICL's active type-II wells over a time period of μs. We compare the results of this model to those derived from the two-level approximation relevant to QCLs [2], and evaluate the importance of such parameters as the second-order and higher-order group velocity dispersions, saturable absorber length and recovery time, ambipolar diffusion coefficient, and polarization relaxation time (homogeneous gain broadening linewidth). We determine the optimal design parameters for experimentally demonstrating both passively mode-locked and FM ICL combs, and outline how they can be realized in practice.

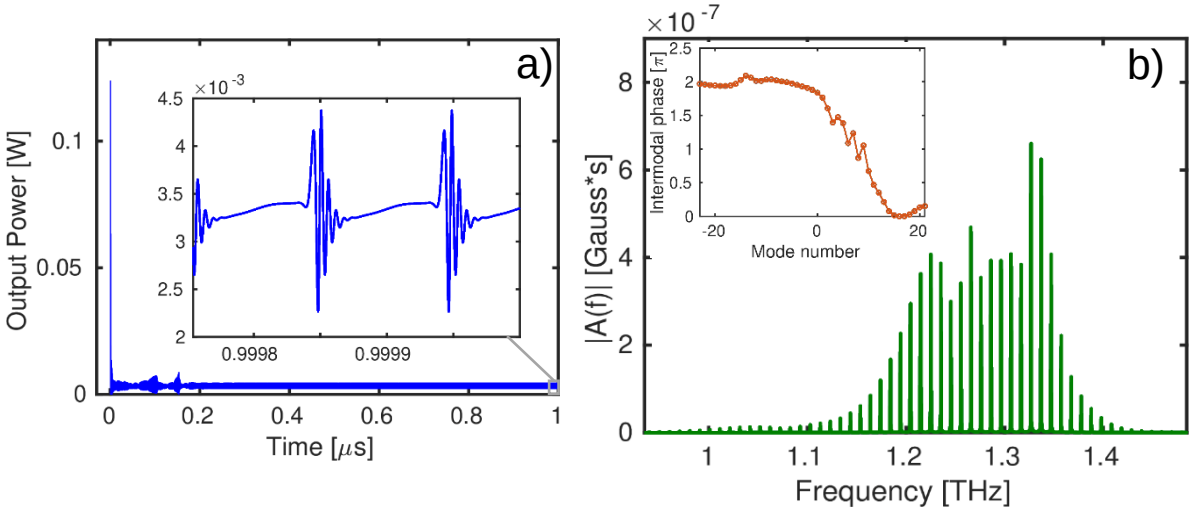

Figure 1. Frequency comb output due to the frequency modulation in an ICL: a) output power; b) output signal modulation spectrum and the intermodal phase difference.

[1] Sterczewski, L. A. *et al*, Opt. Lett. 44, 2113 (2019). [2] Opačak, N. *et al*, Phys. Rev. Lett. 123, 243902(2019).
[+] Author for correspondence: I. Vurgaftman, e-mail: MWIR_laser@nrl.navy.mil

Supplementary Pages

The electromagnetic field is simulated in the slowly varying envelope function approximation, which allows us to use a coarse mesh with points separated by $h > \frac{\lambda}{n_r} \approx 1\ \mu$m, and corresponding time steps $\tau = h/v_g$:

$$\pm\partial_z A^{\pm} + \left(\frac{1}{v_g}\partial_t A^{\pm}\right) + i\frac{\beta_2}{2}\partial_{t^2}^2 A^{\pm} + i^2\frac{\beta_3}{6}\partial_{t^3}^3 A^{\pm} + \ldots + i^{n-1}\frac{\beta_n}{n!}\partial_{t^n}^n A^{\pm} = i\frac{4\pi\omega^2}{\left(\frac{2\pi n_r}{\lambda}\right)c^2}\left(\frac{\Gamma}{w}\right)\left(\frac{2}{(2\pi)^2}\right)P^{\pm} - \frac{\alpha}{2}A^{\pm}, \quad (1)$$

where $A^{\pm}$ are the counter-propagating electric-field amplitudes, $\beta_i = \mathrm{Re}(d^i k/d\omega^i)$ are the group-velocity dispersion (GVD) coefficients, Γ is the mode overlap factor, w is the well width, $P^{\pm}$ are the amplitudes for dipole polarization and α is the absorption coefficient.

The ICL active region is based on a type-II quantum-well heterostructure. Contrary to QCLs, the optical transition energy varies significantly with the electron/hole in-plane wavevector k, so the dipole polarization is a sum of contributions of different k: $P^{\pm} = \int_0^{K\max} d^*(k)\,p^{\pm}(k)(2\pi k)dk$, where $d(k)$ and $p(k)$ are the dipole moment and polarization, respectively. Therefore, to model an ICL it is necessary to know the distribution of electrons and holes over the Brillouin zone at any moment in time. Modeling a non-equilibrium electron gas distribution in both real and momentum space is still a challenging task, so four major assumptions have been made: (1) local charge neutrality; (2) electrons and holes are confined in one direction only, with their transport being quasi-1D along the ICL cavity axis (Fig. S1a); (3) rapid intraband thermalization, meaning both electrons and holes obey the local quasi-Fermi-Dirac distribution; and (4) the spatial dependence of the carrier distribution function along the cavity is approximated as the sum of a large slow-varying envelope $n_0(z)$ and a small first harmonic $n_1(z)$ that oscillates with period $0.5\lambda/n_r$[2]:

$$n^c(z) = n^v(z) = n(z);\ n(z) = n_0(z) + \mathrm{Re}\left(n_1(z)e^{-i\frac{4\pi n_r}{\lambda}z}\right);\ \mu(z) = \mu_0(z) + \mu_1(z);\ \mu_1(z) = \frac{\mu_0(n_0)}{\partial n_0}n_1(z);$$

$$n_{0,1}^{c,v}(z) = \int_0^{K\max} f_{0,1}^{c,v}(k,z)\left(2\cdot 2\pi k\right)dk;\ f_0^{c,v}(k,z) = \frac{1}{\exp\left(\frac{E_{c,v}(k) - \mu_0^{c,v}(z)}{kT}\right)+1};\ f_1^{c,v}(k,z) = \frac{\partial f_0(k,z)}{\partial \mu_0}\mu_1(z) \quad (2)$$

where $\mu(z)$ is the position-dependent quasi-Fermi level.

Starting from these assumptions, a set of equations has been developed in which the quasi-Fermi levels are obtained from the particle conservation law, with the inclusion of uniform injection current, stimulated emission, and Auger nonradiative recombination.

$$\frac{\partial n_0}{\partial t} = \frac{2}{(2\pi)^2}\int_0^{K\max} 2\pi k\left(\frac{\partial f_0}{\partial t}\right)_{rad}dk - \gamma n_0^3 - \frac{n_0}{\tau(z)} + J(z) \quad (3)$$

$$\frac{\partial n_1}{\partial t} = \frac{2}{(2\pi)^2}\int_0^{K_{\max}} 2\pi k\left(\frac{\partial f_1}{\partial t}\right)_{rad}dk - 3\gamma n_0^3 n_1 - \frac{n_1}{\tau(z)} - 4D_a\left(\frac{2\pi}{\lambda}\right)^2 n_1, \quad (4)$$

where $J(z)$ is the injection current density, $1/\tau(z)$ is the defect-assisted recombination rate, which is assumed significant only in an ion-bombarded saturable absorber, D_a is the ambipolar diffusion constant, γ is the Auger recombination constant, and $(\partial f/\partial t)_{rad}$ is the momentum-resolved recombination rate for stimulated emission:

Recent Advances in Interband Cascade Lasers for Mid-Wave Infrared Free-Space Optical Communications

Frédéric Grillot[1]

[1] *LTCI Télécom Paris, Institut Polytechnique de Paris, Palaiseau, 91120, France*
[6] *Center for High Technology Materials, University of New-Mexico, Albuquerque, NM 87106, USA*

Free-space laser communications constitute a promising alternative for transmitting high bandwidth data when fiber optic cable is neither practical nor feasible. This technology has emerged as a strong candidate with a large potential of applications from daily-basis broadband internet to satellite links. Recently, a record transmission speed in free space of up to 1 Tbits/s has been reported over a single wavelength and a distance of 53 km [1]. Although the availability of high-quality transmitters and detectors operating in the near-infrared window makes the 1.55-μm optical wavelength a natural choice for free-space optical systems, two other wavelength ranges can also be considered. First, the mid-wave infrared (MWIR) window between 3 and 5-μm, and second, the long-wave infrared (LWIR) window between 8 and 12-μm. Both are well known for their superior transmission performance through adverse atmospheric phenomena, such as fog, clouds, and dust [2]. In order to develop free-space laser communications in the MWIR, interband cascade lasers (ICL) are currently emerging as very serious candidates [3]. Such advanced semiconductor lasers are based on interband recombinations in a broken-gap configuration, using the same cascade principle as quantum cascade lasers (QCL). However, compared to their QCL counterparts, ICLs offer more advantages. To name a few, they have the ability to bypass fast phonon scattering losses while achieving sufficiently high output powers, on the order of tens of milliwatts [4]. In addition, thanks to their very low threshold currents, ICLs are very much attractive for applications requiring low power consumption. Finally, the development of inter-band cascaded photonic integrated circuits is a key step towards the wider use of ICL technology, which is of growing interest since the first demonstration of an ICL bonded to silicon [5]. A recent work also unveiled the possibility of mitigating a very high dislocation factor, while maintaining the same characteristics as ordinary ICLs grown on GaSb [6]. As a consequence of that, with the advent of new telecommunication standards and the ever-increasing need for data transfer speed, the ICL community is now keenly interested in powerful room-temperature sources operating with high modulation capabilities. In this presentation, we will review our recent progress in the physics and applications of interband cascaded devices. We will discuss their intensity noise and modulation properties and reveal the existence of the oscillation relaxation frequency that is of paramount importance to achieve very fast modulation rates. We will then present state-of-the-art testbed experiments performed with 4.2-μm Fabry-Perot ICLs, which achieved data rates of up to 12 Gbps (OOK) and up to 14 Gbps (PAM-4) under direct modulation of light [7]. In summary, these novel findings in interband cascade devices provide clear scientific guidelines that will be very useful to researchers and engineers in the design and deployment of future free-space MWIR laser communication systems.

[1] Press Release, European Project VERTIGO, Thales Alenia Space, (2022).
[2] Spitz, O., et al., IEEE Journal of Selected Topics in Quantum Electronics 28, 1200109 (2022).
[3] Yang, R. Q., et al., Superlattices Microstruct. 17, 77–83261 (1995).
[4] Meyer, J., et al., *Photonics* 7, 75 (2020).
[5] Spott, A. et al. *Optica*, 5, 996–1005 (2018).
[6] Cerutti, L., et al., *Optica* 8, 1397-1402 (2021).
[7] Didier, P. et al., *Photonics Research* 11, 582-590 (2023).

+ Author for correspondence: frederic.grillot@telecom-paris.fr

Continuous wave room temperature operation of the epitaxially regrown GaSb-based diode PCSELs.

L. Shterengas,[1] W. Lee,[1] R. Liu, A. Stein,[2] G. Kipshidze,[1] G. Belenky[1]
[1] Stony Brook University, Stony Brook, New York 11794, USA
[2] Brookhaven National Laboratory, Upton, New York 11973, USA

Photonic crystal surface emitting laser (PCSEL) device architecture can dramatically improve brightness of semiconductor laser sources. The development of the PCSELs within nitride [1], arsenide [2], phosphide [3], and antimonide [4] material systems is subject of active research to enable high power high brightness surface emitting diode laser operation from UV to mid-infrared. One of the key technological challenges associated with PCSEL development is integration of the high-index-contrast photonic crystal layer into laser heterostructure. The air-pocket-retaining epitaxial regrowth [5] was shown to be effective technique which yielded high-power diode PCSELs. The air-pocket-retaining regrowth within antimonide material system was explored by our research group.

We report on the continuous wave (CW) room temperature operation of epitaxially regrown monolithic GaSb-based ~2 μm diode PCSELs. The devices are based on laser heterostructure containing carrier stopper layer designed to inhibit electron carrier leakage into buried photonic-crystal section. Atomic hydrogen cleaning of the nanopatterned surface followed by optimized epitaxial step resulted in highly uniform air-pocket-retaining regrowth. The laser heterostructure with buried high-index-contrast photonic crystal layer generated about 10 mW of power near 2 μm in CW regime and tens of mW in 5% duty cycle at 20 ^{o}C.

This research was funded by US Army Research Office, grant W911NF2210068, and in part by the U.S. Department of Energy, Office of Basic Energy Sciences, through the Center for Functional Nanomaterials, Brookhaven National Lab, under Contract DE-SC0012704.

[1] K. Emoto, et al, Commun Mater **3**, 72 (2022).
[2] K. Hirose, et al, Nat. Phot. **8**, 406 (2014).
[3] Y. Itoh, et al, Opt. Exp. **30**, 29539 (2022).
[4] L. Shterengas, et al, Phys. Status Solidi RRL **16**, 2100425 (2022).
[5] M. Nishimoto, et al, Appl. Phys. Exp. **6**, 042002 (2013).

[+] Author for correspondence: leon.shterengas@stonybrook.edu

Single-Mode Tunable Interband Cascade Lasers with a Wide Tuning Range

Jingli Gong,[1] Zhanyi Wang,[1] Jian-Jun He,[1] Rui Q. Yang[2,+]
[1] State Key Laboratory of Modern Optical Instrumentation, College of Optical Science and Engineering, Zhejiang University, Hangzhou, China 310027
[2]School of Electrical and Computer Engineering, University of Oklahoma, Norman, OK USA 73019.

Type-II interband cascade lasers (ICLs) [1,2] are efficient and compact mid-infrared light sources with many applications such as gas sensing and environmental monitoring. Here, we report the demonstration of single-mode tunable ICLs with a wide tuning range based on V-coupled cavity [3,4]. By optimizing the coupling coefficient and the cavity structure design, the tuning range of V-coupled cavity single-mode ICLs is significantly extended with a side mode suppression ratio (SMSR) exceeding 37 dB in continuous wave operation near 3.4 μm. At a fixed temperature, a tuning range of up to 97 nm has been demonstrated. By combining two temperatures at 82K and 100K, a total tuning range of about 150 nm has been achieved, as shown in Fig. 1. The total tuning range exceeded 150 nm when operation temperature extended to 110K. More details and updated results will be presented at the conference.

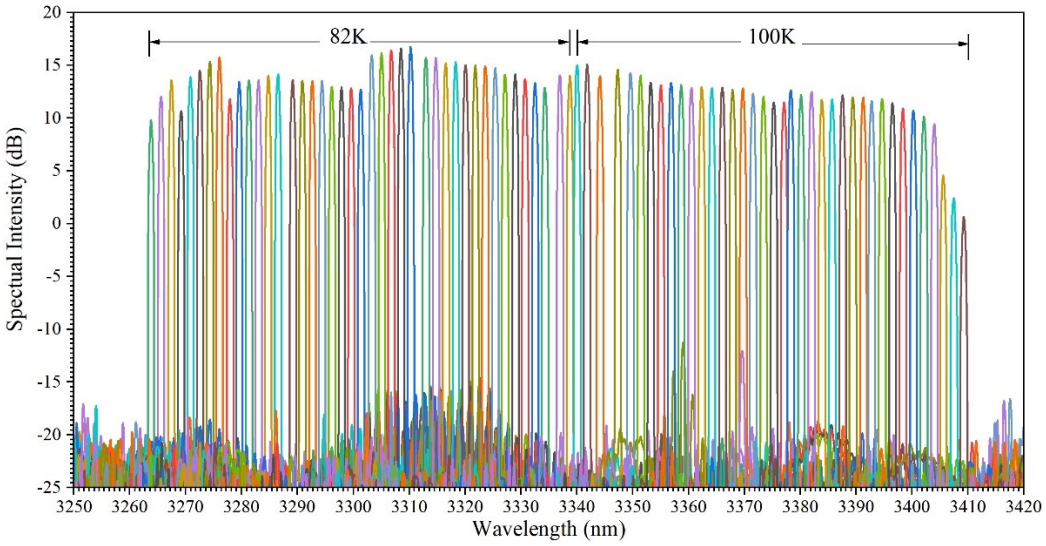

Fig. 1 CW emission spectra of a V-coupled cavity ICL with a total tuning range of 150 nm.

Acknowledgments: The work at Zhejiang University was supported by the National Natural Science Foundation of China (61960206001 and 62027825). The work at University of Oklahoma was partially supported by NSF (No. ECCS-1931193) and OCAST (AR21-024).

[1] R. Q. Yang, Superlattices Microstruct., **17**, 77 (1995).
[2] J. R. Meyer, *et al*., Photonics **7**, 75 (2020)
[3] J.-J. He and D. Liu, Opt. Express, **16**(6), 3896 (2008)
[4] J. L. Gong, R. Q. Yang, Z. Wang, and J. J. He, IEEE Photo. Technol. Lett. **35**, 309 (2023).

[+] Author for correspondence: Rui.q.Yang@ou.edu

Expanding the Frontiers of Long Wavelength Interband Cascade Lasers using Innovative Quantum Well Active Regions

Yixuan Shen,[1] J. A. Massengale,[1] Rui Q. Yang[1,+], S. D. Hawkins[2], A. J. Muhowski[2]
[1]School of Electrical and Computer Engineering, University of Oklahoma, Norman, OK.
[2]Sandia National Laboratories, PO Box 5800, Albuquerque, NM 87185-1085, USA

Interband cascade lasers (ICLs) [1-2] based on type-II quantum wells (QWs) are an efficient mid-infrared light source for many practical applications due in large part to their low power consumption. High performance operation of ICLs has been demonstrated at room temperature across a wavelength range from 2.7 µm to about 6 µm [2-4]. However, extending the operation of ICLs to longer wavelengths with similar performance as their short wavelength counterparts is challenging due to factors such as the reduced wavefunction overlap in the type-II QW and the increased free-carrier absorption loss. In this work, we report significant progress in long wavelength ICLs from newly designed and grown ICL wafers by employing an innovative QW active region containing strained InAsP layers [5]. These ICLs were able to operate at wavelengths near 14.3 µm as shown in Fig. 1, the longest ever demonstrated for III-V interband lasers, suggesting great potential of ICLs to cover an even wider wavelength range. Devices from another wafer were able to lase at a low threshold current density (*e.g.*, 15 A/cm^2 at 80 K) and at temperatures up to 210 K near 12.3 μm as shown in Fig. 2. Detailed results will be presented at the conference.

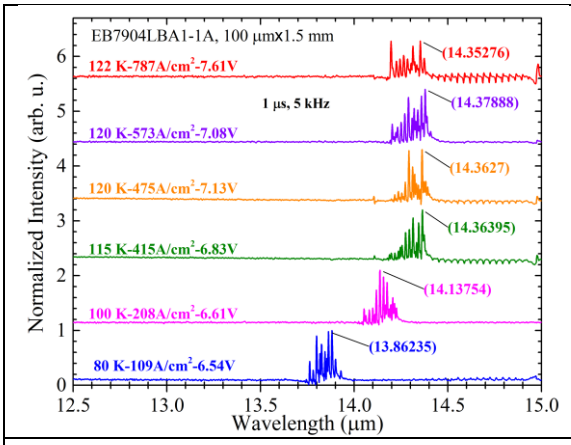

Fig. 1 Pulsed lasing spectra of an ICL from EB7904.

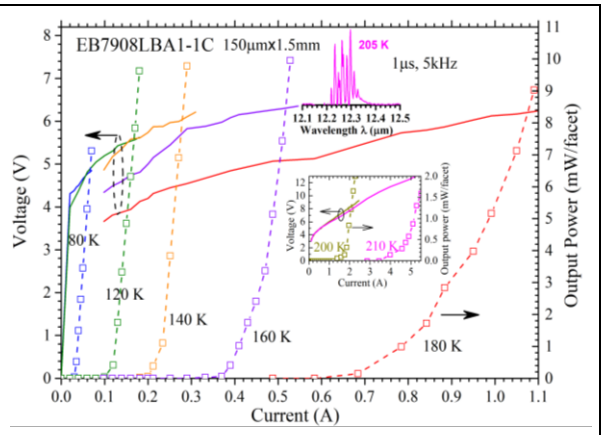

Fig. 2. IVL characteristics and a lasing spectrum.

This work at OU was partially supported by NSF (No. ECCS-1931193), and was performed, in part, at the Center for Integrated Nanotechnologies, an Office of Science User Facility operated for the U.S. Department of Energy (DOE) Office of Science. SNL is managed and operated by NTESS under DOE NNSA contract DE-NA0003525.

[1] R. Q. Yang, Superlattices Microstruct., **17**, 77 (1995).
[2] J. R. Meyer, *et al*., Photonics **7**, 75 (2020)
[3] R. Q. Yang, *et al*. IEEE J. Sel. Top. Quantum Electron. **25**, 1200108 (2019).
[4] J. Nauschutz, *et al*., Laser & Photonics Reviews, 2200587 (2023).
[5] J. A. Massengale, *et al*., Semicond. Sci. Technol. **38**, 025009 (2023).

[+] Author for correspondence: Rui.q.Yang@ou.edu

Stabilization of terahertz quantum-cascade VECSELs

Christopher A. Curwen,[1] Jonathan H. Kawamura,[1] Darren J. Hayton,[1] Sadhvikas J. Addamane,[2] John L. Reno,[2] Boris S. Karasik[1], and Benjamin S. Williams,[3]

[1] *Jet Propulsion Laboratory, California Institute of Technology, Pasadena, CA 91109*

[2] *Center for Integrated Nanotechnologies at Sandia National Laboratories, Albuquerque, NM 87185*

[3] *Department of Electrical and Computer Engineering at the University of California, Los Angeles, CA 90095*

Terahertz metasurface quantum-cascade (QC) vertical external cavity surface emitting lasers (VECSELs) are excellent candidates for frequency agile local oscillators and spectroscopic sources, that emit milliwatts to tens-of-milliwatts continuous-wave power with excellent beam power. We present the first high resolution studies of the free-running laser behavior of QC-VECSELs at 2.5 THz and 3.4 THz, and demonstrate phase-locking to a microwave reference, by using subharmonic Schottky-diode mixer instrumentation to downconvert the THz signal to a GHz intermediate frequency (IF). Feedback from reflections at the mixer are observed to have a strong influence on the free-running QC-VECSEL frequency stability as a result of efficient coupling to free-space compared to more typical ridge waveguide lasers. Instabilities in feedback result in free-running linewidths of tens of MHz. The QC-VECSEL IF signal is phase locked to a 100 MHz reference using the bias on the device as a means of error correction. Between 90-95% of the QC-VECSEL signal is locked within 2 Hz of the multiplied RF reference, and amplitude fluctuations on the order of 1-10% are observed, depending on the bias point of the QC-VECSEL. The bandwidth of the locking loop is ~1 MHz. Many noise peaks in the IF signal corresponding to mechanical resonances in the 10 Hz-10 kHz range are observed. These peaks are generally -30 to -60 dB below the main tone, and are below the phase noise level of the multiplied RF reference which ultimately limits the phase noise of the locked QC-VECSEL.

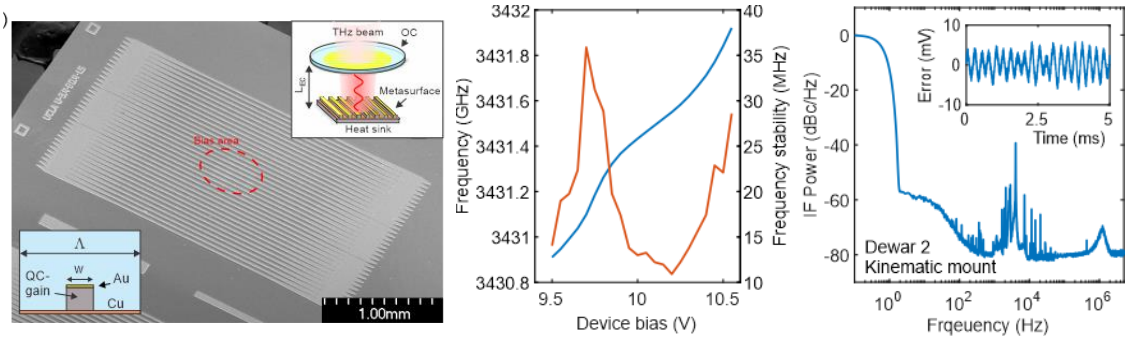

Figure 1. (left) SEM of the 3.4 THz metasurface. Insets illustrate a period of the metasurface, and the QC-VECSEL cavity. (center) Tuning characteristic and free-running linewidth of QC-VECSEL. (right) Phase-locked IF power spectrum and bias fluctuations.

[1] C. A. Curwen, J. H. Kawamura, Darren J. Hayton, Sadhvikas J. Addamane, John L. Reno, Benjamin S. Williams, and Boris S. Karasik, "Phase locking of THz QC-VECSELs to a microwave reference," https://www.techrxiv.org/articles/preprint/Phase_locking_of_THz_QC-VECSELs_to_a_microwave_reference/21893031/1 .

[+] Author for correspondence: bswilliams@ucla.edu

RF injection locking of THz metasurface quantum-cascade-VECSEL: effect of cavity length variation

Yu Wu,[1] Christopher A. Curwen,[2] John L. Reno,[3] Benjamin S. Williams[1]
[1] *Department of Electrical and Computer Engineering, University of California, Los Angeles, California 90095, USA*
[2] *Jet Propulsion Laboratory, California Institute of Technology, Pasadena, California 91109, USA*
[3] *Sandia National Laboratories, Center of Integrated Nanotechnologies, MS 1303, Albuquerque, New Mexico 87185, USA*

Quantum-cascade (QC) lasers are ideally suited for high-resolution, high speed spectroscopy techniques in terahertz (THz) spectral region. Their inherently high optical nonlinearity promotes the generation of spontaneous frequency combs via four-wave mixing in Fabry-Pérot or ring QC-lasers, based on which THz dual-comb spectroscopy has been demonstrated. Besides that, THz QC-laser has recently been implemented in the vertical-external-cavity surface-emitting laser (VECSEL) architecture, which is considered as a great candidate for THz frequency comb or mode-locking operations.

Here, we demonstrate RF injection locking in THz metasurface QC-VECSEL for the first time. An intra-cryostat focusing VECSEL cavity design is applied to reduce the intra-cavity diffraction loss and enable continuous wave lasing at 3.4 THz in an external cavity length over 30 mm (Fig. 1(a)). RF current modulation is applied to the QC-metasurface at a frequency close to the cavity round-trip frequency. Under weak RF power, pulling and locking of the round-trip frequency to the injected RF signal has been observed with locking bandwidth characterized using Adler's equation; Under strong RF power, broadening of the lasing spectrum with a maximum observable bandwidth around 110 GHz has been demonstrated under an injected RF power of 20 dBm (Fig. 1(b)). Injection locking phenomenon using metasurfaces with different gain/dispersion and tunable external cavity lengths has also been explored, taking the advantage of design flexibility of the VECSEL configuration. This experimental setup is suitable for further exploration of active mode-locking in THz QC-VECSELs.

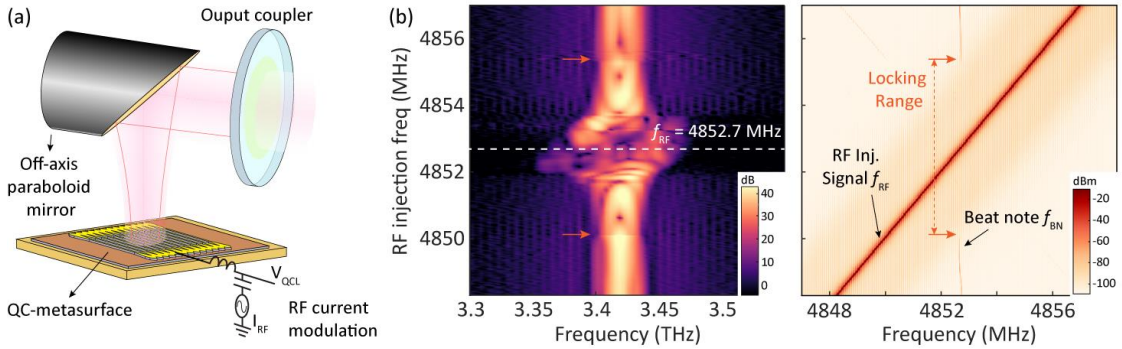

Figure 1. (a) Schematic of the QC-VECSEL based on an intra-cryostat focusing cavity design. (b) Lasing spectral broadening is observed under constant RF power of 20 dBm. The corresponding beat note map shows beat note locking to the injected RF signal with the estimated locking range pointed out by the red arrows.

THz Quantum Photodetector based on LO-phonon scattering-assisted extraction

J. Pérez Urquizo,[1] Z.Z. Zhang,[2] J.C. Cao,[2] D. Gacemi,[1] A. Vasanelli,[1] C. Sirtori,[1] H. Li,[2] Y. Todorov [1]

[1] *Laboratoire de Physique de l'École Normale Supérieure ENS, Université PSL, CNRS, Sorbonne Université, Université de Paris, F-75005 Paris, France*

[2] *Key Laboratory of Terahertz Solid State Technology, Shanghai Institute of Microsystem and Information Technology, Chinese Academy of Sciences, 865 Changning Road, Shanghai 200050, China*

The use of the LO-phonon scattering mechanism has proven effective to enhance electron transfer between quantum wells in diverse intersubband devices, such as Mid IR QCDs [1] and Mid IR and THz QCLs [2,3]. In this work we present a THz quantum detector based on GaAs/$Al_{0.25}Ga_{0.75}As$ heterostructure which is designed to exploit LO phonon scattering as an extraction mechanism for photoexcited electrons. As shown in Figure 1a) the absorbing quantum well has an intersubband transition of 15.5 meV. When an electric field is applied, a miniband is formed in the subsequent quantum wells, the edge of which is aligned resonantly with the first subband of the next period's absorbing quantum well, exhibiting a transition at roughly the LO phonon energy in GaAs E_{LO}= 37 meV. Spectral-resolved measurements were performed on samples processed into arrays of patch microcavities [4]. Figure 1 b) shows the responsivity spectrum of the device taken at 20 K exhibiting a peak response at 3.5 THz with a maximum value of 80 mA/W. This type of quantum detectors allows exploiting the degrees of freedom of quantum confinement for a constant Al content.

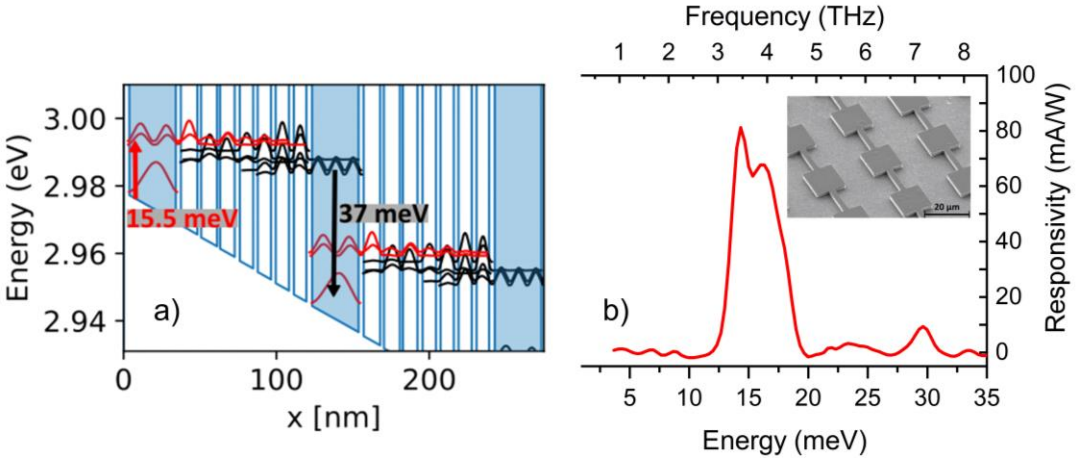

Figure 1 a) Conduction band profile of the device based on a GaAs/$Al_{0.25}Ga_{0.75}As$ system, under an electric field of $F = -2.8$ kV/cm. Two complete periods are displayed, each of them starting with an active quantum well which is highlighted in blue. b) Responsivity spectrum of the device taken at 20 K. Inset: SEM image of a section of a patch microcavity array.

[1] F. R. Giorgetta, et al. IEEE J. Quantum Electron. Vol. 45, no. 8 (2009).
[2] M. Beck, et al. Science. 295,5553 (2001).
[3] B.S. Williams, et al. Appl. Phys. Lett. 82, 1015-1017 (2003).
[4] Y. Todorov et al. Opt. Express 18, 13886-13907 (2010).

+ Author for correspondence: joel.perez-urquizo@phys.ens.fr

Multi-Octave THz Wave Generation in PNPA Crystal at MHz Repetition Rates

L. A. Sterczewski,[1,+] J. Mnich,[1] and J. Sotor[1]
[1]*Faculty of Electronics, Photonics and Microsystems, Wroclaw University of Science and Technology, Wyb. Wyspianskiego 27, 50-370 Wroclaw, Poland*

Terahertz (THz) wave generation using organic nonlinear optical (NLO) crystals has received considerable attention in the past decades as a viable method to convert broadband near-infrared radiation to the far-infrared region. Nowadays, the rapid development of fiber laser oscillators at telecom wavelengths creates a demand for novel NLO crystals optimized for longer-wavelength excitation and lower pulse energy compared to conventional solutions optimized for millijoule-level pulses with kHz repetition rates at near-visible wavelengths. This requirement is partially addressed by well-established NLO materials like DAST, DSTMS, or OH-1. However, further improvements in terms of conversion efficiency are still desired. Very recently, PNPA ((E)-4-((4-nitrobenzylidene)amino)-*N*-phenylaniline) has been identified as a potential candidate to address this need. Spectra in the 0.2–5 THz range have been obtained using mJ-level 100 fs long pump pulses with kHz repetition rates, yet lower-energy MHz-rate excitation has not been tested to date. In this work, we demonstrate multi-octave THz generation from PNPA pumped by a simple all-fiber femtosecond laser providing 17 fs pulses at a 1550 nm wavelength with 50 MHz repetition rate (4 nJ pulse energy). Increasing the repetition rate 5×10^4 times accompanied by a 5-fold decrease in the pulse duration grants us access to the longwave infrared and THz region from 10 μm of wavelength (30 THz) to 300 μm (1 THz). Using the THz-induced lensing technique we optically sample the emitted field as shown in Fig. 1a. Without purging the measurement chamber, persistent oscillations of water molecules persist over tens of picoseconds, which appear as sharp absorption dips in the spectrum (Fig. 1b). We will discuss the time-frequency characteristics of the waveform and compare them with other well-established THz emitters like DSTMS.

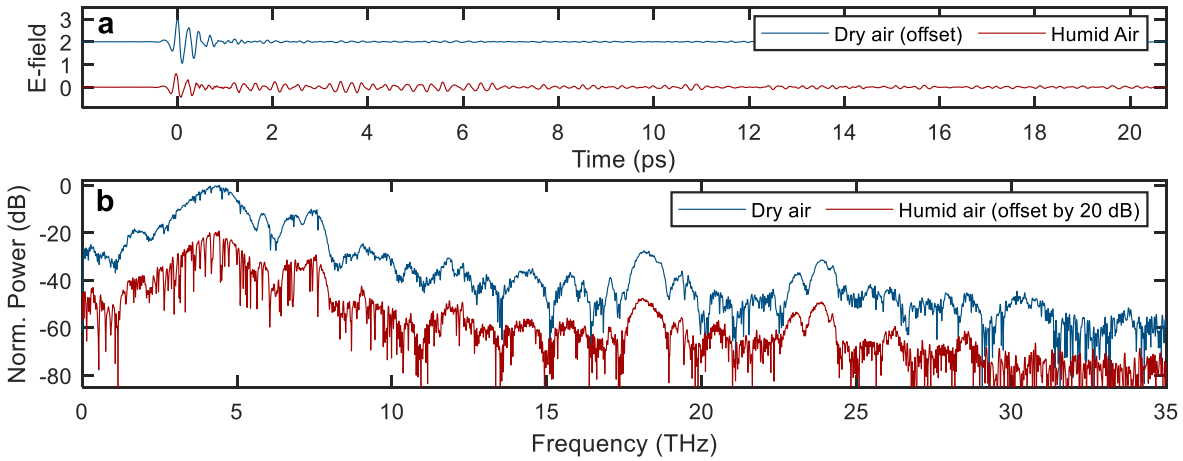

Fig. 1. Broadband THz generation from the PNPA crystal. (a) Sampled *E*-field. (b) Optical spectra obtained by Fourier-transforming the time-domain *E*-field waveforms.

[1] C. Rader et al., ACS Photonics **9**, 3720 (2022).

[+] Author for correspondence: lukasz.sterczewski@pwr.edu.pl; Funding from the European Union's Horizon 2020 research and innovation programme under the Marie Sklodowska-Curie grant agreement No 101027721.

Supplementary Pages (Optional)

A time-frequency analysis (spectrogram) of the *E*-field emitted by the PNPA crystal is shown in Fig. S1. Interestingly, the emitted waveform is highly chirped – low frequency components are generated first. Next, the longwave infrared part (i.e. between 10–30 THz / 30–10 μm) appears in the emission spectrum, yet it persists for only ~2 picoseconds. This resembles earlier observations of organic nonlinear optical crystals, whose longwave infrared (LWIR) emission features correspond to a different generation mechanism than simple optical rectification [S1]. The high-frequency components are potentially attributable to molecular vibrations with picosecond-level dynamics that produce coherent infrared emission.

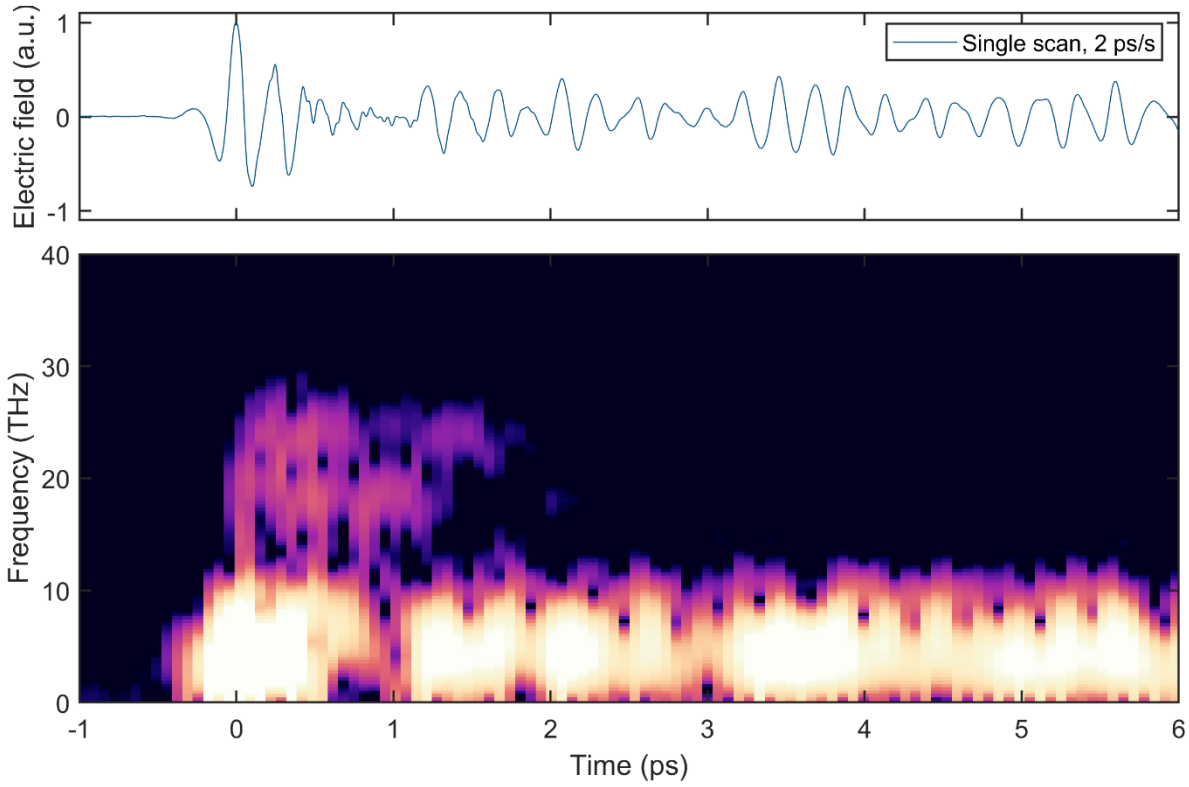

Fig. S1. Time-frequency analysis of the *E*-field waveform generated by the PNPA crystal pumped by a 17-fs 1550 nm laser.

Supplementary references

[S1] C. Somma, G. Folpini, J. Gupta, K. Reimann, M. Woerner, and T. Elsaesser, Ultra-Broadband Terahertz Pulses Generated in the Organic Crystal DSTMS, Opt. Lett. **40**, 3404 (2015).

Low Threshold Long Wavelength Interband Cascade Lasers

Jeremy A. Massengale,[1] Y. Shen,[1] Rui Q. Yang,[1,+] S. D. Hawkins,[2] A. J. Muhowski[2]
[1]School of Electrical and Computer Engineering, University of Oklahoma, Norman, OK.
[2]Sandia National Laboratories, PO Box 5800, Albuquerque, NM 87185-1085, USA

Interband cascade lasers (ICLs) [1-2] employ type-II quantum wells (QWs) as the active region and can cover a wide range of mid-IR spectrum with high performance especially in wavelength range from 3 μm to about 6 μm [2-4]. In this work, we report significant improvements in long wavelength ICLs in terms of reduced threshold current density J_{th} and voltage V_{th} compared to previous ICLs [5]. For example, in cw operation, the J_{th} at 80 K is below 9 A/cm^2 with output power exceeding 100 mW/facet and with a lasing wavelength near 10.7 μm close to 140 K as shown in Fig.1. Such a low J_{th} indicates a weak SRH recombination, suggesting a good material quality. The threshold voltage V_{th} at 80K is 3.61 V with a voltage efficiency of 73%, which is quite high considering that the photon energy (126meV) is low at such a long wavelength (9.83 μm at 80 K). ICLs from another wafer EB7910 lased at a longer wavelength in cw mode near 11.4 μm at 80 K with a J_{th} of 24.9 A/cm^2 and V_{th} of 3.95 V, corresponding a voltage efficiency of about 55%. These ICLs were able to operate at wavelengths exceeding 12 μm in pulsed mode at 135 K as shown in Fig. 2, the longest ever reported for ICLs with standard W-shape QW active regions. Detailed results will be presented at the conference.

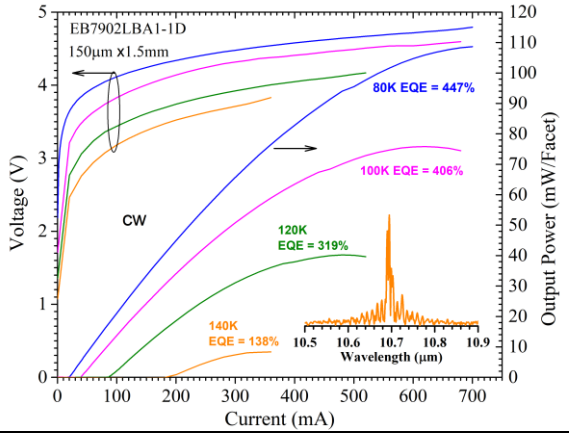

Fig. 1 IVL and a spectrum of an ICL from EB7902.

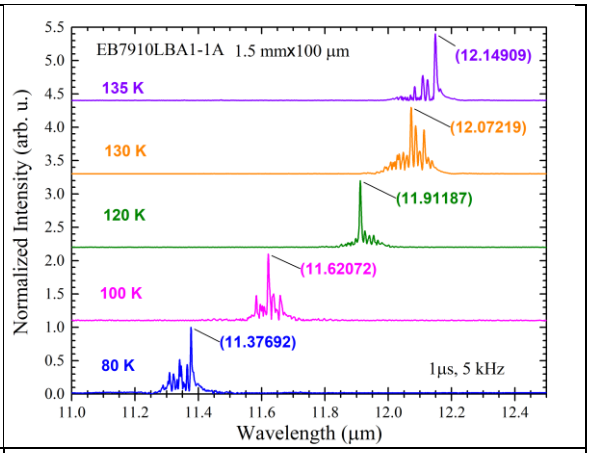

Fig. 2. pulsed lasing spectra of ICL from EB7910.

This work at OU was partially supported by NSF (No. ECCS-1931193), and was performed, in part, at the Center for Integrated Nanotechnologies, an Office of Science User Facility operated for the U.S. Department of Energy (DOE) Office of Science. SNL is managed and operated by NTESS under DOE NNSA contract DE-NA0003525.

[1] R. Q. Yang, Superlattices Microstruct., **17**, 77 (1995).
[2] J. R. Meyer, *et al*., Photonics **7**, 75 (2020)
[3] R. Q. Yang, *et al*. IEEE J. Sel. Top. Quantum Electron. **25**, 1200108 (2019).
[4] J. Nauschutz, *et al*., Laser & Photonics Reviews, 2200587 (2023).
[5] J. A. Massengale, *et al*., Semicond. Sci. Technol. **38**, 025009 (2023).

[+] Author for correspondence: Rui.q.Yang@ou.edu

Progress in Terahertz Quantum Cascade Lasers supporting clean n-level systems.

Nathalie Lander Gower[1], Shiran Levy[1], Silvia Piperno[1], Sadhvikas J. Addamane[2], John L. Reno[2], Asaf Albo[1, a)]

[1] *Faculty of Engineering, Bar-Ilan University, Ramat Gan 5290002, Israel.*

[2] *Center for Integrated Nanotechnologies, Sandia National Laboratories, MS 1303, Albuquerque, New Mexico 87185-1303, USA*

Although Terahertz Quantum Cascade Lasers (THz-QCLs) have a lot of potential, since they were first demonstrated in 2002, their use has been restricted due to lack of portability due to the requirements of cooling machinery. Therefore, raising the T_{max} is the main goal in the field. In 2021, a new T_{max} of ~250 K was achieved and demonstrated [1], enabling the launch of the first high-power portable THz-QCL. Although portable, this device, still required thermoelectric cooling, and the T_{max} was reached in pulsed operation. Moreover, up to date, other groups did not report similar T_{max} values, indicating how big of a challenge this represents.

The design that reached the T_{max} of ~250 K [1] is a two-well (TW) design supporting a clean three-level system (meaning the electron transport occurs only within the laser´s active subbands and all thermally activated leakage paths for electrons were suppressed). This design is like the design demonstrated beforehand with small variations (Design HB2 in Ref. [2]), and it is not the only design with a clean n-level system. Other designs that showed to have successfully suppressed thermally activated leakage channels are a resonant-phonon design presented in 2016 [3], and a split-well direct-phonon (SWDP) proposed in 2019 [4]. However, it is not clear why designs with very similar characteristics show very different T_{max} values, hence, the investigation is still ongoing.

Within our study, we suggest two other novel designs with clean n-level system. The first one is a highly diagonal split-well resonant-phonon (SWRP) scheme [5] and the second is a two-well injector direct-phonon (TWI-DP) scheme. Just as the structures mentioned earlier, both these new designs support clean 4-level systems.

The focus of the research we are presenting is on investigating these designs and comparing their device performance with other designs supporting clean n-level systems. Considering that THz-QCL designs supporting clean n-level systems are not limited by thermal leakage, a detailed comparison of their temperature performance should be the key for improvements beyond the state-of-the-art.

[1] A. Khalatpour, A. K. Paulsen, C. Deimert, Z. R. Wasilewski, and Q. Hu, 'High-power portable terahertz laser systems', *Nat. Photonics*, Nov. 2020, doi: 10.1038/s41566-020-00707-5.

[2] A. Albo, Y. V. Flores, Q. Hu, and J. L. Reno, 'Two-well terahertz quantum cascade lasers with suppressed carrier leakage', *Appl. Phys. Lett.*, vol. 111, no. 11, p. 111107, 2017, doi: 10.1063/1.4996567.

[3] A. Albo, Q. Hu, and J. L. Reno, 'Room temperature negative differential resistance in terahertz quantum cascade laser structures', *Appl. Phys. Lett.*, vol. 109, no. 8, p. 081102, 2016, doi: 10.1063/1.4961617.

[4] A. Albo, Y. V. Flores, Q. Hu, and J. L. Reno, 'Split-well direct-phonon terahertz quantum cascade lasers', *Appl. Phys. Lett.*, vol. 114, no. 19, p. 191102, 2019, doi: 10.1063/1.5089854.

[5] S. Levy, N. Lander Gower, S. Piperno, S. J. Addamane, J. L. Reno, A. Albo," Split-well resonant-phonon terahertz quantum cascade laser", Submitted (2023).

[+] Author for correspondence: *asafalbo@gmail.com*

Supplementary Pages

To keep improving the temperature performance of THz-QCLs, we need to better understand the physics and obstacles that were overcome over the years to reach the developments that led to the T_{max} of ~250 K [1].

The thermally activated longitudinal optical (LO) phonon scattering from the upper lasing level (ULL) to the lower lasing level (LLL) is the main mechanism that limits the operation temperature of standard vertical-transition THz-QCLs [2]. This limitation was overcome by designing highly diagonal structures, which significantly reduce thermally activated LO phonon scattering [3, 4]. In highly diagonal THz-QCLs structures the main mechanism observed to limit the temperature performance, is the thermally activated leakage into the continuum [4], mainly when using barriers containing just 15% Al. Thermally activated leakage of charged carriers into excited bound states [5, 6] also proved to be harmful for the temperature performance, even with barriers containing 30% Al. Combining high barriers with thin wells proved to push the excited and continuum states to higher energies and suppress these leakage paths [6-8]. Carefully engineered devices, showed clear negative differential resistance (NDR) behavior in the current voltage (I-V) curves all the way up to room temperature [6–8]. A clear NDR region means that the electron transport occurs only within the laser´s active subbands, meaning all thermally activated leakage paths for electrons were suppressed. This way, a clean n-level system was obtained, n being the number of the laser's active subbands [6–8]. Taking this into account, the strategy has been to design THz-QCLs that have as close as possible to clean n-level systems, especially at elevated temperatures. This strategy of achieving a clean n-level system, led to the highest recorded T_{max} [1] and this is the strategy used in our research as well.

The design that reached the T_{max} of ~250 K [1] is a two-well (TW) design supporting a clean three-level system, like the design demonstrated beforehand with small variations (Design HB2 in Ref. [7]), and it is not the only design with a clean n-level system. Other designs that showed to have successfully suppressed thermally activated leakage channels are a resonant-phonon design presented in 2016 [5], and a split-well direct-phonon (SWDP) proposed in 2019 [8]. However, it is not clear why designs with very similar characteristics show very different T_{max} values, hence, the investigation is still ongoing.

Here, we suggest two other novel designs with clean n-level system. The first one is a highly diagonal split-well resonant-phonon (SWRP) scheme (Fig.1a) [9], based on the same design principles as the split-well direct-phonon (SWDP) design previously described in Refs. [8-10]. However, in the SWDP device there is a high overlap between the doped region and the active laser states [10] and in the new SWRP design, this overlap is reduced, and effects related to gain broadening should be lower. The second design is a two-well injector direct-phonon (TWI-DP) structure (Fig.2a), which combines both two-well injector and direct-phonon scattering schemes. The TWI-DP design keeps the direct-phonon scheme for the depopulation of the lower laser level (LLL), while overcoming its main disadvantages, such as the large overlap between the doped and active laser regions. Just as the structures mentioned earlier, both these new designs support clean 4-level systems, as shown by the NDR signature in their I-V curves all the way up to room temperature (Fig.1b and Fig.2b respectively).

The focus of the research we are presenting is on investigating these designs and comparing their device performance with other designs supporting clean n-level systems. Considering that THz-QCL designs supporting clean n-level systems are not limited by thermal leakage,

Improving Transverse Mode Quality of QCLS with Novel Waveguides

M. Suttinger,[1] R. Go,[1] C. Lu[1]
[1] *Air Force Research Laboratory, 3550 Aberdeen Ave SE, Kirtland AFB, NM 87117*

Quantum Cascade Lasers (QCLs) are reaching a level of commercial maturity. With multiple watts of CW power available from a single QCL source with near transform limited ("fundamental mode-like") beam quality. This beam quality is achievable due to the standard configuration of the QCL waveguide, with an laser core having transverse dimensions of 1-2 µm X 8-12 µm relative to the 4-5 µm wavelengths produced by higher power Midwave infrared (MWIR) devices. However, remaining with this form factor will limit the amount of available power produced by the laser, as the longitudinal extent of the waveguide cannot be indefinitely extended without issue. Multiple geometries have been explored to expand the total achievable power of single emitter beyond that of the narrow Fabry-Perot cavity, most immediately available being the broad area QCL. In this presentation, results of novel QCL waveguides fabricated at Air Force Research Laboratory are discussed.

In the "ultrawide" Fabry-Perot waveguide, extremely wide laser cores exceeding the standard configuration width by an order of magnitude allow for the scaling of average power, but with severely reduced and divergent beam quality. Through a modification of waveguide to bring the waveguide mode closer to the electrical contact, and splitting said contact into a Dual Contact Strip, the mode quality can be rectified to fundamental-like behavior.

Another approach to improving mode quality relative to the Fabry-Perot geometry is through an angled cavity waveguide. On its own, an angled cavity with a severe enough tilt may induce improved transverse mode quality, but at the expense of overall power potential through losses induced by sidewall interaction. A similar effect may be achieved by using a less pronounced angle and interrupting the waveguide with "notches" etched out of areas far from the internal beam path of the fundamental mode. This allows losses to preferentially disrupt higher order modes. Power can then be scaled by overlapping multiple angled cavities to produce a coherent array with an output beam envelope reflected by that of the output of its components in isolation.

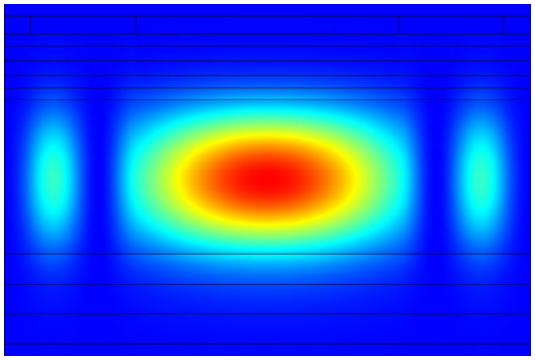

Figure 1 Simulated mode of an ultrawide QCL with Dual Contact Strip geometry.

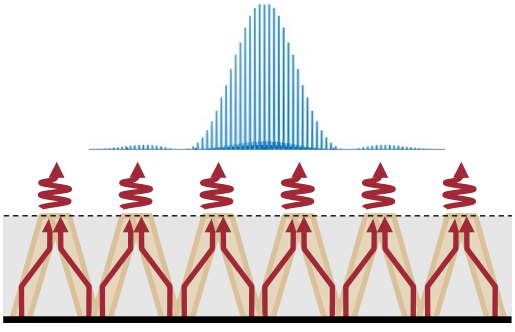

Figure 2 An overlapped angled cavity array with simulated far field.

Broadly Tunable Single Spatial Mode Quantum Cascade Lasers in an External Cavity

B. Knipfer,[1] D. Ruiz,[1] S. Ruder,[1] K. Oresick,[1] D. Caffey,[1] M. Klaus,[1] C. Galstad,[1] M. Dwyer,[1] and T. Earles[1]
[1] DRS Daylight Solutions

Broadly tunable laser sources spanning mid- to long-wave IR are highly sought after for their ability to characterize materials with non-destructive spectroscopy techniques. The wavelengths of interest typically span 3-13 µm, or approximately 2500 cm^{-1}. Given such a large spectrum window finding materials adequately suited can be a challenge, however, given the scalability of MOCVD growth, and the wavelength agility of quantum cascade lasers, MOCVD-grown QCLs fill this niche perfectly.

Previous work has shown heterogeneous quantum cascade lasers emitting in the LWIR that span, up to 760 cm^{-1}, however, at relatively low pulsed powers and in a double-channel ridge configuration [1]. We have previously reported on tuning capabilities within an external cavity in the 4.0-4.8 µm regime [2] and here we push wavelengths across the MW- to LWIR while optimizing CW and pulsed powers with superb beam pointing stability.

This work shows advances in the tuning capabilities of single-core and heterogeneous quantum cascade structures within an external cavity. Previous state-of-the-art products would use four QCL chips to cover 1000 cm^{-1}, but here we are able to further expand the tuning range of individual chips such that the same range can be covered by only three QCLs, shown in Figure 1. Typically, the expansion of tuning range is achieved by broadening the spectral gain through either broadening of a single core, the introduction of additional cores supporting different wavelengths, or both. These different methods typically correspond to a decrease in output power; however, we show this expansion is achieved while maintaining high single mode powers. Through optimization of the active region, a relatively flat modal gain can be achieved across the desired emission range.

These devices exemplify the ability of QCLs to span significant wavenumbers, at high pulsed and CW power levels while maintaining strong single spatial mode operation which has been verified through pointing stability measurements. Beam measurements show deviations of less than 100 µrad over the range of tuning under CW and pulsed operation.

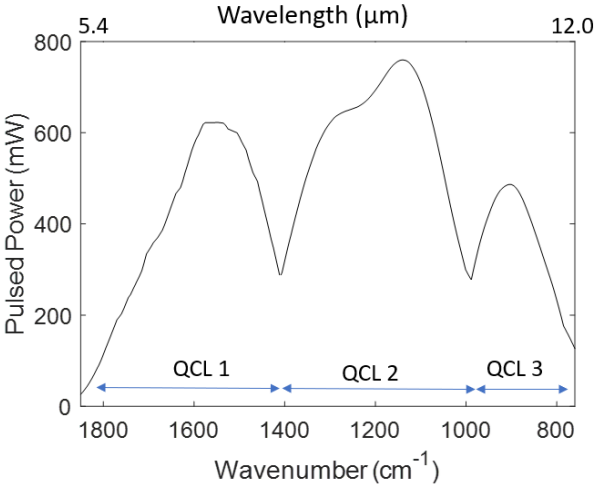

Figure 1 Three individual QCLs spanning > 1000 cm^{-1} wavenumbers under pulsed conditions

[1] D. Caffey et al. Proceeding of SPIE, (2011)
[2] N. Bandyopadhyay et al. Opt. Exp. Vol. 23, Iss. 16, pp. 21159-21164 (2015)

+ Author for correspondence: Benjamin.Knipfer@drs.com

Hybrid passive photonics in the longwave-infrared

Dingding Ren[1,2], Chao Dong[1], Sadhvikas Addamane[3], and David Burghoff[1]

[1] *Department of Electrical Engineering, University of Notre Dame, IN, United States*

[2] *Department of Electronic Systems, Norwegian University of S&T (NTNU), Norway*

[3] *Center for Integrated Nanotechnologies, Sandia National Lab, Albuquerque, NM, USA*

The development of passive low-loss material platforms is vital for advancing quantum and nonlinear photonics. Recently, mature nanophotonic platforms like Si_3N_4 and Si-on-insulator have emerged in the near- and midwave-infrared. These platforms have enabled the creation of a wide range of devices that exploit nonlinear effects, including frequency comb generation, supercontinuum generation, quantum frequency conversion, and generation of entangled biphotons. However, none of these platforms are suitable for the longwave-infrared (6 to 14 μm), as most optical materials become too lossy.

Recent advances in low-loss longwave-infrared photonic platforms, such as diamond[1], chalcogenide glasses[2], and germanium[3], have now made it possible to explore novel applications of nonlinear photonics. In this talk, we will discuss our recent work on the development of low-loss platforms based on hybrid photonic integration[3] and will outline a roadmap for novel nonlinear photonic devices using similar schemes. Hybrid approaches could enable novel sensing modalities using supercontinuum and frequency comb technology, with significant implications for chemical and biological sensing, healthcare, and environmental monitoring.

In particular, we will highlight our work demonstrating ultra-high-quality factor microresonators based on Ge-on-glass. By coupling the output of a quantum cascade laser (QCL) into a partially suspended Ge-on-glass waveguide and coupling it into a waveguide, we demonstrate resonators with an intrinsic quality factor of 2.5×10^5, approximately two orders of magnitude better than the prior state-of-the-art. In addition, we will discuss our more recent results demonstrating that the same approach can be used to create fully-integrated Ge-on-ZnSe waveguides with losses nearly as low. Our results demonstrate the importance and potential of using high-quality native materials for passive photonics in the longwave infrared range and will allow for a number of new device topologies.

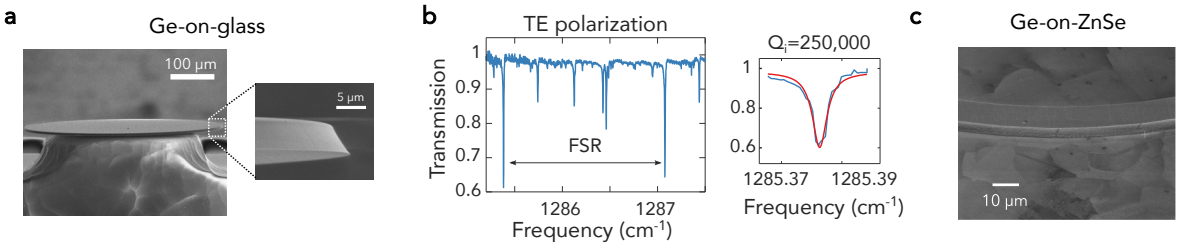

Figure 1. a. Ultra-low-loss microdisks based on a Ge-on-glass platform. By relying on native materials and mechanical processing rather than material growth, microresonators can be fabricated with losses lower than epitaxially-grown Ge and III-V materials. b. Transmission scan of a resonance, demonstrating the first clear resonances in the LWIR. c. Fully integrated hybrid Ge-on-ZnSe platform.

[1] Y.-J. Lee et al., Opt. Express **28**, 5448 (2020).

[2] B. Gholipour et al., J. Phys. Photonics **5**, 012501 (2023).

[3] D. Ren et al., Nat. Commun. **13**, 5727 (2022).

[+] Author for correspondence: dburghoff@nd.edu

Modeling of GaSb-Based Monolithically Integrated Passive Photonic Devices at λ > 2 μm

M.S.I. Sumon[1], S. Sankar[1], S.S.S. Nikor[1], W. You[1], I.I. Faruque[2], S. Dwivedi[3], S. Arafin[1,*]

[1]Department of ECE, The Ohio State University, Columbus, Ohio 43210, USA
[2] QET Labs, University of Bristol, BS8 1TL Bristol, U.K.
[3]Rockley Photonics, Pasadena, CA 91101, USA

Photonic integrated circuits for the extended short and mid-wave infrared (eS-MWIR) wavelength regime are crucial for potential applications including on-chip chemical and biological sensing and non-invasive medical diagnosis. The lack of high-performance lasers on an SOI wafer and material limitations in InP necessitate an alternative material system. A monolithic platform based on GaSb addresses these concerns through the tight integration of both passive and active components since it is an optimal material system for realizing long-wavelength lasers and photodetectors. In this work, we modeled and optimized various fabrication-compatible passive components including 1×2 power splitters/combiners based on directional coupler (DC), multimode interferometer (MMI), and Y-branch as well as a grating coupler on GaSb substrates at 2.56 μm.

Surface ridge waveguides designed on GaSb-based epitaxial layers are schematically shown in Figure 1(a). Figure 1(b) shows the effective refractive indices n_{eff}, of a few lowest-order guided modes as a function of the ridge width W, and the inset shows the mode profile of TE_0 at W = 4 μm. Figure 1(c) shows the transmission through the two output ports of DC-, MMI-, and Y-branch- splitters with 1-dB bandwidth, $\Delta\lambda \sim 1$ μm at a center wavelength of 2.56 μm. For all the splitters, we achieve 50:50 power splitting with an excess loss lower than 0.12 dB. For the grating coupler, a coupling efficiency of -5.4 dB and a 3-dB bandwidth of 80 nm are achieved at 2.56 μm. Details of the design and simulation results of all these passive photonic devices will be presented at the conference.

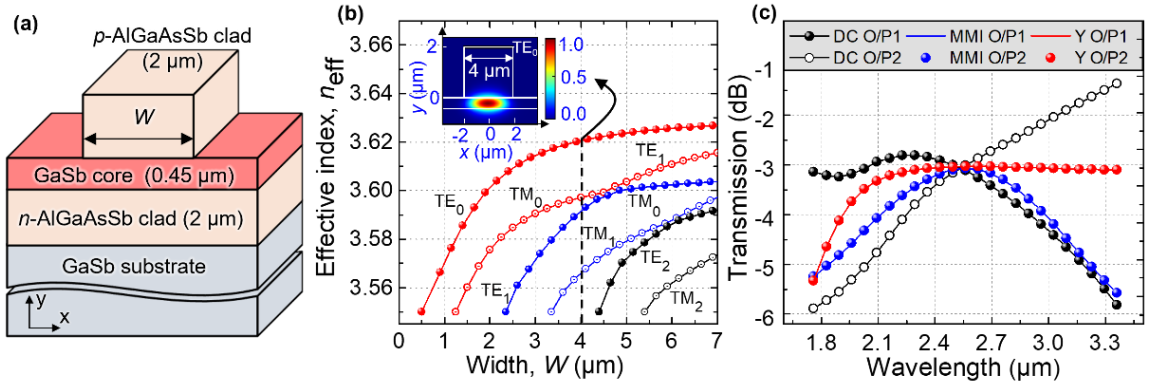

Figure 1. (a) Schematic cross-section of the GaSb-based single-mode surface ridge waveguide, (b) mode effective index as a function of waveguide width, W. Inset: fundamental TE_0 mode at 2.56 μm, and (c) transmission through the two output ports of DC (black), MMI (blue), and Y-branch (red) at a center wavelength of 2.56 μm.

* Author for correspondence: arafin.1@osu.edu

Supplementary Pages

Figure 1(b): Up to a width of 2.4 μm, the waveguide supports only single TE modes. However, in experiments, devices with wider widths are found to emit a single fundamental mode. The first higher-order odd mode TE_1 in a laser cavity receives very little gain due to a null at the waveguide center and is not usually considered while defining the single-mode waveguide cut-off condition [1]. TM modes were also not considered since the III-V laser structure employs compressively strained quantum wells which favor only TE-polarized light. Thus, the calculated ridge width supporting single mode is 4.4 μm, as represented by the vertical dashed line.

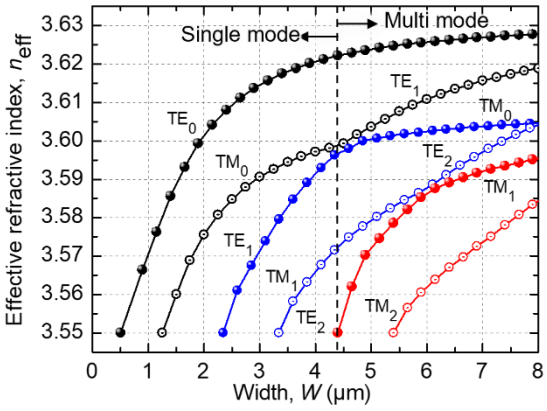

[1] Arafin, Shamsul, Alexander Bachmann, and Markus-Christian Amann. "Transverse-mode characteristics of GaSb-based VCSELs with buried-tunnel junctions." IEEE Journal of Selected Topics in Quantum Electronics 17.6 (2011): 1576-1583.

Acknowledgments

This work was supported by the National Science Foundation (NSF) under Grant 2144375.

GaSb-based ICLs grown on GaSb, GaAs and Si substrates

M. Fagot, D. Díaz-Thomas, A. Gilbert, G. Ndemengoye, Y. Rouillard, A.N. Baranov, J.B. Rodriguez, E. Tournié and L. Cerutti[+]

IES, Univ. Montpellier, CNRS, 34000 Montpellier, France.

GaSb-based Interband Cascade lasers (ICLs) have emerged as the leading optoelectronic source in the 3-6 µm wavelength range **[1]**. Although ICLs are very attractive for various applications such as laser spectroscopy or free-space communication, the cost and size of substrates pose a significant limitation to their widespread commercialization. However, recent studies have shown that the unique band diagram of the ICLs active zone, is tolerant to mid-gap defect states induced by dislocations [2]. Thus, the growth of ICLs on large, inexpensive, and mismatched substrates presents a viable solution for the low-cost production of high-performance mid-infrared (MIR) lasers and MIR photonic sensors on GaAs or Si-photonic integrated circuits (PIC).

In this study, we have examined the performance of ICLs designed to emit at 3.3 µm, which were grown simultaneously on GaSb, GaAs, and on-axis Si (001) substrates. The ICL structures consisted of two n-type AlSb/InAs superlattice claddings and a 5-stage interband cascade active region sandwiched between two n-type GaSb separate confinement layers. After the growth, the structures were processed into 8 µm x 2 mm laser devices and bonded epi-side up, with the bottom contact taken into the bottom cladding.

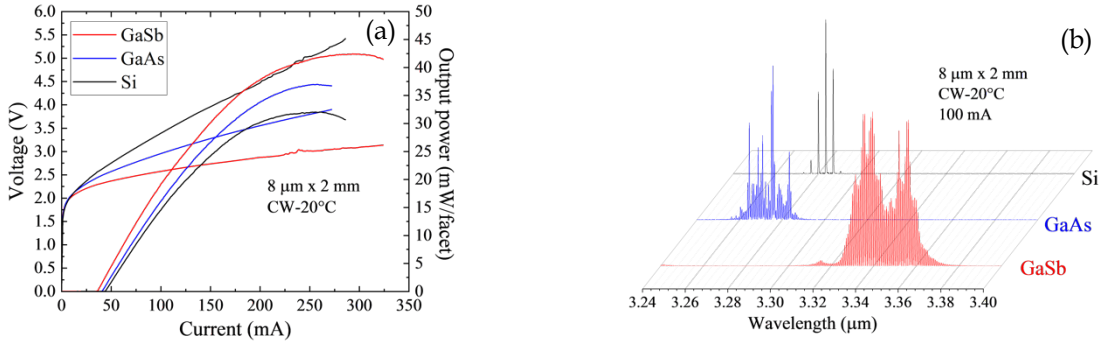

Figure 1: P-I-V (a) and spectra (b) of ICLs grown on GaSb, GaAs and Si measured in CW at 20°C

All the lasers operated in the continuous wave (CW) regime at RT and emitted around 3.3 µm (Fig.1). The threshold current is approximately 40 mA whereas the maximum output power decreased from 42 mW for the lasers on GaSb to 37 and 32 mW for the devices on GaAs and Si substrates, respectively (Fig.1). We attribute the observed decrease in the optical power to a higher voltage drop which results in overheating of the active region. The higher series resistance in these devices can be explained by poorer lateral electrical conductivity of the cladding in presence of threading misfit dislocations in the mismatched structures. These encouraging results open the way to the development of low cost ICLs and integrated photonic sensors for PIC.

[1] J. R. Meyer et al., Photonics. **7**, 75, p. 2-58 (2020).
[2] L. Cerutti et al., Optica. **8**, 11, 1397 (2021).

This work was partially supported by the French "Investment for the Future" program (EquipEx EXTRA, ANR-11-EQPX-0016), the French Occitanie Region (LASIDO project) and the French Agency for Defense and Innovation (AID-DGA).

[+] Author for correspondence: laurent.cerutti@umontpellier.fr

Electrically injected GeSn laser on Si substrate operating up to 130 K.

S. Acharya,[1] S. Ojo,[1] Y.Zhou[2], S. Amoah[2], W.Du[2], B. Li[3] ,S. Yu[1,2]

[1] Material Science and Engineering, University of Arkansas, Fayetteville, Arkansas 72701 USA

[2]Department of Electrical Engineering, University of Arkansas, Fayetteville, Arkansas 72701 USA

[3]Arktonics, LLC, 1339 South Pinnacle Drive, Fayetteville, AR, USA 72701

Germanium-tin (GeSn) semiconductors have gained significant attention over the last years as a group IV material for the development of novel Si-based optoelectronic devices. Specifically, direct band gap GeSn alloys with Sn fractions above 8% are of interest as light emitting sources in the near- and mid-infrared spectral range. In addition, GeSn epitaxy is monolithic on Si and also fully compatible with the complementary metal-oxide semiconductor (CMOS) technology, making it a promising candidate for the integrated light source on the Si platform, with advantages such as cost-effectiveness, reliability, and compactness [2]. Recently, GeSn lasers on Si substrate were demonstrated both under optical pumping and electrical injection. In this work, we report an electrically injected GeSn/SiGeSn laser grown on Si substrate operating up to 130 K. Our study is mainly focused on the cap layer effect on the optical loss for lasing devices. The GeSn/SiGeSn heterostructure was grown using chemical vapor deposition (CVD) technique. The laser devices were fabricated in ridge waveguide structures with 80 µm, 100 µm and 120 µm wide ridges. The lasing performance was investigated under pulsed conditions. The electroluminescence signal was collected through a monochromator and liquid-nitrogen-cooled InSb detector (response range 1–5.5 µm). The L-I characteristics of devices with different cavity lengths were studied at different temperatures. Our results suggest pathways for enhancing the lasing performance of electrically injected GeSn laser diodes.

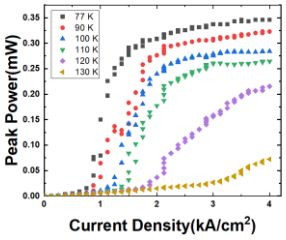

Figure1 Temperature dependent L-I curve.

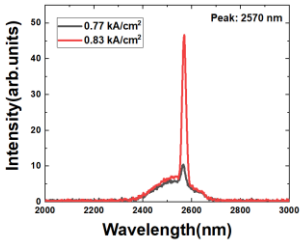

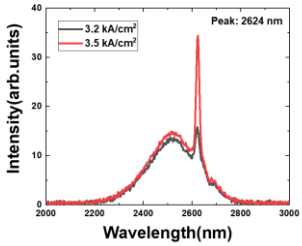

Figure 2(a, b) : Lasing spectra at and above threshold for 77K and 130 K temperature respectively

[1] Yiyin Zhou, Yuanhao Miao, Solomon Ojo, Huong Tran, Grey Abernathy, Joshua M. Grant, Sylvester Amoah, Gregory Salamo, Wei Du, Jifeng Liu, Joe Margetis, John Tolle, Yong-hang Zhang, Greg Sun, Richard A. Soref, Baohua Li, and Shui-Qing Yu, "Electrically injected GeSn lasers on Si operating up to 100 K," Optica 7, 924-928 (2020)

[2] Solomon Ojo, Yiyin Zhou, Sudip Acharya, Nicholas Saunders, Sylvester Amoah, Yue-Tong Jheng, Huong Tran, Wei Du, Guo-En Chang, Baohua Li, Shui-Qing Yu, "Silicon-based electrically injected GeSn lasers," Proc. SPIE 11995, Physics and Simulation of Optoelectronic Devices XXX, 119950B (4 March 2022); https://doi.org/10.1117/12.2615476

Temperature and Band Structure Dependent Properties of GeSn Double Heterostructure Lasers

A. R. Ellis,[1+] I. P. Marko,[1] D. A. Duffy[2], S. Ojo,[3] W. Du,[3] S.-Q. Yu,[3] S. J. Sweeney[1,2]
[1] James Watt School of Engineering, University of Glasgow, G12 8LT, United Kingdom
[2] ZiNIR Ltd., Eastbourne, BN22 7QP, United Kingdom
[3] Dept. Electrical Engineering, University of Arkansas, Fayetteville, Arkansas 72701, USA

The development of monolithically integrated group-IV lasers remains a key challenge in realising Si-based integrated optoelectronic circuits [1]. With its direct bandgap and the possibility for wavelength tuning through strain and composition engineering, GeSn has emerged as an interesting approach. However, GeSn lasers have been primarily limited to low temperature operation. Understanding the carrier recombination behavior is therefore vital to develop improved devices with higher operating temperatures. Here, we investigate bulk $Ge_{0.89}Sn_{0.11}$ lasers grown using chemical vapor deposition [2]. In this study, high pressure, low temperature measurements are used to vary the electronic band structure for a fixed thermal carrier distribution, enabling purely band structure dependent mechanisms to be probed. Analysis of the threshold current density with pressure indicates an L-valley occupation of ~1% at 85K, determined from the fit in Fig. 1 a). Above this temperature, the fractional L-valley occupation increases strongly, indicated by a sharp rise in the threshold carrier density (assuming only mirror losses), illustrated by the red line in Fig. 1 b). This increases the pump threshold leading to device heating, increasing the L-valley occupation further and heightening free carrier absorption losses. The implications for this in terms of optimising the laser design for ambient temperature operation will be discussed.

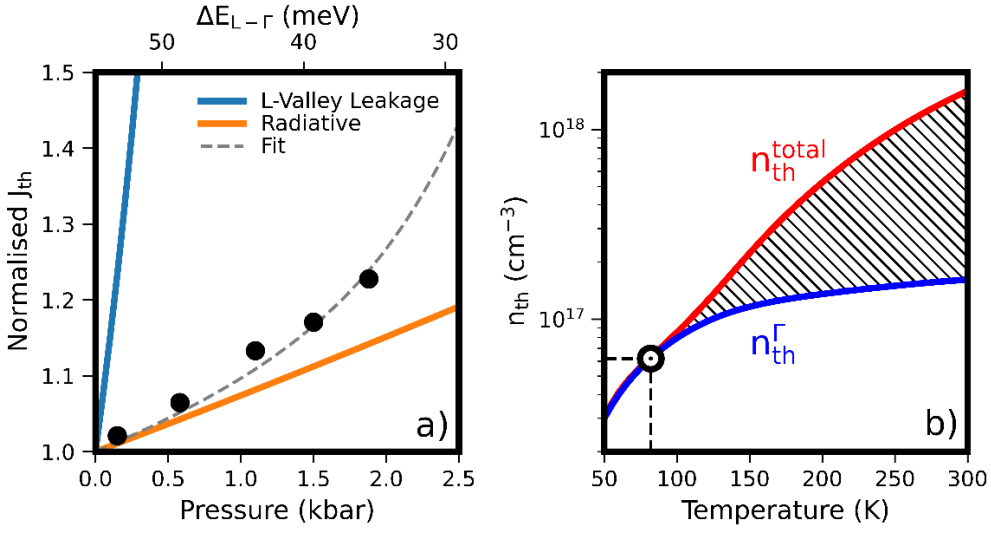

Figure 1. a) Normalised variation of threshold current density with pressure and **Γ**-L separation, $\boldsymbol{\Delta E_{L-\Gamma}}$, showing the effect of L-valley leakage. b) Increase in total threshold carrier density with temperature above the 80K break point due to enhanced fractional L-valley occupation.

[1] Wang, B. *et al.* *Light Sci Appl* **10**, 232 (2021).
[2] Zhou, Y. *et al.* Optica **7**, 924-928 (2020).

[+] Author for correspondence: a.ellis.1@research.gla.ac.uk

Integrating GaSb-based infrared detectors with Si substrates via interfacial misfit arrays

Trent A. Garrett,[1] Jacob A. Tenorio,[1] Madison Drake,[1] Pooja Reddy,[2] Kunal Mukherjee,[2] Kevin A. Grossklaus,[3] Shimon Maimon,[4] and Paul J. Simmonds[1, 5]

[1]Micron School of Materials Science & Engineering, Boise State University, ID 83725, USA
[2]Materials Science & Engineering, Stanford University, CA 93405, USA
[3]Department of Electrical and Computer Engineering, Tufts University, Medford, MA 02155, USA
[4]NetzVision LLC, Rochester, NY 14618, USA
[5]Department of Physics, Boise State University, ID 83725, USA

With applications from night vision and aerial target acquisition, to space telescope operation, infrared (IR) detectors are of great interest to the defense and scientific communities alike. The functionality of these detectors hinges on achieving a high signal-to-noise ratio so that weak signals can still be resolved. Of the many IR detector designs, the nBn device has emerged as a leading choice. As the name suggests, nBn detectors comprise an electron-blocking barrier between *n*-type absorber and contact layers [1]. nBn-based IR detectors are typically grown on GaSb substrates, which are expensive and only widely available up to 4–6" diameter. In addition, integrating a detector grown on a GaSb substrate with the Si-based ROIC via direct bonding interconnect processing is difficult. nBn detectors produced directly on Si substrates would overcome these problems. However, this approach comes with its own set of challenges, primarily due to the large lattice mismatch between GaSb and Si. We therefore adopt the use of interfacial misfit (IMF) arrays grown by molecular beam epitaxy (MBE) to manage strain at the III-Sb/Si heterointerface. IMFs consist of the spontaneous formation of a 2D array of 90º dislocations that lie in the plane of the heterointerface. Previous studies show that thin initiation AlSb layers between the GaSb and Si are critical. GaSb deposited onto an AlSb/Si IMF heterostructure has dramatically improved material quality and lower threading dislocation density (TDD) [2]. We will discuss how choices regarding AlSb growth initiation, substrate temperature, annealing, AlSb thickness, and AlSb growth rate affect the quality of GaSb overlayers. By optimizing these MBE growth parameters, initial results suggest that we can grow GaSb layers with quality comparable to the current state-of-the-art, giving us a benchmark against which to measure further improvements. We will discuss the performance of nBn devices integrated with our optimized GaSb-on-Si buffers. Promising initial results include background limited infrared photodetection (BLIP) at 150 K (Fig. 1), and the ability to carry out thermal imaging with a 300 K blackbody background. This work is supported by the Office of Naval Research through grant #N00014-21-1-2445 and by the National Science Foundation grant GRFP #1946726.

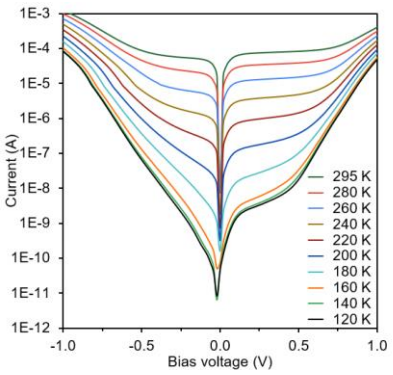

Figure 1: Temperature dependent IV curves for an nBn device on a Si(100) substrate. We see BLIP at 150 K, while 10× dark current decrease per 30 K of cooling indicates good material quality.

[1] S. Maimon and G.W. Wicks, Applied Physics Letters **89**, (2006).
[2] K. Akahane, N. Yamamoto, S.-I. Gozu, and N. Ohtani, Journal of Crystal Growth **264**, 21 (2004).

Supplementary Page

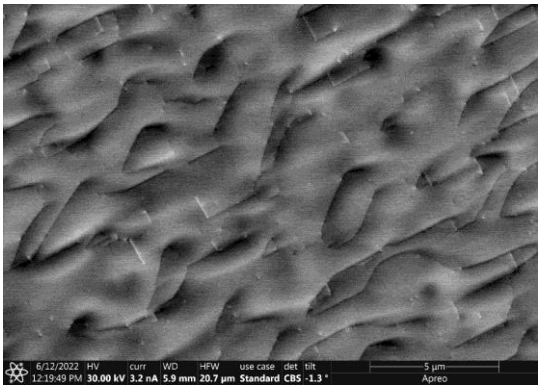

Figure 1 supp.: Electron channeling contrast imaging scan showing threading dislocations in a sample containing a dislocation filtering superlattice. For this sample we found TDD = 2.8×10^7 cm^{-2}

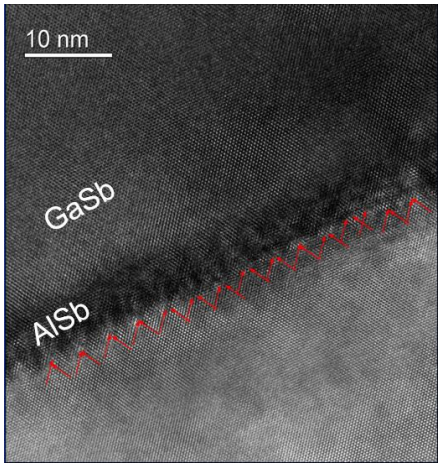

Figure 2 supp.: High resolution transmission electron microscopy image displaying the III-Sb/Si heterointerface where red arrows indicate the location of periodic misfit dislocations forming the IMF array.

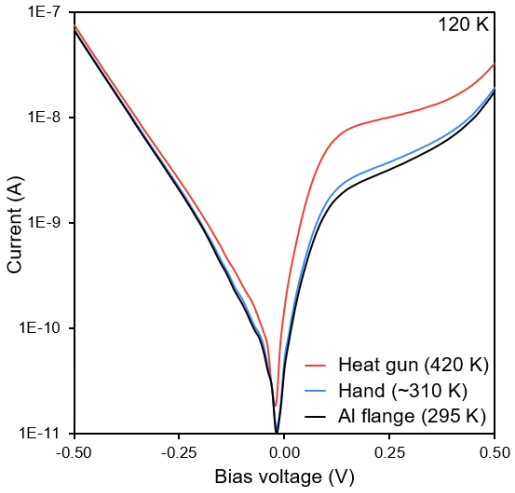

Figure 3 supp.: IV response at 120 K of a single-element nBn detector fabricated on a Si(100) substrate, to illumination with: a room temperature Al metal flange (~295 K, 10% emissivity), a hand at ~310 K (90% emissivity), and a heat-gun at ~420 K. Critically, the ability to distinguish the hand from the flange suggests we could use this device for thermal imaging with a 300 K blackbody background.

Interband Cascade Technology for Long Wavelength GaSb based Lasers and LEDs

R. Weih[1], J. Nauschütz[1], H. Knötig[2], N. Schäfer[1], B. Schwarz[2], J. Koeth[1]
[1] *nanoplus Advanced Photonics Gerbrunn GmbH, Oberer Kirschberg 4, Gerbrunn, Germany*
[2] *Institute of Solid State Electronics, TU Wien, Gusshausstrasse 25-25a, Vienna 1040, Austria*

Since the first demonstration of continuous wave operation [1] Interband Cascade Lasers (ICLs) have shown tremendous improvement in their performance. Not only cw operation up to a temperature of more than 100°C has been shown [2] but also the capability of the interband cascade concept to operate to wavelengths beyond 13µm [3]. Recently we demonstrated another design improvement which focusses on the mitigation of intervalence band absorption [4]. This in turn led to a significant improvement of laser performance in the wavelength region around 6 µm [5]. A spectrum and LIV characteristics of an epi down mounted laser are shown in Figure 1. Furthermore, the latest results on resonant cavity ICLEDs and long wavelength ICLEDs with emission um to 10.2µm will be shown.

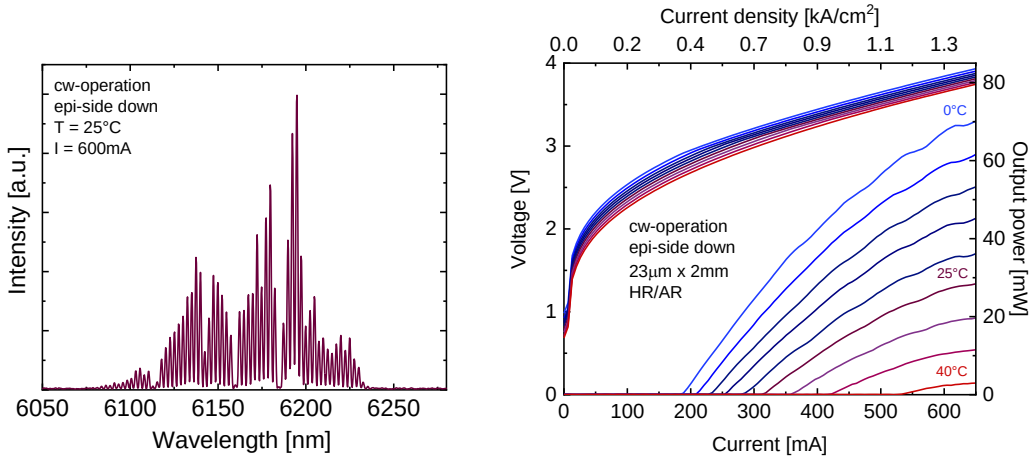

Figure1: Spectrum and LIV characteristics of an ICL operating beyond 6µm in cw.

[1] M. Kim, C. L. Canedy, W. W. Bewley, C. S. Kim, J. R. Lindle, J. Abell, I. Vurgaftman and J. R. Meyer, Appl. Phys. Lett. **92**, 191110 (2008).
[2] I. Vurgaftman, W.W. Bewley, C.L. Canedy, C.S. Kim, M. Kim, C.D. Merritt, J. Abell, J.R. Lindle and J.R. Meyer, Nat. Commun. **2:585** (2011).
[3] J. A Massengale, Y. Shen, R. Q. Yang1, S. D. Hawkins and J. F. Klem, Semicond. Sci. Technol. **38** (2023).
[4] H.Knötig, J. Nauschütz, N. Opacak, S. Höfling, J. Koeth, R. Weih, and B. Schwarz, Laser Photonics Rev. **2200156** (2022).
[5] J. Nauschütz, H. Knötig, R. Weih, J. Scheuermann, J. Koeth, S. Höfling and B. Schwarz, Laser Photonics Rev. **2200587** (2023).

+ Author for correspondence: robert.weih@nanoplus.com

Metamorphic growth of MWIR ICLED on Silicon

F. F. Ince,[1] T. J. Rotter,[1] M. Frost,[1] G. Balakrishnan,[1] M. R. McCartney,[2] D. J. Smith,[2] C. L. Canedy,[3] W. W. Bewley,[3] S. Tomasulo,[3] C. S. Kim,[3] M. Kim,[4] I. Vurgaftman,[2] and J. R. Meyer.[2]

[1] University of New Mexico, Albuquerque, NM 87108
[2] Department of Physics, Arizona State University, Tempe, AZ 85287
[3] U.S. Naval Research Laboratory, Washington, DC 20375
[4] Jacobs Corporation, Hanover, MD 21076, USA.

Interband cascade light emitting diodes (ICLEDs) grown on GaSb substrates have emerged as an effective continuous wave (CW) room temperature emitter technology in the 3 – 5 µm wavelength range [1,2]. The integration of ICLEDs directly on a silicon substrate can lead to significant benefits in manufacturability for applications including chemical sensing and IR scene projectors (IRSPs).

This presentation will discuss the growth at NRL of high performance ICLEDs on GaSb/Si buffers that were grown at UNM. The growths on GaSb *vs*. GaSb/Si are compared for crystallographic quality using cross section transmission electron microscopy (XTEM) and X-Ray reciprocal space maps (RSM). XTEM images show the presence of threading dislocations in the GaSb buffer grown on Si, with a higher density near the silicon substrate and reduced closer to the ICLED. We measure a range from 5×10^7 to 2×10^8 cm^2 in different samples. Individual threading dislocations in the GaSb buffer can reach the ICLED and multiply once they reach the active stages (figure 1). Another artifact of growth on silicon is an undulation in the ICLED layers. Our presentation will provide a detailed mechanism for both of these observations, and we will compare the results to those for an ICLED grown lattice-matched to a GaSb substrate (figure 2). We will also discuss possible strategies for improving the epitaxial quality and device performance.

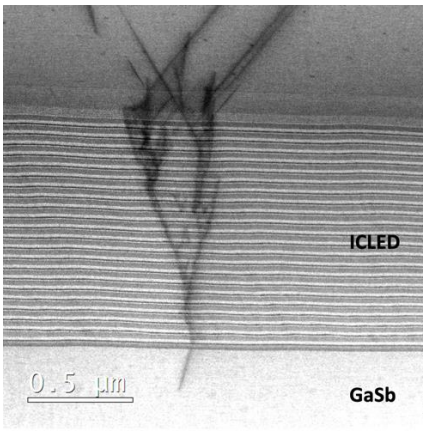

Figure 1 - Threading dislocation multiplication seen in an ICLED grown on GaSb/Silicon.

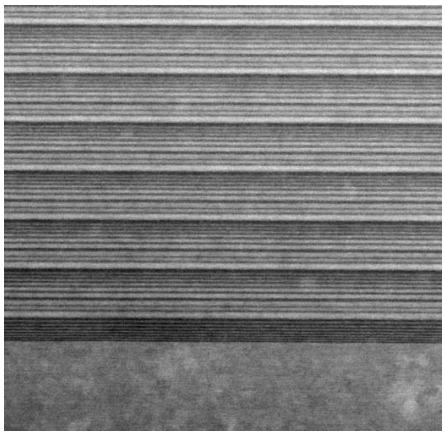

Figure 2 - Highly planar and defect free layers in an ICLED grown lattice-matched on GaSb.

[1] C. S. Kim et al., Opt. Engr. 57, 011002 (2018).
[2] N. Schäfer et al., Opt. Engr. 58, 117106 (2019).
[+] Author for correspondence: incef@unm.edu

Supplementary Pages

Epitaxial process for growth of ICLED on GaSb/Silicon: The first step in the process involves GaSb buffer layers that are grown on (001) silicon with an offcut of 4° towards (111). The native oxide on the silicon is removed using a dilute HF etch resulting in a hydrogen passivated surface. The III-V nucleation on the Silicon is achieved by growing a ≈ 10 nm thick AlSb layer at a substrate temperature of 500 °C, followed by the growth of a 1µm thick GaSb buffer layer. The GaSb/Si wafers are then transferred to NRL with an antimony cap to prevent oxidation. An additional GaSb buffer 2-3 µm thick is now grown followed by the ungrouped active ICLED stages. A control structure is also grown to the same 22-stage design on a GaSb substrate. The epi-up ICLED grown on silicon exhibits efficiencies 75% of those for epi-down ICLEDs grown on GaSb when differences in architecture are accounted for. At 100 mA, 200-µm-diameter mesas produce 184 µW CW at 25°C and 140 µW at 85°C.

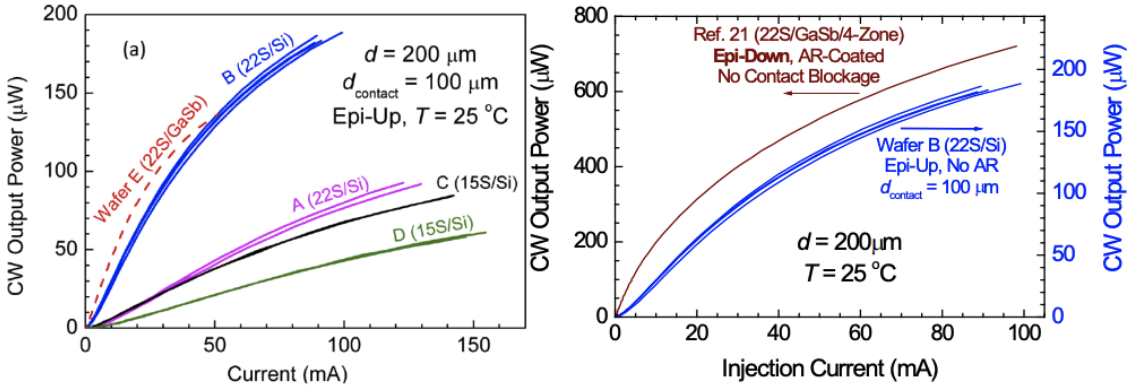

Figure 1 (Left) – Cw L-I characteristics at room temperature for multiple 200-µm-diameter ICLEDs from Wafers A-D on silicon and control Wafer E on GaSb; Figure 2 (Right) - RT cw L-I characteristics of multiple epi-up ICLEDs on silicon, compared to that for an epi-down and AR-coated ICLED on GaSb with active stages divided into 4 groups positioned at antinodes of the optical field, all with 200 µm mesa diameter. Adjustment of the right power scale by a factor of 3.3 accounts for architectural differences.

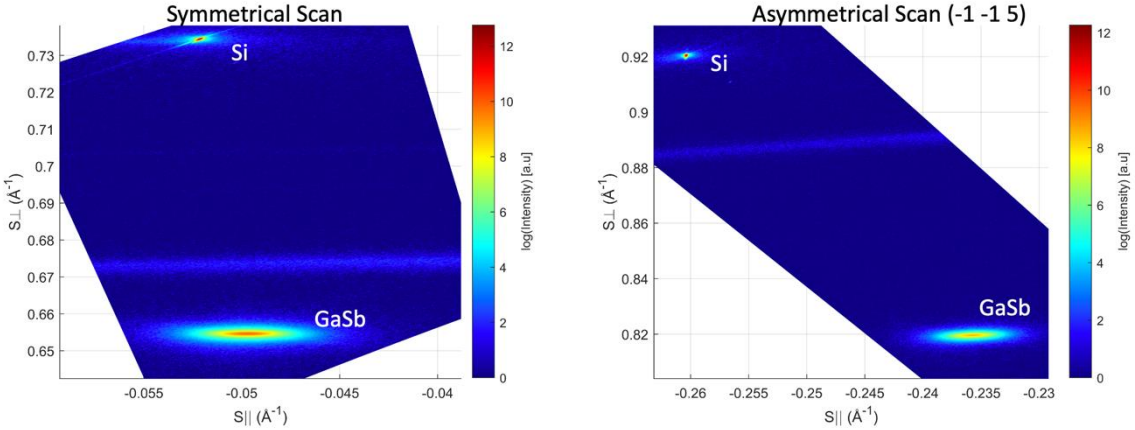

Figure 3 – XRD Reciprocal Space Map of GaSb on Silicon buffer grown at UNM. Threading dislocation density is ~ 10^8/cm^3 and the GaSb is 99.2% relaxed.

Production MBE Growth of QuiC SLED with Emission in the Longwave Infrared for Custom Gas Sensing Solutions

E. Fraser[1], J. Shao[1], B. Barnes[1], P. Frensley[1], P. Pinsukanjana[1], Y. C. Kao[1], and M. S. Miller[2]

[1] *Intelligent Epitaxy Technology, Inc., 1250 E. Collins Blvd., Richardson, TX, 75081*
[2] *Terahertz Device Corporation, 4525 Wasatch Blvd. Suite 325, Salt Lake City, Utah 84124*

We have demonstrated quantum interband cascaded superlattice light emitting diodes (QuiC SLED) operating in the longwave infrared for gas sensing applications. Production scale growth of strained layer superlattice (SLS) based materials presents challenges associated with volume material manufacturing and requires solutions for both uniformity and consistency of material output. We have developed a MBE growth methodology for routine production of SLS materials for focal plane array applications and applied these capabilities to growth of QuiC SLED materials for the gas sensing market. The QuiC SLED materials were developed based on Terahertz Device's Version 1.5 technology node architecture and produced by IntelliEPI on an Sb-equipped Riber MBE6000 multi-wafer production MBE system. The multi-wafer growth run was characterized for defect levels, uniformity of deposition and wafer warpage. The QuiC SLED materials were processed into surface emitting diodes based on standard photolithography and wet chemical etching. Electroluminescence emission was measured by FTIR spectrometer at various operating temperatures and show emission within the LWIR spectral band. The emission peak wavelength decreased with drive current from 10.6 µm to 10.2 µm.

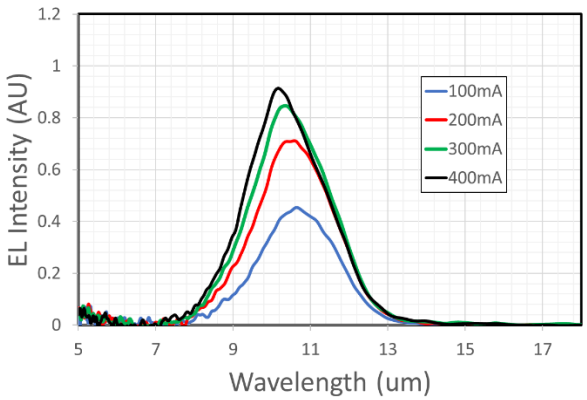

Figure 1: Electroluminescence emission at 77K operating temperature for QuiC SLED LW device.

[+] Author for correspondence: efraser@intelliepi.com

Interband cascade laser on silicon for high-speed applications in the mid-infrared domain

S. Zaminga[1], P. Didier[1,2], O. Spitz[1,3], D. A. Díaz-Thomas[4], A. N. Baranov[4], H. Knötig[5], A. Lardschneider[5], B. Schwarz[5], L. Cerutti[4], F. Grillot[1,6]

[1] *LTCI Télécom Paris, Institut Polytechnique de Paris, Palaiseau, 91120, France*
[2] *mirSense, Campus Eiffel, Bâtiment E-RDC, 1 rue Jean Rostand, Orsay, 91400, France*
[3] *now with CREOL, University of Central Florida, Orlando, Florida 32816, USA*
[4] *IES, Université de Montpellier, CNRS UMR 5214, Montpellier, 34000, France*
[5] *Institute for Solid State Electronics, TU Wien, Gußhausstraße 25-25a, 1040 Vienna, Austria*
[6] *Center for High Technology Materials, University of New-Mexico, Albuquerque, NM 87106, USA*

Quantum cascade structures are nowadays becoming mature solutions enabling mid-infrared (MIR) light-generation for diverse applications, such as free-space communications [1] and precision spectroscopy [2]. In the 3-6-µm transmission window, the interband cascade laser (ICL) is an excellent candidate over the quantum cascade laser (QCL) due to its low-threshold drive power [3]. Such reduced energy consumption meets the requirement for ultracompact devices and photonic integration: the utilization of epitaxial growth of III-V materials on silicon (Si) presents a compelling cost advantage compared to other material platforms [4]. The laser under study is a type-II Fabry-Perot (FP) ICL grown on Si, operating continuous-wave (CW) at room temperature (RT). Despite the high dislocations density and high non-radiative carrier recombination rates [5], the ICL still exhibits performances very similar to those grown on the native GaSb substrate. As shown in the light-intensity-voltage (LIV) characteristics in Figure 1a, the threshold current is 59 mA at 293 K; the maximum output power is around 11 mW per facet, the slope efficiency (per facet) is 0.12 W/A, and the external differential quantum efficiency (related to the two facets) is about 70%. The frequency response in Figure 1b shows a sharp cut-off around 1 GHz, which is promising for multi-Gbit/s wireless transmissions. Ulterior results in this direction will be presented during the conference.

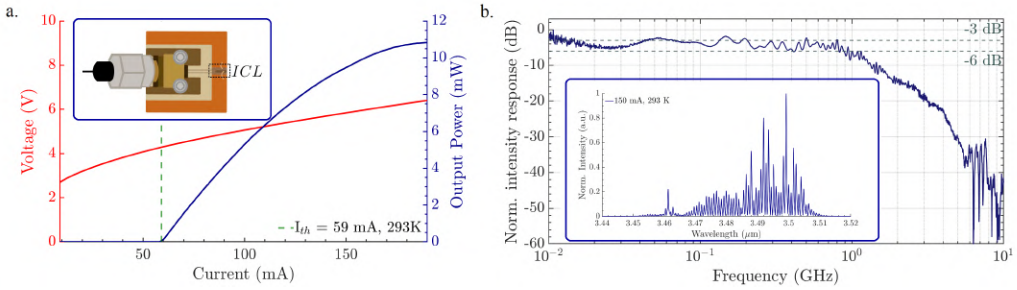

Figure 1: **a.** Light-Intensity-Voltage (LIV) curve of the 3.5 µm ICL. (inset) Schematic of the ICL and its dedicated mounting for high-speed operation. **b.** Frequency response of the ICL for a bias current of 150 mA. (inset) Emission spectrum of the multi-mode ICL, biased at 150 mA at 293 K.

[1] Didier, P. et al., *Photonics Research* 11, 582-590 (2023).
[2] Sterczewski, L., et al., *Optical Engineering* 57, 011014 (2018).
[3] Meyer, J., et al., *Photonics* 7, 75 (2020).
[4] Liu, A. Y., et al., *IEEE Journal of Selected Topics in Quantum Electronics* 24, 6, 6000412 (2018).
[5] Cerutti, L., et al., *Optica* 8, 1397-1402 (2021).

+ Author for correspondence: sara.zaminga@telecom-paris.fr

Supplementary Pages

Structural characterization

In this work, a type-II ICL is fabricated by molecular beam epitaxy (MBE) on a 2-inch silicon substrate with a slight misorientation of 0.5° along the crystal axis [110] on which 1500 nm of GaSb buffer has been previously epitaxied [6]. The growth starts with a lower optical confinement layer with a thickness of 3 µm, composed of a n-doped AlSb/InAs superlattice. It is followed by the waveguide consisting of 2 layers of n-doped GaSb, surrounding the 7 stages of the interband cascade active region. The type-II quantum wells with a "W" geometry are composed of 2 electron wells of InAs, surrounding the hole quantum well in GaInSb. The thicknesses are chosen to obtain an emission at 3.5 µm. Finally, the top confinement layer is also an n-type superlattice, 1.8 µm thick. After epitaxy, the structure undergoes several technological steps to realize the laser component. Since the realization of ohmic contacts on the silicon substrate is difficult using the technological processes for III-V semiconductors, the two contacts are placed on the front side: one contact was formed on top of the ridge and another one in the AlSb/InAs bottom cladding layer. The 8-µm wide laser mesas are created by UV photolithography and dry etching. The width of the laser is below the 10-µm thickness, where cracks appear in GaSb-based laser grown on Si [7]. The lasers are then cleaved to form a 2-mm cavity and epitaxial side-up soldered. The facets present no coating, so they are not processed [8].

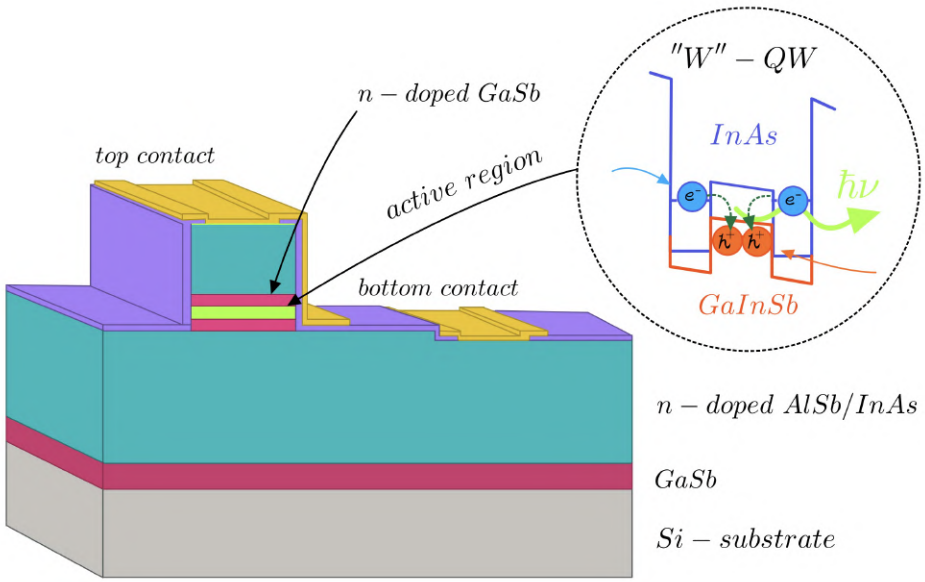

Figure 2: Schematic representation of the processed ICL grown on Si-substrate.

Optical characterization

Figure 3 displays the experimental setup to perform the optical response measurement. The continuous bias is provided by a low-noise current source (ILX Lightwave, LDX-3232), while the ICL is kept at a temperature of 293 K by a temperature controller (ILX Lightwave, LDT-5412) and a thermistor. A converging lens is employed to focus the beam on an interband cascade infrared photodetector (ICIP) [9], placed at a distance of roughly 20 cm. The ICIP is connected to a Pasternack bias tee: the DC part serves for the detector biasing through a Keithley source; the AC contribution is connected to the receiver of a 40-GHz-bandwidth vector network analyzer (VNA, Rohde&Schwartz-ZVK). It performs

All-Epitaxial Nanophotonic Architectures for Mid-Infrared Optoelectronics

L. Nordin, A. Kamboj, P. Petluru, M. Bergthold, Y. Wang, N. Mansfield, A. Muhowski, and D. Wasserman

Electrical and Computer Engineering, University of Texas at Austin, Austin, Texas 78758, USA

The mid-infrared (mid-IR) provides a design space where a wide range of engineered and intrinsic light matter interactions can be harnessed to develop a new generation of optical materials and devices. In particular, the highly-doped semiconductor class of materials offers an intriguing opportunity to control the permittivity of epitaxially-grown semiconductors, and can serve as low-index dielectrics, epsilon-near-zero materials, or even as plasmonic materials. Because these materials can be directly integrated with epitaxially-grown optoelectronic device active regions, there exists an opportunity to develop new mid-IR device architectures leveraging co-design of optical and electronic properties, all in a monolithic material system.

In this presentation I will discuss recent results showing strongly enhanced performance of mid-IR structures and devices leveraging all-epitaxial photonic enhancement of response, including distributed Bragg reflectors, leaky cavity LEDs and detectors, guided mode LEDs and detectors, and plasmonic infrared detectors, operating across the mid-infrared. I will present the opportunities and challenges for these new device architectures, and discuss potential future approaches for further enhancement and systems integration.

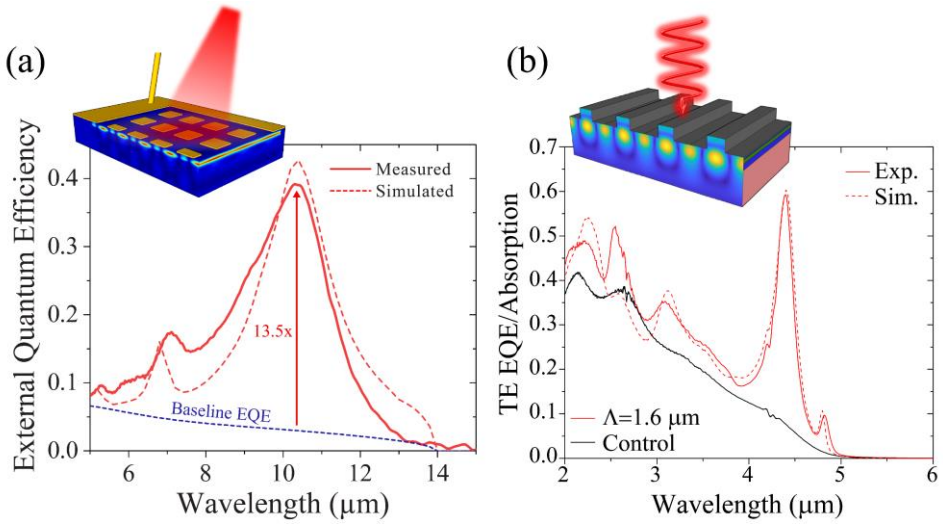

Figure 1: (a) Measured (solid) and simulated (dashed) T=195K external quantum efficiency (EQE) for a long-wave infrared plasmonic nBn detector with simulated EQE of the same detector without the plasmonic enhancement. (b) Measured (solid) and simulated (dashed) room temperature EQE for a mid-wave infrared guided mode resonance detector, compared to same detector structure without grating.

+ Author for correspondence: dw@utexas.edu

Strategies for Electrical Tuning of Thermal Emissivity in Metamaterials

B. Shrewsbury, A. Ghanekar, R. Audhkhasi, M. Sakib, M. L. Povinelli
Ming Hsieh Department of Electrical and Computer Engineering, University of Southern California, 3737 Watt Way, PHE 614, Los Angeles, CA 90089-0271

Achieving tunable control over the thermal emission spectrum of materials is expected to enable new possibilities in applications including thermophotovoltaics, waste heat recycling, and infrared communication and sensing. In recent work, we have introduced several strategies for achieving electrical control over thermal emission based on resonant coupling and symmetry breaking in infrared metamaterials.

In one thrust of our work, we consider control over emissivity amplitude. We employ metamaterials comprised of several, coupled resonators in each unit cell. By tuning the dimensions of each resonator, we can arrange for either a bright mode (one that couples to normally incident light) or a dark mode (one that does not) to fall within a specified region of the spectrum. This leads to several possibilities for spectral control. In an exemplar strategy, we consider two, initially bright modes that couple to form a dark mode. At zero applied voltage, the system is mirror symmetric, and the dark mode does not produce any observable feature in the emission spectrum. When a voltage is applied to tune the refractive index in a portion of the unit cell, mirror symmetry is broken. The formerly dark mode becomes bright, switching on an emissive peak. We present design strategies for implementing this concept within both graphene and III-V semiconductor platforms.

In a second thrust, we consider control over directionality of thermal emission. In this case, we consider a metamaterial based on weakly coupled resonators, which give rise to a nearly flat photonic band. We then consider the effect of a small index perturbation of the refractive index of the structure. We show that for fixed wavelength, the flatness of the photonic band magnifies the change in angle for emitted radiation. We present several practical designs for realizing this effect in a III-V semiconductor platform.

Nonlocal effects in heavily doped semiconductor

P. Loren,[1] E. Sakat,[2] J.-P. Hugonin,[3] L. Cerutti,[1] F. Gonzalez-Posada,[1] A. Moreau,[4] T. Taliercio[1]

[1] IES, Univ Montpellier, UMR CNRS 5214, Montpellier, France
[2] Université Paris-Saclay, CNRS, C2N, 91120 Palaiseau, France
[3] Université Paris-Saclay, CNRS, Laboratoire Charles Fabry, 91127 Palaiseau, France
[4] Université Clermont Auvergne, CNRS, SIGMA Clermont, Institut Pascal, F-63000 Clermont-Ferrand, France

The Drude model is the most adapted model to describe the optical properties of metal and nano-antennas. Unfortunately, it starts to fail when the size of the nanostructures becomes small enough, that is a few nanometers for noble metals or a few tens of nanometers in the case of heavily doped semiconductors. It is then necessary to consider a nonlocal susceptibility tensor to describe accurately the optical properties of these metallic nanostructures. The best-suited approaches are the semi-classical quantum model [1] or the hydrodynamic Drude model (HDM). HDM can describe accurately the ultra-confined light of the plasmonic mode by the introduction of an electron quantum pressure in the equation of motion of the free electron gas.[2] It is particularly well adapted to be implemented in electromagnetic modeling. In this work, we compared experimental measurements of the volume plasmon modes with HDM. Figure 1 shows volume plasmon modes measured by attenuated total reflectance (Diamonds) on heavily Si-doped InAsSb layers with thickness varying between 20 nm and 200 nm. InAsSb:Si is grown by solid source MBE on GaSb substrate.[3] HDM is represented in Fig. 1 by the gray map. The light gray curves show the volume plasmon modes introduced by the nonlocal effect. Modeling is in good agreement with the experimental data.

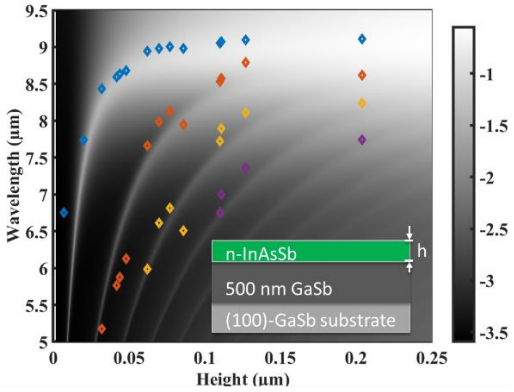

Figure 1 Optical resonances of InAsSb:Si layers of varying thicknesses measured by attenuated total reflectance (ATR). The gray map corresponds to the HDM simulations, and the diamonds are the modes measured by ATR for different layer thicknesses.

[1] L. Wendler and E. Kändler, Phys. Status Solidi B 177, 9 (1993).
[2] E. Sakat, A. Moreau and J.-P. Hugonin, Phys. Rev. B 103, 235422 (2021).
[3] M. J. Milla, *et al.* Nanotechnology 27, 425201 (2016).
+ Author for correspondence: thierry.taliercio@umontpellier.fr

Low doping level and carrier lifetime measurements in InAs with a novel THz characterization technique

J. Guise,[1] **S. Blin**,[1] **H. Ratovo**,[1] **J.-B. Rodriguez**,[1] **L. Cerruti**,[1] **E. Centeno**,[2] **R. Smaali**,[2] **F. Gonzalez-Posada Flores**,[1] **M. Thual**,[3] **J. Hesler**,[4] **T. Reck**,[4] **and T. Taliercio**[1]

[1] *IES, Univ Montpellier, CNRS, Montpellier, France*

[2] *Univ. of Clermont-Auvergne, 63170 Aubière, France*

[3] *Univ. of Rennes, 22305 Lannion, France*

[4] *VDI Inc., VA 22902-6172 Charlottesville, USA*

In this abstract, we present a novel, contactless opto-THz technique for measuring low doping levels and carrier lifetime in InAs. Preliminary studies proved that THz waves can be modulated using an optically-pumped InAs slab [1]. This optically-driven modulation is efficient in the 0.75–1.1-THz frequency band because of its vicinity with the plasma frequency of electrons, that leads to a strong dependence of the real and imaginary parts of the dielectric permittivity of InAs on free carrier density, the latter being strongly increased using optical pumping. Additionally, without any optical pumping, we show that n-type doping levels around 10^{16} cm^{-3} could be measured thanks to THz transmission measurements analyzed using a single-variable Drude-Lorentz model, as shown in Fig. 1(a), thus offering an original and accurate technique to measure very low doping levels. Using an amplitude-modulated optical pump, we could also easily retrieve the effective carrier lifetime by measuring the transmission of a THz probe signal, as shown in Fig. 1(b).

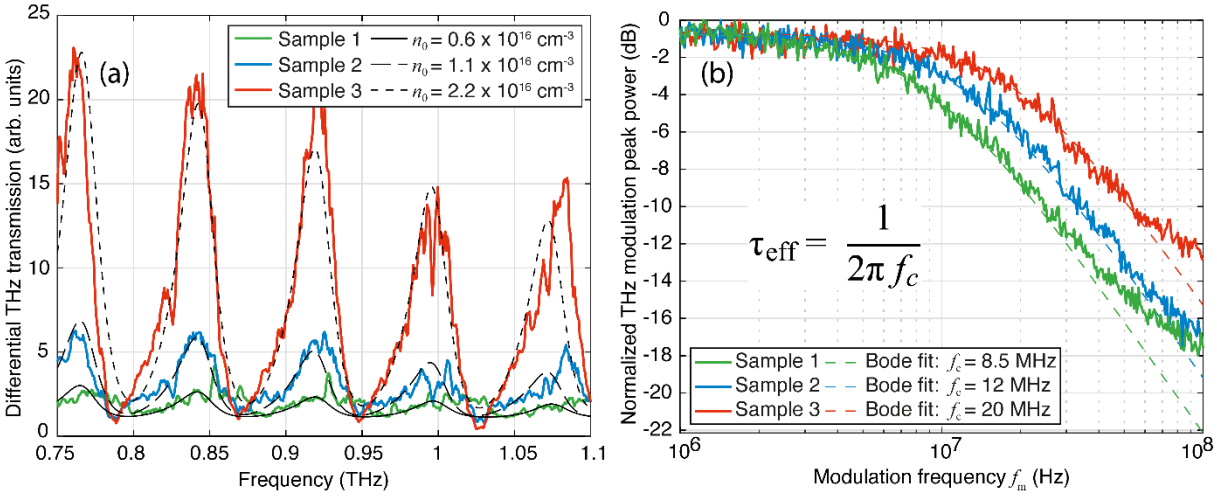

Figure 1. (a) Differential THz transmission measurement: transmission through substrate only (500 µm of GaAs) divided by the sample transmission (5 µm of InAs on GaAs substrate). Black curves correspond to the model fittings. **(b)** Typical THz modulation Bode spectrum at 0.81 THz under 10 W/cm^2 mean optical density. The bandwidths give information about the carrier effective lifetime in the three InAs samples.

[1] E. Alvear-Cabezón, Appl. Phys. Lett. 117(11), 111101 (2020).

+ Author for correspondence: julien.guise @umontpellier.fr

Temperature dependence of the infrared dielectric function and the direct band gap of InSb from 25 to 800 K

Sonam Yadav, Melissa Rivero Arias, Carlos A. Armenta, Carola Emminger, Cesy M. Zamarripa, Nuwanjula S. Samarasingha, Jaden R. Love, Stefan Zollner

Department of Physics, New Mexico State University, Las Cruces, NM 88003-8001, USA

In experiment, the infrared dielectric function of InSb in the region of the direct band gap at temperatures from 77 to 725 K using Fourier-transform infrared spectroscopic ellipsometry is determined. At the highest temperatures, the free carrier concentration due to thermally excited electron-hole pairs becomes very large and the Fermi level is above the conduction band minimum. The observed band gap increases again at 600 K (Burstein-Moss shift).

Theoretically, the temperature dependence of the chemical potential μ for an ideal intrinsic semiconductor (InSb) at fixed temperatures is calculated by using Polylogarithm forms of FD integrals. It is known that at absolute zero, the chemical potential (μ) is equal to the Fermi energy (ε_F). μ versus T is plotted for Degenerate and Non-Degenerate case (this calculation assumes parabolic bands, a constant band gap, and constant effective masses). On comparing both graphs we can see at higher temperature degenerate graph goes up (deviate up) but for non-degenerate case, it remains linear. Due to the small electron to hole mass ratio, the optical activation energy (OAE, i.e., the experimental band gap measured with transmission or ellipsometry measurements) is almost the same as the chemical potential, once μ is larger than the band gap (above about 400 K). It is apparent that there is a thermal Burstein-Moss shift for temperatures above 400 K, because the chemical potential and the OAE are larger than the intrinsic band gap.

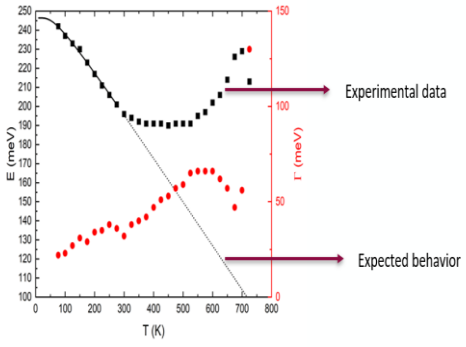

Fig1: Direct band gap E_0 (▪) and broadening (·) of InSb as a function of temperature. (Experimental Result)

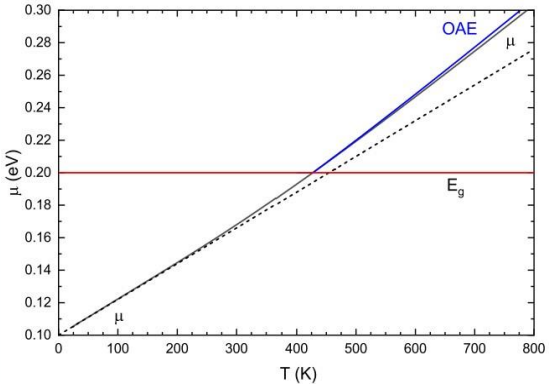

Fig 2: Chemical potential for intrinsic InSb v/s temperature in the degenerate (solid) and non-degenerate (dotted) case. The red horizontal line shows the band gap of 0.2 eV. The blue line shows the optical activation energy (OAE, i.e., the experimental band gap)

+ Author for correspondence: yadsonam@nmsu.edu

Supplementary Pages (Optional)

In Experimental work, the temperature dependence of the complex pseudo-dielectric function of bulk InSb (100) near the direct band gap was measured with Fourier-transform infrared ellipsometry between 30 and 500 meV at temperatures from 80 to 725 K in ultrahigh vacuum. Using the Jellison-Sales method for transparent glasses, the thickness of the native oxide was found to be 25±5 ˚A, assuming a high-frequency dielectric constant of about 3.8 for the native oxide. After this surface correction, the dielectric function was fitted with a Herzinger-Johs parametric semiconductor model to determine the band gap and with a Drude term to determine the electron concentration and the mobility. We find that the band gap decreases from 230 meV at 80 K to 185 meV at 300 K, as expected from thermal expansion and a Bose-Einstein model for electron-phonon scattering renormalization of the band gap. Between 450 and 550 K, the band gap remains constant near 150 meV and then increases again at even higher temperatures, presumably due to a Burstein-Moss shift resulting from thermally excited electron-hole pairs. The broadening of the direct band gap increases steadily with temperature. (See Fig. (a))

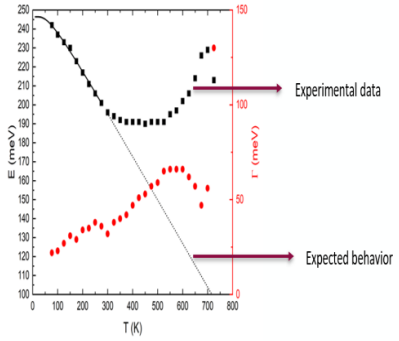

Fig: (a)

We described a theoretical model that is used to explain these experimental results.

For an undoped (intrinsic) semiconductor with parabolic bands, the electron and hole concentrations as a function of temperature T are given by,

$$n\,(T) = \frac{1}{4}\left(\frac{2m_0\, m_e k_B T}{\pi\hbar^2}\right)^{\frac{3}{2}} F_{\frac{1}{2}}\left(\frac{\mu - E_0}{k_B T}\right),\; p(T) = \frac{1}{4}\left(\frac{2m_0\, m_h k_B T}{\pi\hbar^2}\right)^{\frac{3}{2}} F_{\frac{1}{2}}\left(\frac{-\mu}{k_B T}\right)$$

where m_e and m_h are the effective density-of-states masses of the conduction and valence bands and $\hbar$ is the reduced Planck's constant. μ is the chemical potential, and E_0=0.2 eV is the direct band gap, which we have assumed to be constant. We also assumed constant effective masses. For sufficiently low temperatures, the argument of the Fermi-Dirac integral $F_{1/2}$ becomes very large, and the Fermi integral can be expanded into essentially using Maxwell-Boltzman statistics to describe the electron and hole populations.

$$\mu \approx \frac{E_0}{2} + \frac{3k_B T}{4}\, ln\left(\frac{m_h}{m_e}\right), \qquad \mu \approx 2\left(\frac{m_0 k_B T}{2\pi\hbar^2}\right)^{\frac{3}{2}} (m_e m_h)^{\frac{3}{4}} \exp\left(-\frac{E_0}{2k_B T}\right)$$

For InSb, these expressions can be used up to 300 K, but deviations become noticeable at higher temperatures. Above 300 K, we must use the exact definition of the Fermi-Dirac integral.

Sb-based Mid-Wave Infrared Laser Arrays

Rowel Go[1], **Andy Lu**[1], **Matthew Suttinger**[1]
[1] *Air Force Research Laboratory, 3550 Aberdeen Ave SE, Kirtland AFB, NM 87117*

Mid-wave infrared lasers have advanced in both spectral coverage and power level in the past decade. Particularly, Sb-based semiconductor laser structures are of interests for many applications such as remote sensing, direct diode pump sources, and defense countermeasures. Here we report high power diode laser arrays using these laser structures. The laser structures as shown in Fig 1. were grown using molecular beam epitaxy on GaSb substrates with designed emission wavelengths of 2.0µm, 2.4µm, and 2.7µm. All structures share the same lattice-matched AlGaAsSb quaternary cladding doped with Te for n-type and Be for p-type clad layers. The waveguide consists of lattice-matched quaternary or quinary alloy and compressively strained InGaAsSb quantum wells laced at the center with inter-well spacings. Changing in wavelength is controlled by adjusting In content in the waveguide. Single and four-bar stack arrays were processed, fabricated, and packaged with water-cooled microchannel coolers. Some of the laser performance results tested in various conditions are shown in Fig 2.

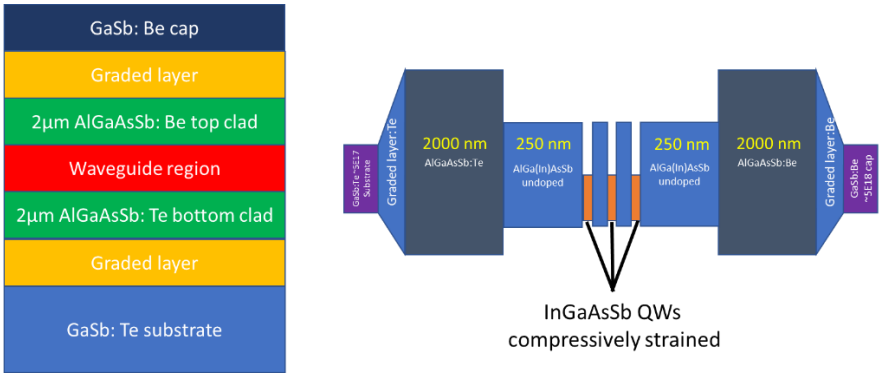

Figure 1 Laser Structure.

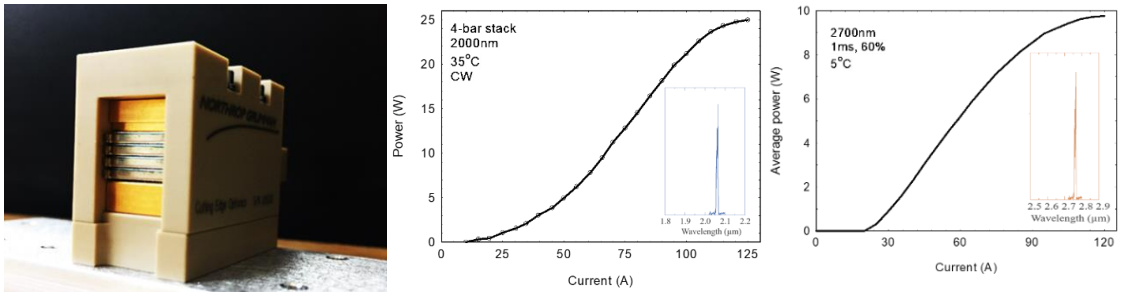

Figure 2 Packaged four-bar stack arrays (left). 2.0µm continuous-wave (CW) operation (middle). 2.7µm 60% duty cycle quasi-CW operation (right).

+ Author for correspondence: Rowel.Go@us.af.mil

Carrier Concentration-Dependent Optical Properties of Narrow Gap Semiconductors

Yixuan Shen,[1,+] Rui Q. Yang,[1] and Michael B. Santos[2]
[1] School of Electrical and Computer Engineering, University of Oklahoma, Norman, OK
[2]Homer L. Dodge Department of Physics and Astronomy, University of Oklahoma, Norman, OK USA 73019.

This work provides a comprehensive assessment of the optical properties of narrow bandgap semiconductors based on the k·p method [1] across a wide range of carrier concentrations and wavelengths. Based on a commonly used two-band model [2] and a less explored three-band model that include the spin-orbit split-off band, the refractive index and absorption coefficient due to free-carrier absorption are evaluated and compared with experimental data to assess their suitability for different scenarios. It is found that the values of electron energy based on the two models can substantially differ as the carrier concentration is increased. Fig. 1 shows the energy calculations for InAs, with the resulting effective masses shown in Fig. 2. The refractive index and absorption coefficient calculated from the two models will have some differences that depend on the carrier concentration. The results provide a guideline for selecting the appropriate model in different wavelength and carrier concentration ranges for various applications. The attained results may help with the optimization of interband cascade laser performance and other applications, and lead to improved device performance and more accurate measurements.

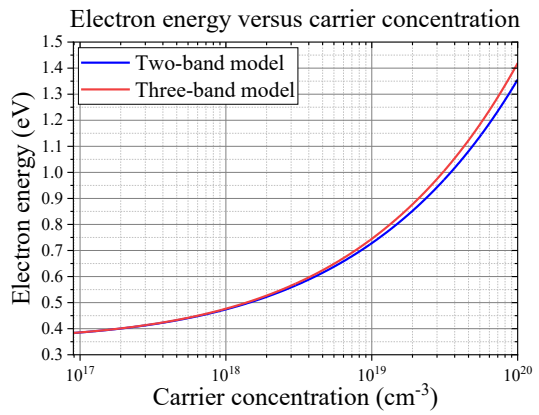

Fig. 1 Electron energy versus carrier concentration based on the two models for InAs.

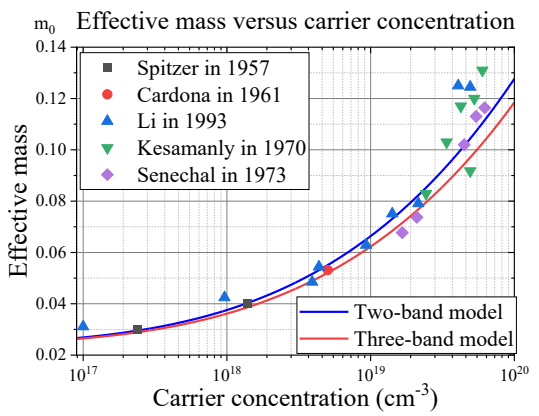

Fig. 2. Calculated effective mass versus carrier concentration based on the two models compared with experiment data from literature.

This work was partially supported by NSF (No. ECCS-1931193) and OCAST (AR21-024).

[1] E. O. Kane, "Physics of III-V compounds," Chapter 3 in Semiconductors and Semimetals, edited by R. K. Willardson and A. C. Beer (Academic, New York, 1966), Vol. 1.
[2] Y. B. Li *et al.*, "Infrared reflection and transmission of undoped and Si-doped InAs grown on GaAs by molecular beam epitaxy," *Semiconductor Science and Technology,* vol. 8, no. 1, pp. 101-111, 1993.

[+] Author for correspondence: yixuan_shen@ou.edu

Tuning the plasmonic response of heavily-doped semiconductors in epsilon-near-zero regime

P. Fehlen,[1,2,*] J. Guise,[2] G. Thomas,[1] F. Gonzalez-Posada,[2] L. Cerutti,[2] J-B. Rodriguez,[2] D. Spitzer,[1] T. Taliercio[2]

[1] *Nanomaterials for systems under extreme stress, UMR3208 ISL/CNRS/UNISTRA, Saint-Louis, France*

[2] *IES, Univ., Montpellier, UMR CNRS5214, Montpellier, France*

Epsilon-near-zero (ENZ) materials display vanishing permittivity at precise frequencies, e.g., plasma frequency ω_p. They exhibit several peculiar properties such as a unique field enhancement or ultrafast nonlinear efficiencies, and will be useful in the field of integrated Photonics. Heavily doped semiconductors have a tunable ENZ regime over the infrared spectral range by adjusting their doping level and thus their plasma frequency ω_p.

In this work, we investigate the correlation between the localized surface plasmon-polariton resonance and the nano-antenna size within a metal-insulator-metal structure composed of heavily-doped semiconductor InAsSb:Si (Fig. 1 a)). In this study, while the metals have a high plasma frequency ω_{p1}, the insulator is also doped InAsSb:Si at lower plasma frequency ω_{p2}. In doing so, we uncover the origin of the resonance pinning, which has been previously mentioned in the literature, as the spacer permittivity approaches zero [1]. Plus, we demonstrate that doping is an excellent additional degree of freedom to engineer the optical response of plasmonic structures, especially in the ENZ regime where the response becomes nearly geometry-independent, and is rather dispersive dependent (Fig. 1 b)).

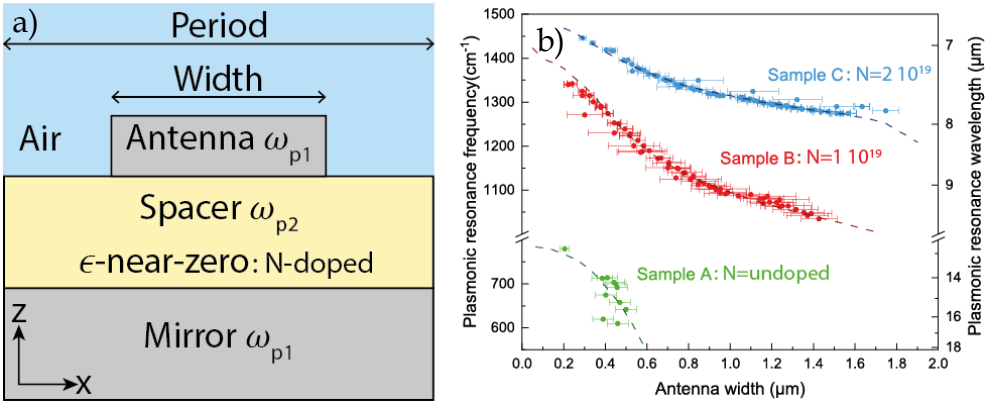

Fig. 1) a) Diagram of the samples. b) Plasmonic resonance as a function of the antennas width (dashed: simulations, points: experimental). We observe the influence of the spacer layer doping level on the geometry-independent behavior, notably Sample C.

[1] Kim, J., Dutta, A., Naik, G. V., Giles, A.J., Bezares, F.J., Ellis, C.T., Tischler, J.G., Mahmoud, A.M., Caglayan, H, Glembock.i, O.J,. Kildishev, A.V., Caldwell, J.D., Boltasseva, A., Engheta, N. 2016, *Optica*, 3, 339-346.

*Author for correspondence: pierre.fehlen@isl.eu

Interfacial Misfit dislocation array assisted MBE growth of InSb quantum well on InAs using AlInSb buffer layer

F. F. Ince,[1] Alex T. Newell,[1] T. J. Rotter,[1] and G. Balakrishnan,[1] M. R. McCartney,[2] D. J. Smith [2]

[1] University of New Mexico, Albuquerque, NM 87108

[2] Department of Physics, Arizona State University, Tempe, AZ 85287

Mid-wave infrared (MWIR) detectors are commonly used in medical devices, remote sensing, and spectroscopy. InSb-based infrared focal plane arrays (FPAs) offer spatial uniformity, temporal stability, scalability, and affordability. Type-II superlattices and metamorphic buffers are used to cover the MWIR spectrum and reach the long-wave infrared (LWIR) region. We propose using interfacial misfit dislocations to grow fully relaxed InSb on InAs substrate, and direct growth of $Al_xIn_{1-x}Sb$ buffer layers on InAs, for developing tunable InAsSb absorbers for MWIR and LWIR applications [1], [2].

In this presentation will discuss the interfacial misfit dislocation growth mode to form instantly relaxed buffer layer on top of InAs substrates. We analyze both directly grown AlInSb and InSb epilayers on InAs substrates using HR-XRD ω-2θ scans as well as reciprocal space mapping. HR-XRD results indicate a relaxation of 99.4% for InSb directly grown on InAs, and a slightly reduced value for the $Al_{0.1}In_{0.9}Sb$ and $Al_{0.2}In_{0.8}Sb$ epilayers. Reciprocal space mapping allows us to estimate the screw and mixed dislocation density for the layers. Additionally, TEM analysis shows the formation of misfit dislocation arrays at the AlInSb/InAs interface. We investigate InSb quantum wells grown with different $Al_xIn_{1-x}Sb$ barrier layers using photoluminescence (PL). We will present a comprehensive analysis of the buffer layers with respect to threading dislocation density using XRD scans and TEM images. Furthermore, we will provide a detailed analysis of the InSb QWs based on PL and TRPL results.

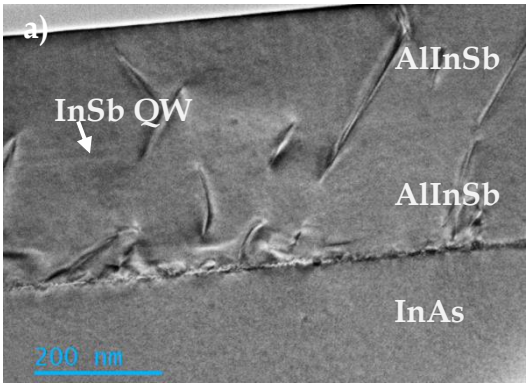

Figure 1 – TEM image of InSb QW using AlInSb buffer layer

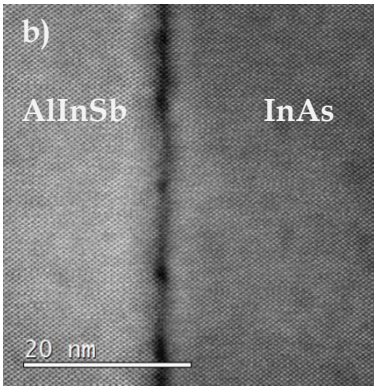

Figure 2 – HRTEM shows the formation of interfacial misfit dislocations

[1] W. L. Sarney, S. P. Svensson, Y. Xu, D. Donetsky, and G. Belenky, "Bulk InAsSb with 0.1 eV bandgap on GaAs," J. Appl. Phys., vol. 122, no. 2, p. 025705, Jul. 2017.

[2] A. Rogalski, "Next decade in infrared detectors," in Electro-Optical and Infrared Systems: Technology and Applications XIV, Warsaw, Poland, 2017.

[+] Author for correspondence: incef@unm.edu

Supplementary Pages

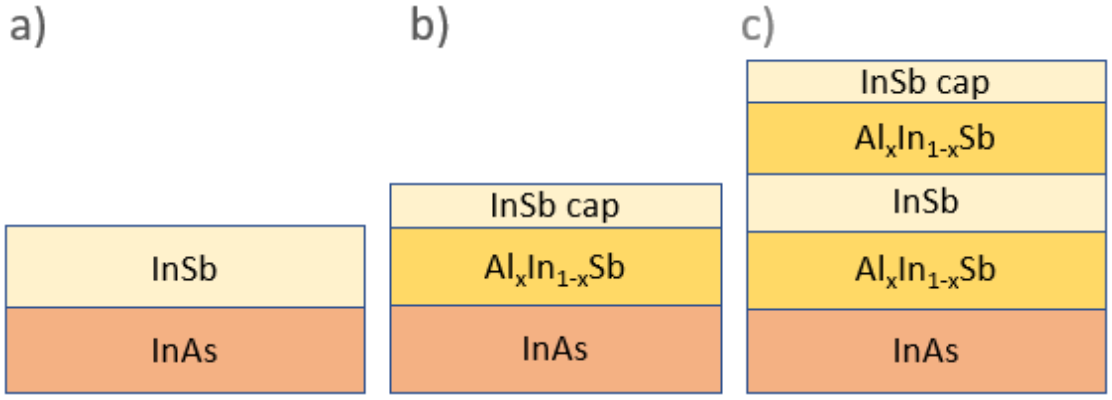

Figure 1: Schematic of different configurations of the IMF samples

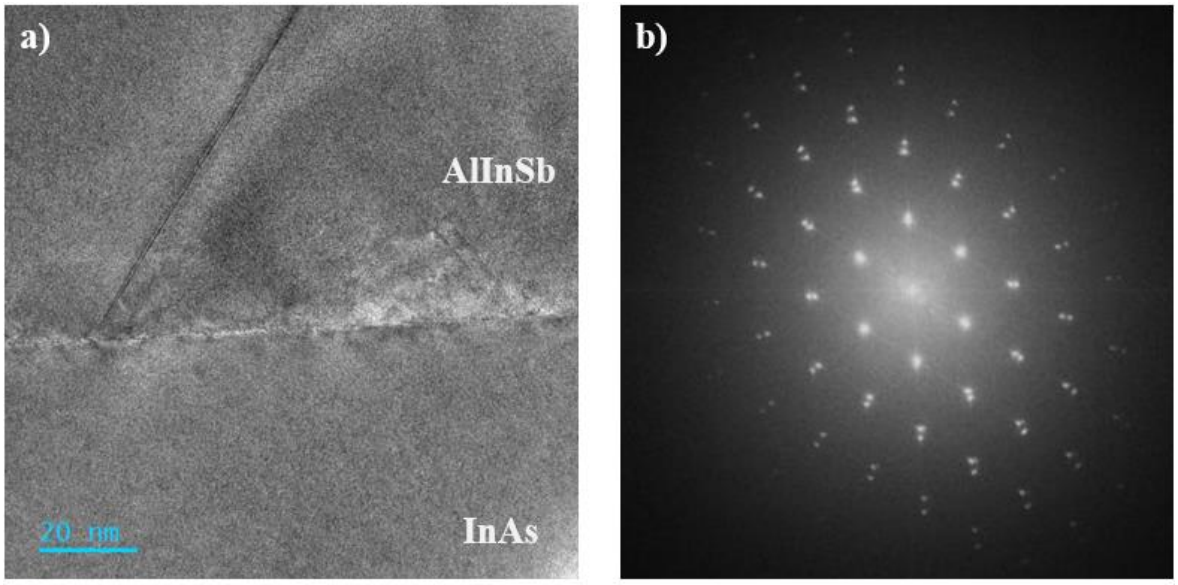

Figure 2: *TEM of the $Al_{0.2}In_{0.8}Sb$/InAs buffer layer interface showing a stacking fault formation and FFT of the image shows two distinct lattice parameters $Al_{0.2}In_{0.8}Sb$ and InAs*

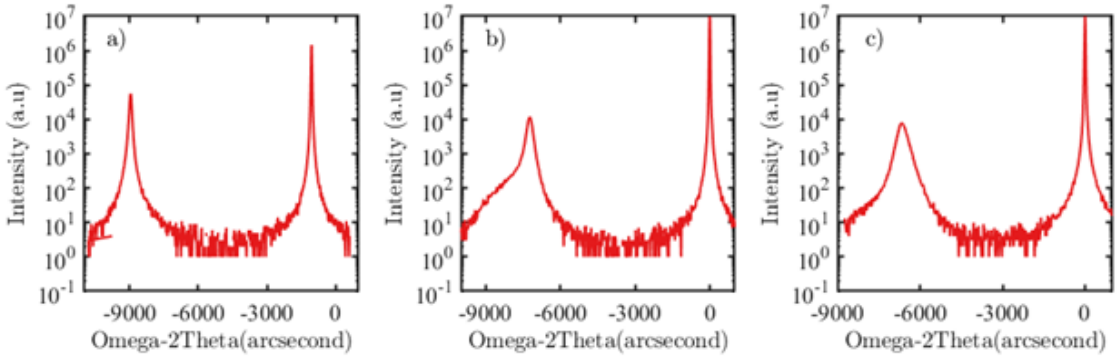

Figure 3 – *HR-XRD ω-2θ scans of a) InSb/InAs b) $Al_{0.1}In_{0.9}Sb$ and c) $Al_{0.2}In_{0.8}Sb$ buffer layers*

High Efficiency Room Temperature HgTe Colloidal Quantum Dot Photodiodes

J. C. Peterson,[1] P. Guyot-Sionnest[1]

[1] *The James Franck Institute, 929 E. 57th St., The University of Chicago, Chicago, IL, 60627, USA.*

Colloidal quantum dots offer an inexpensive, solution-processed alternative to conventional, crystalline material devices for mid-infrared photodetection. Photodiodes of size 1 mm by 1 mm made using HgTe quantum dots previously reached the background limit at cryogenic temperatures but suffered from a 30-fold decrease in signal near room temperature. This was attributed to a decreased carrier diffusion length at higher temperatures, where the thermal carrier concentration is high. An alternative explanation based on a simple circuit model suggests that it is instead due to the effects of a finite series resistance, coming mainly from the semitransparent indium tin oxide electrode.
Using microfabrication, devices were prepared which use an insulating polymer to restrict the active device area to 50 by 50 microns. This decrease in size increases the shunt resistance to be greater than the series resistance even at room temperature. It was also found to be important to employ a guard ring in the final design to only collect carriers within this restricted area, which limits crosstalk between nearby devices and allows one to measure the true resistance of the devices. As a result of these alterations, greater signal is collected, leading to 15% EQE and a four-fold improvement in the detectivity in excess of 10^9 Jones near room temperature for photodiodes with a cutoff at 4 microns.

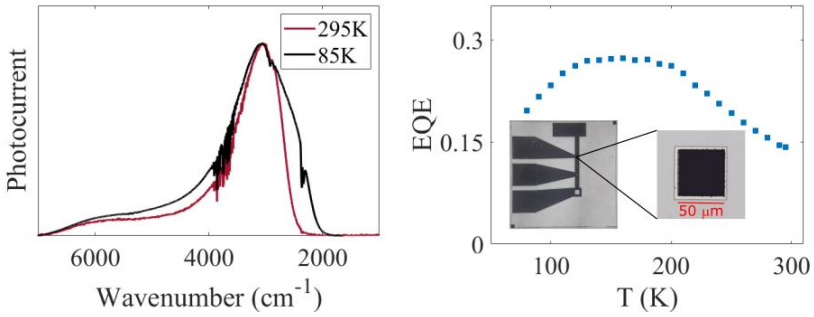

Figure 1: Photocurrent spectrum of HgTe pn photodiode (left) and associated external quantum efficiency (right). Inset is a picture of the device substrate. [1]

[1] J. C. Peterson, P. Guyot-Sionnest, Room-Temperature 15% Efficient Mid-Infrared HgTe Colloidal Quantum Dot Photodiodes. ACS Applied Materials & Interfaces. Article ASAP, (2023).

+ Author for correspondence: jcpeterson@uchicago.edu

Experimental study of band offsets at the GeSn/SiGeSn interface by Internal Photon Emission

J. Rudie,[1] H. Tran,[1] S. Amoah,[1] S. Ojo,[1] M. Shah,[2] S. Yu[1]
[1] University of Arkansas, 1 University of Arkansas Fayetteville, AR 72701
[2] University of Arkansas at Pine Bluff, 1200 University Dr, Pine Bluff, AR 71601

In heterojunction semiconductor devices the band structure of the interfacing materials plays a pivotal role in the resulting device's performance and characteristics. Therefore, measuring and understanding the band offsets of emerging materials is crucial since the type of band alignment (Type I, Type II, Type III) and the magnitude of energy offsets determine the magnitude of the potential barriers, and thus, the possible carrier confinement in any resulting device. [1]

The band offsets between GeSn and SiGeSn in a quantum well photoconductor device were measured using internal photon emission (IPE). This technique was used as it is precise with values reported with sub millielectronvolt resolution and is not limited by surface depth penetration like many electron spectroscopy techniques.[1],[2] IPE is characterized by the product of a device's responsivity and energy of incident exciting photons. This product is known as quantum yield (Y) and is proportional to photon energy exceeding the energy threshold required for photocurrent generation from an emitter material to a collector material.[2] In the measurement of the GeSn/SiGeSn device it was determined that the band alignment was Type-1 with a VBO of 0.06 eV and a conduction band offset (CBO) of 0.02 eV.

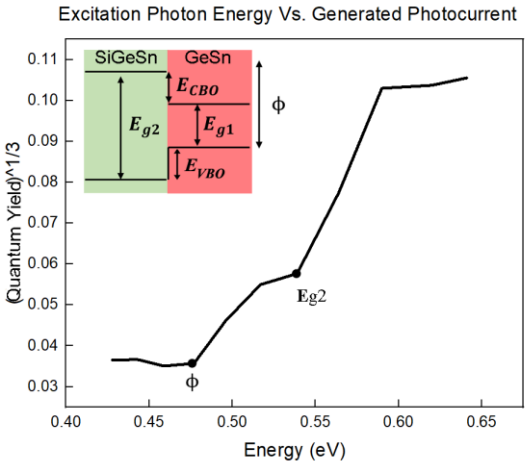

Figure 1 – Quantum yield from the measured photocurrent vs. the incident energy of excitation photons.

[1] Afanas′ev, Valery V. Internal Photoemission Spectroscopy: Fundamentals and Recent Advances. Elsevier, 2014.
[2] Y. F. Lao and A. G. U. Perera, "Physics of Internal Photoemission and Its Infrared Applications in the Low-Energy Limit," *Adv. Optoelectron.*, vol. 2016, pp. 1–18, Jan. 2016, doi: 10.1155/2016/1832097.

[+] Author for correspondence: jrudie@uark.edu

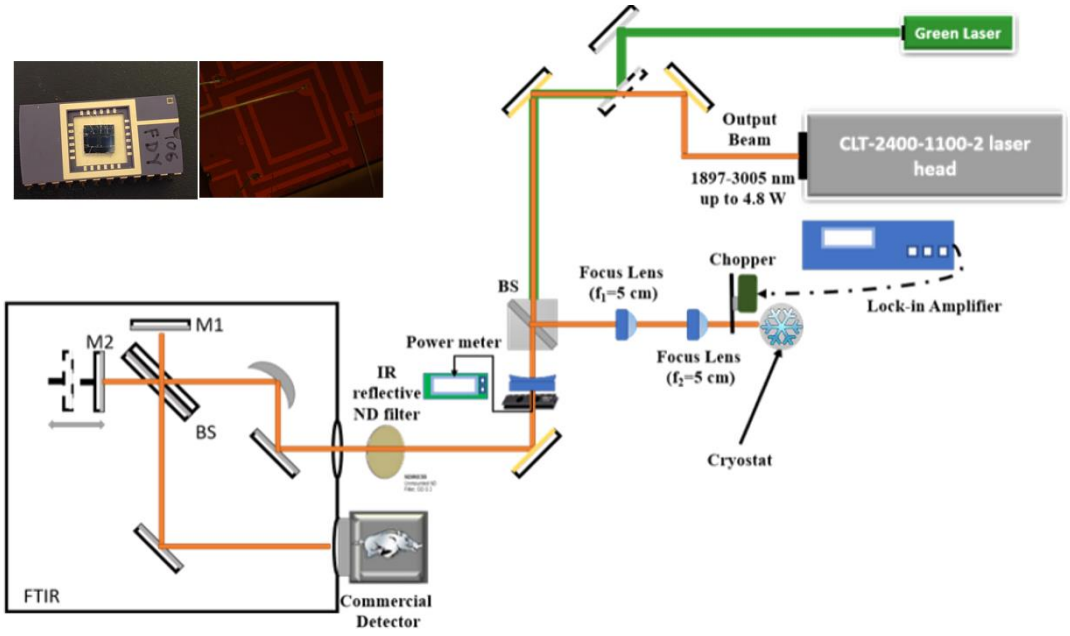

Figure 2 – IPE measurement setup and sample. The measurements used a tunable 1.9 – 3 um laser which was aligned with a visible green laser on a common path. The beam passed through a CaF2 50:50 beam splitter. The split beam struck the sample in a cryostat and a power meter at a equal distance so the measurement could be conducted and the incident beam power could be measured simultaneously. An FTIR and commercial detector were used to determine the wavelength of the laser during each collection. The sample was a square device single quantum well photoconductor.

Design

	Si (%)	Sn (%)	Thickness (nm)
Barrier 2	3	8	15
Well 1	0	15	20
Barrier 1	3	8	100
GeSn buffer	0	8~11	>800
Ge Buffer	0	0	900
Substrate	100	0	735,000

SIMS

	Si (%)	Sn (%)	Thickness (nm)
Barrier 2	2.4	8.4	71.5
Well 1	0	11.8	39.1
Barrier 1	2.2	8.4	73.8
GeSn buffer	0	6~9	850
Ge Buffer	0	0	560
Substrate	100	0	735,000

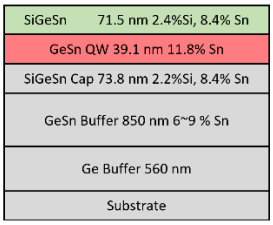

Figure 3 – GeSn/SiGeSn quantum well sample design and composition information. The thick buffer layers are intended to reduce potential defects in the top active layers.

A comparative study of ion-implantation of As and B in GeSn epilayers grown on Si (001) by chemical vapor deposition.

S. Amoah,[1] G. Abernathy,[1,2] H. Stanchu,[3] W. Du,[1,3] B. Li,[4] S.Q Yu[1,3]

[1]*Department of Electrical Engineering, University of Arkansas, Fayetteville, Arkansas 72701, USA*

[2]*Microelectronics-Photonics Program, University of Arkansas, Fayetteville, Arkansas 72701, USA*

[3]*Institute for Nanoscience and Engineering, University of Arkansas, Fayetteville, Arkansas 72701, USA*

[4]*Arktonics, LLC, 1339 South Pinnacle Drive, Fayetteville, Arkansas 72701, USA*

Recently, direct band gap GeSn alloy semiconductors with Sn concentration above 6-8% have attracted considerable attention as a tunable mid- and near-infrared materials of group IV for light emitting and detection applications with the advantage of monolithic integration on Si substrate and CMOS compatibility [1]. Due to the low miscibility of Sn and Ge, Sn-rich metastable GeSn alloys are typically grown under non-equilibrium conditions, such as by chemical vapor deposition (CVD) and molecular beam epitaxy (MBE). With these techniques, *in-situ* doping is somehow limited, in particular for the fabrication of devices with laterally selected doping regions. Alternatively, *ex-situ* ion implantation is a commonly used process for engineering the structure and precise control of different dopant species in materials.

The poor thermal stability of Sn-rich GeSn materials imposes a low thermal budget for dopant activation. At elevated annealing temperatures, phase separation into thermodynamically favored elemental Ge and β-Sn is ubiquitous. Recently, an annealing study of ion-implantation of As in Ge have shown a 60% substitutional occupation of As atoms in the Ge lattice for annealing temperatures below 200 °C and almost 100% substitutional occupation at higher temperatures [2]. In this work, the implantation of As and B in GeSn epilayers is investigated under different conditions.

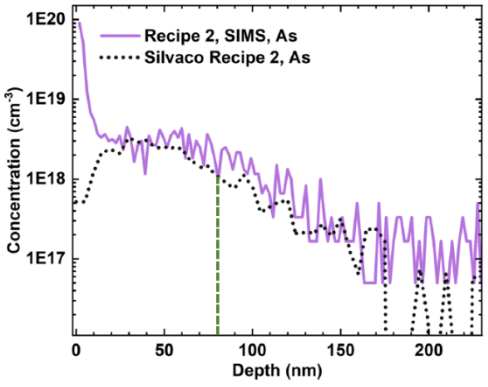

Figure 1 Arsenic doping profile with recipe 1 from SIMS compared with Silvaco simulation.

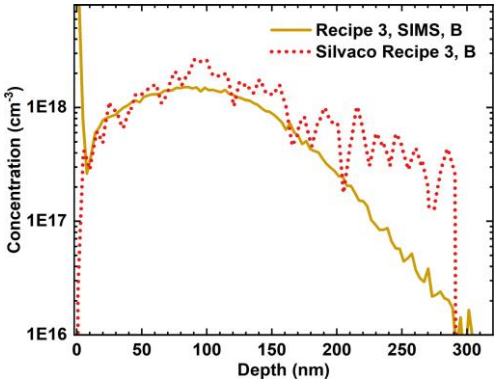

Figure 2 Boron doping profile with recipe 3 from SIMS compared with Silvaco simulation.

[1] K. P. Homewood and M. A. Lourenço, Nature Photonics **9**, 78–79 (2015).
[2] S. Decoster *et al.*, J. Appl. Phys. **111**, 053528 (2012).

+ Author for correspondence: samoah@uark.edu

Suplementary Pages (Optional)

Table 1: Detail of doping parameters for As and B

Recipe #	Dopant	Dose	Energy	Tilt
1	As	2 x 10^{13}/cm^2	150keV	7 degrees
2	B	3 x 10^{13}/cm^2	30keV	7 degrees

The implantation parameters for As and B into GeSn epilayer are shown in table 1. The angle of tilt is to ensure that the dopant elements align to the lattice structure of GeSn for enhanced implantation. For both recipes, the implantation parameters were simulated using Silvaco to achieve a target depth of ~80 nm. At the target depth, the dopant has maximum concentration. After ion implantation, the samples were measured using SIMS. This was to compare the simulated doping profile with the actual. Figure 1 shows a comparison of the simulated versus the SIMS measured doping profile for both recipes. From the plot, it can be seen that the simulated doping profile is commensurate with the actual.

Snowflakes Patterns Formation Enhances Performance of Nanostructure-based MWIR PbSe Photoconductive Detector

Richard S. Kim,[1] Jeung Hun Park,[1] Russ Dahl[1]
[1] *Research and Development, Optodiode, 1260 Calle Suerte, Camarillo, CA 93012*

We present a novel approach to fabricate a PbSe thin film photoconductive detector using the chemical bath deposition technique, resulting in the formation of various snowflakes-like patterns on the active area of the detector. Our findings reveal the presence of clusters of nanostructures, primarily nanoprisms, beneath the snowflakes patterns, which enhance the performance of the PbSe photoconductive detector. This is a new observation that has not been previously reported.

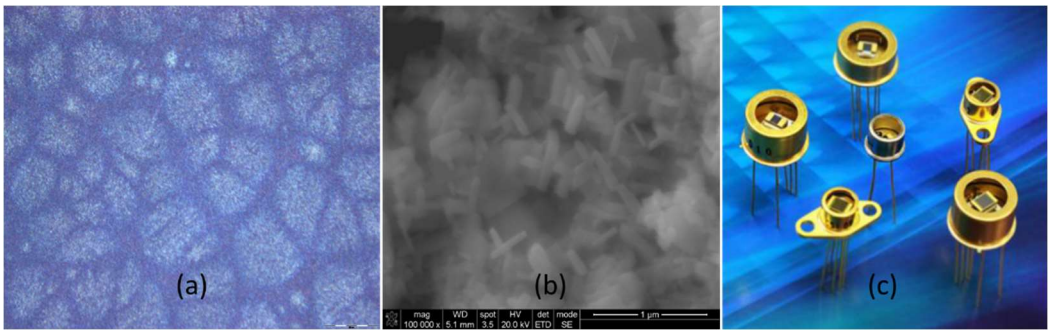

Figure 1(a) shows a micrograph of the snowflakes patterns, while Figure 1(b) shows the formed nanoprisms entangled with each other, which were revealed after etching the oxide phases of the PbSe matrix. Examples of PbSe detectors (www.optodiode.com) fabricated based on such nanostructures are shown in Figure 1(c). It is clear that underneath the snowflakes patterns, many nanoprisms are developed, massively entangled together, and form clusters of nanostructures.

Our investigations have shown that when snowflakes-like patterns appear on the surface of the detector's active region, a large number of PbSe nanostructures are formed within the PbSe thin film. We have also found a strong correlation between the size and compactness of the snowflakes patterns, and thus the nanostructures, and the performance of the PbSe photoconductive detector. As the snowflakes patterns get larger, the detection signal tends to be stronger.

We have examined changes in the microstructure and carrier concentrations resulting from sensitizing treatments such as oxygen and iodine. Our findings suggest that the snowflakes patterns are a direct evidence of the crystallization process. Finally, we have thoroughly examined the FTIR spectral response of the nanostructure-embedded PbSe photoconductive detector at various temperatures ranging from 77K to 340K.

[+] Author for correspondence: rkim@optodiode.com

GaSb-based Interband Cascade Lasers with Hybrid Cladding Layers Operating in the 3-4 µm Wavelength Region

Yixuan Shen,[1] Jeremy A. Massengale,[1,2] Rui Q. Yang,[1,+] Tetsuya D. Mishima,[2] and Michael B. Santos[2]

[1] School of Electrical and Computer Engineering, University of Oklahoma, Norman, OK
[2]Homer L. Dodge Department of Physics and Astronomy, University of Oklahoma, Norman, OK USA 73019.

We report the demonstration of interband cascade lasers (ICLs) [1] with hybrid cladding layers [2-4] in the 3-4 µm wavelength region. These ICLs were grown on GaSb substrates and employed n^+-doped $InAs_{0.91}Sb_{0.09}$ cladding layers and n-doped InAs/AlSb superlattice (SL) intermediate cladding layers. In contrast to a regular ICL with only SL cladding layers, an ICL with the hybrid cladding layers can have an enhanced optical confinement and improved thermal dissipation. A room temperature (RT) threshold current density (J_{th}) as low as 177 A/cm^2 was measured for a broad area device emitting at 3.28 µm (Fig. 1) with pulsed operation extending up to 390 K. The characteristic temperature (T_0) was nearly 60 K, which is the highest value among RT ICLs with similar lasing wavelengths. ICLs from two wafers grown later exhibited a RT pulsed J_{th} as low as 151 A/cm^2 for emission near 3.82 µm (Fig. 2), which is comparable to the best ICLs with only SL cladding layers [5]. Considering the substantial deviations (>10%) in the grown layer thicknesses from the design values, it is expected that ICLs with hybrid cladding layers will have significantly better performance once the growth process is improved. Updated results will be reported at the conference.

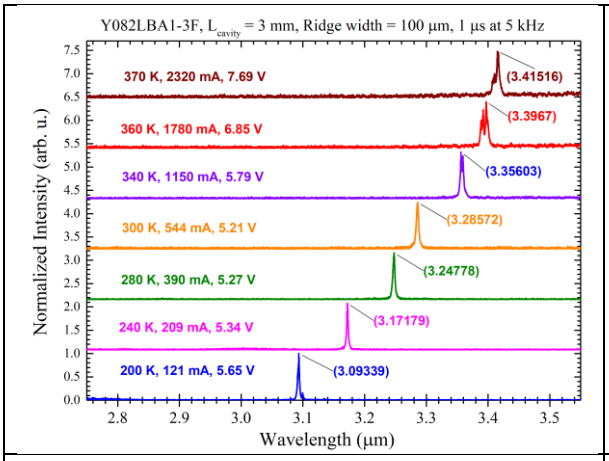

Fig. 1 Pulsed lasing spectra of an ICL from Y082L.

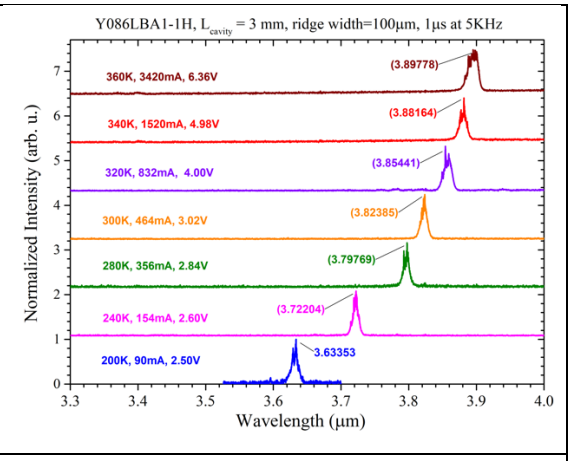

Fig. 2 Pulsed lasing spectra of an ICL from Y086L.

This work was partially supported by NSF (No. ECCS-1931193) and OCAST (AR21-024).

[1] R. Q. Yang, Superlattices Microstruct., **17**, 77 (1995).
[2] L. Li, *et al*., Appl. Phys. Lett. **106**, 251102 (2015).
[3] C. L. Canedy, *et al*. Proc. SPIE **10111**, 101110G (2017).
[4] Y. Lin, *et al*., J. Infrared & Millimeter Waves. **39**, 137 (2020).
[5] J. R. Meyer, *et al*., Photonics **7**, 75 (2020).

[+] Author for correspondence: Rui.q.Yang@ou.edu

16th International Conference on Mid-IR Optoelectronics: Materials and Devices MIOMD-XIV (MIOMD 2023) MIOMD1: Materials Development, Growth, and Characterization for Infrared Optoelectronics

Mirchandani[1]

[1] *Syrnatec Photovoltaic Inc., 95 Pond PL, Middletown, Connecticut 06457-8736, United States*

Halide perovskites have recently attracted significant attention as a promising material for optoelectronic applications due to their high absorption coefficient, long carrier lifetime, and low-cost processing. In particular, $CsPbBr_3$ perovskite has emerged as a promising candidate for infrared optoelectronic applications because of its narrow bandgap and high quantum efficiency. However, the synthesis and growth of high-quality $CsPbBr_3$ perovskites with controlled morphology and crystal structure remains a challenge.

Syrnatec has developed innovative technology for the growth, characterization, and development of halide perovskites. The technology is based on a two-step solution process, which involves the deposition of a precursor film followed by annealing to form the perovskite.

The precursor film was deposited using a novel spin-coating method that utilizes a mixture of $PbBr_2$ and CsBr in dimethyl sulfoxide (DMSO). The deposition was followed by annealing at a temperature of 150°C for 15 minutes to convert the precursor film to the perovskite.

The synthesized $CsPbBr_3$ perovskite was characterized using various techniques such as X-ray diffraction, scanning electron microscopy, and photoluminescence spectroscopy. The X-ray diffraction patterns of the perovskite showed sharp diffraction peaks, indicating excellent crystallinity. The scanning electron microscopy images revealed that the perovskite had a well-defined morphology with a cubic shape. The photoluminescence spectra of the perovskite showed a narrow emission peak at around 510 nm, indicating a narrow bandgap of 2.25 eV and indicative of high quantum efficiency.

The unique technology also enables the control of the crystal structure and morphology of the synthesized $CsPbBr_3$ perovskite. By adjusting the annealing temperature and time, we were able to obtain different crystal structures of the perovskite, including tetragonal and orthorhombic structures. We were also able to control the morphology of the perovskite by varying the concentration of the precursor solution.

Our experiments demonstrated that the synthesized $CsPbBr_3$ perovskite has potential applications in United States optoelectronics. The photodetector showed excellent photoresponse with 23.4% external quantum efficiency and a fast response time of 40ms.

Finally, this proposed technology will be having a potential for the large-scale production of $CsPbBr_3$ perovskite for US infrared optoelectronic applications like solar cells, photodetectors, and light-emitting diodes. The technology will provide a simple and low-cost solution-based approach for the synthesis and growth of high-quality $CsPbBr_3$ perovskite with controlled crystal structure and morphology. The potential of the technology for large-scale production of $CsPbBr_3$ perovskite which makes it a promising candidate for the commercialization of infrared optoelectronics applications in US.

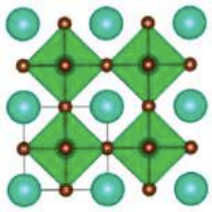

Figure 1: Structure of CsPbBr3

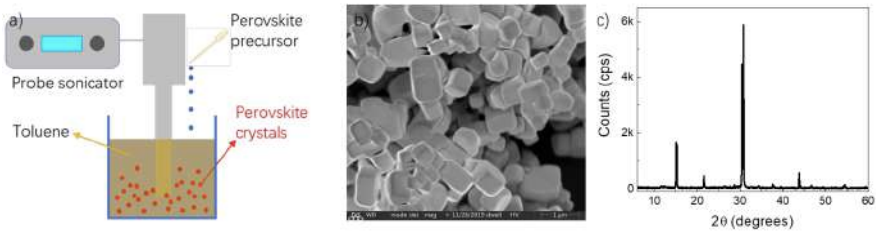

Figure 2: a. Proposed experimental set up for perovskite crystal synthesis, b. SEM image of synthesized CsPbBr3, c. XRD characterization of crystal

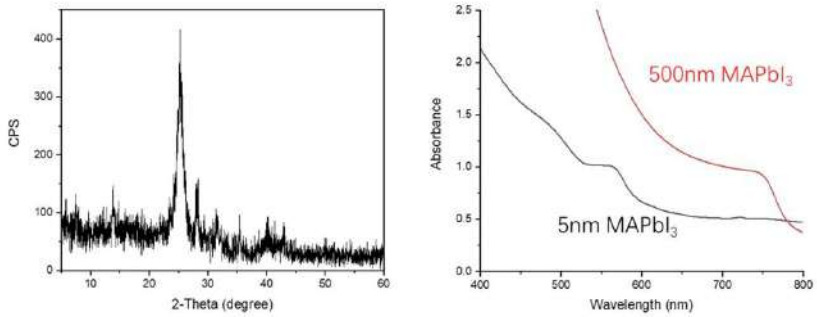

Figure 3: The XRD results. Absorbance spectra shows a significant blue shift from near IR absorption edge (750nm-800nm) to orange-red light wavelength (560nm-600nm), indicating the small size crystals exhibited the "quantum confinement," which occurs usually when crystal size goes below 5nm.

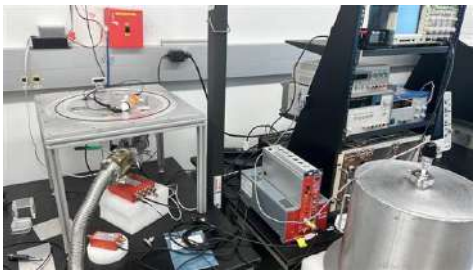

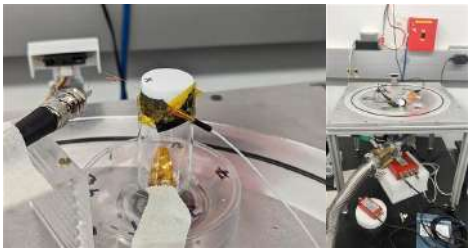

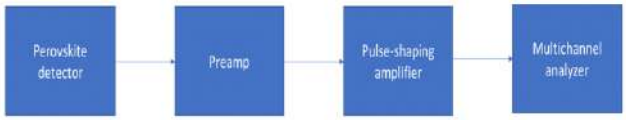

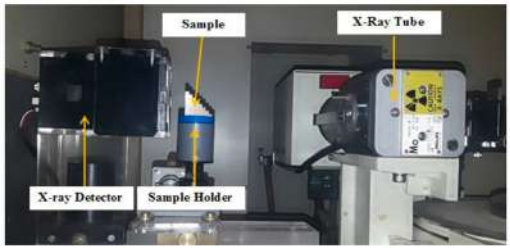

Figure 4: Proposed experimental set up

X-ray Tube Voltage (kV)	Max. X-ray Energy	X-ray Tube Current (μA)
10	10 keV	10, 20, 40, 60, 80, 100, 120, 140, 160, 180, 200
20	20 keV	10, 20, 40, 60, 80, 100, 120, 140, 160, 180, 198
30	30 keV	10, 20, 40, 60, 80, 100, 110, 120, 132
40	40 keV	10, 20, 30, 40, 50, 60, 70, 80, 90, 99
50	50 keV	5, 10, 20, 30, 40, 50, 60, 70, 79

Infrared Endovascular Navigation for Enhanced Sensing and Treatment

D. R. DeVries,[1] M. L. Salter,[1] S. E. Balzora,[1] L. J. Olafsen,[1+] J. S. Olafsen,[1] K. E. Schubert,[1] S. Dayawansa,[2] and J. H. Huang[2]

[1] Baylor University, One Bear Place #97356, Waco, TX 76798, United States

[2] Baylor Scott and White Health, 2401 S. 31st St., Temple, TX 76508 United States

We present recent results toward development of an endovascular navigation system comprised of a programmable surgical wire with infrared (IR) emitters and detectors on the tip. This system is intended for enhanced sensing and medical treatment, particularly for remote treatment sites, including telemedicine. Successful demonstration of this system has the potential to enhance urgent care provided by field surgeons and medics, as well as to open opportunities for remote practitioners minimally to observe and provide expertise and maximally to operate or assist in the field by expertly guiding the wire. The proposed device has great potential (1) to enable imaging and sensing deeper in the head and body, (2) to increase the sensitivity of infrared measurements of biomarkers, (3) to result in more efficient and safer navigation of catheters and surgical instruments for treatment of aneurysms and other endovascular procedures, especially in remote settings, and (4) to reduce exposure of patient and surgeon to harmful radiation by employing ultrasound or infrared imaging techniques. This endovascular device uses wire made of a shape-memory alloy, such as Nitinol, to navigate arteries for treatment. Nitinol has prior FDA approval and a long record of biocompatibility, especially when an oxide and/or another passivating layer is applied. The wire is programmed to bend at temperatures above core body temperature and navigate arterial branches using current control. Blind navigation of wires by physical pushing can result in rupture of vessel walls with lethal consequences. Stents have been used to deploy deep brain stimulation devices, but no deep system for *in vivo* near-infrared spectroscopy exists. The ability to effectively insert and guide an infrared emitter to the brain for neurological monitoring and treatment would be of significant benefit in the operating room, particularly during cardiothoracic surgery or neurosurgery.

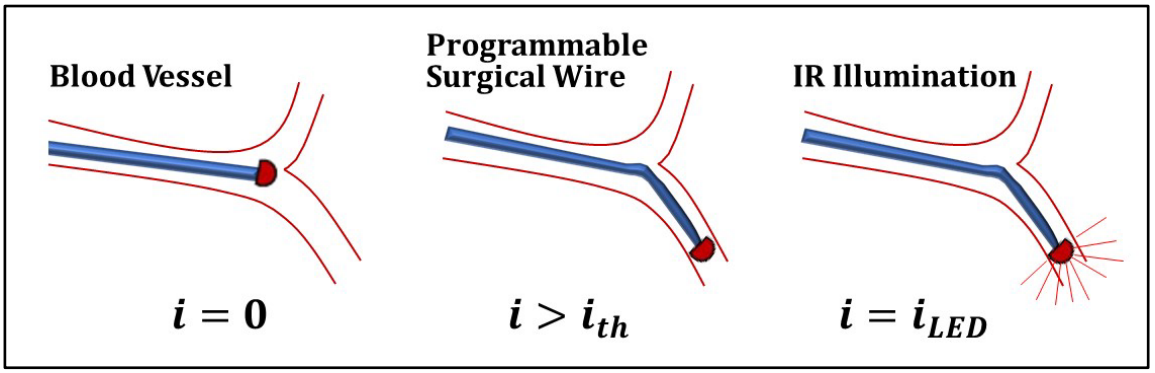

Figure 1 Current-controlled endovascular navigation and IR sensing using a programmable surgical wire comprised of a shape-memory alloy.

[+] Author for correspondence: Linda_Olafsen@baylor.edu

Residual Gas Analysis of Reactions between Germane and Tin Tetrachloride for the Optimization (Si)GeSn CVD Growth

J. Grant,[1] E. Yang,[1] A. Golden,[2] W. Du,[1,3] B. Li,[4] and S.-Q. Yu, [+,1,3]
[1]Department of Electrical Engineering, University of Arkansas, Fayetteville, AR 72701 USA
[2]Material Science and Engineering Program, University of Arkansas, Fayetteville AR 72701 USA
[3]Institute for Nanoscience and Engineering, University of Arkansas, Fayetteville, AR 72701 USA
[4]Arktonics LLC, 1339 S. Pinnacle Dr., Fayetteville, AR 72701 USA

Since the introduction of (Si)GeSn alloys to the world of semiconductors for silicon based photonic applications, the material has become highly desired for both detectors and sources [1]. By capitalizing on the ability to tailor the band gap of the material by varying the Sn content, transforming an indirect bandgap material to a direct, holds great potential for Near to Mid-IR wavelength photonics. The growth of GeSn for devices and material study has been performed by Molecular Beam Epitaxy (MBE) and Chemical Vapor Deposition (CVD), with Plasma-enhanced Chemical Vapor Deposition (PECVD) and its low thermal requirements [2, 3] gaining popularity. The CVD growth of GeSn has been performed using the commercially available precursors Tin tetrachloride (SnCl4) and Germane (GeH4) [4]. To better understand the growth mechanisms of GeSn on a Si (100) substrates using $SnCl_4$ and GeH_4 during the CVD process. Reactions between the two precursors was studied utilizing a differential pumping system for a 300 amu Residual Gas Analyzer (RGA) that was isolated from the CVD reactor. The focus of this talk will be to present the most recent findings from the mass spectra of the interactions between the two precursors.

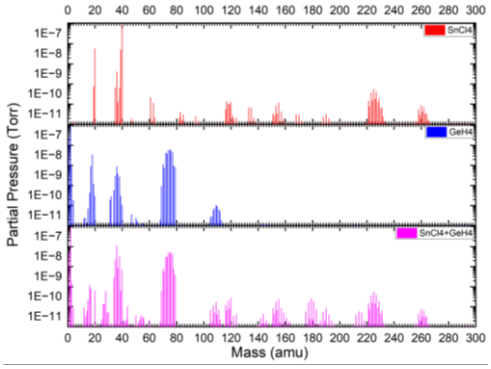

Figure 1: Plot from RGA of $SnCl_4$ (top), GeH_4 (middle), and the combined precursors (bottom).

[1] S.-Q. Yu, G. Salamo, W. Du, B. Li, G. Sun, R. A. Soref, Y.-H. Zhang, and G.-E. Chang., 2022 Device Research Conference (DRC), 1-2(2022).
[2] W. Dou, B. Alharthi, P. C. Grant, J. M. Grant, et al., Optical Materials Express, **8**(10),3220-3229(2018.)
[3] B. Clain, G.J. Grzybowski, M.E. Ware, S. Zollner, and A.M. Kiefer., Frontiers in Materials, 7-44, 2020.
[4] S. Al-Kabi, S. A. Ghetmiri, J. Margetis, et al., Journal of Electronic Materials,**45**,6251-6257(2016).

[+] Author for correspondence: syu@uark.edu

Low Temperature Plasma Enhanced Growth of $Si_{1-x}Sn_x$ by Chemical Vapor Deposition

A. Golden,[1] J. Grant,[2] E. Yang,[2] S. Acharya,[1] S.Q. Yu[2]
[1] *Material Science & Engineering, University of Arkansas, Fayetteville, AR 72701, USA*
[2] *Department of Electrical Engineering, University of Arkansas, Fayetteville, AR 72701, USA*

Thin films of Silicon-tin alloys ($Si_{1-x}Sn_x$) were grown on Si (001) substrate using low temperature plasma-enhanced chemical vapor deposition. These alloys have potential in the application of optoelectronic devices however their growth conditions have not been studied as thoroughly as similar GeSn materials [1]. Precursors like silane have a high breakdown temperature compared to the CMOS process and the solid solubility of Sn in Si is very low and is further complicated by segregation at higher temperatures. Therefore, the growth mechanism of $Si_{1-x}Sn_x$ needs to be better understood [2]. The thin film growth of $Si_{1-x}Sn_x$ in this work was accomplished by adjusting plasma intensity and controlling the precursor flow fractions. The film thickness was measured by Spectroscopic Ellipsometry, and the Sn incorporation and crystallinity were estimated using X-ray Diffraction measurements. In particular, an increase of Sn composition in the $Si_{1-x}Sn_x$ epilayers was concluded by observing the migration of the (004) peak towards the lower angles on the X-ray diffraction 2θ/ω scans, Figure 1, which corresponded to an overall improvement of Sn incorporation of more than 10% relative to the previous work. Moreover, a significant enhancement in material quality was concluded by comparing the line widths (FWHM) of the SiSn peak to those reported previously [3].

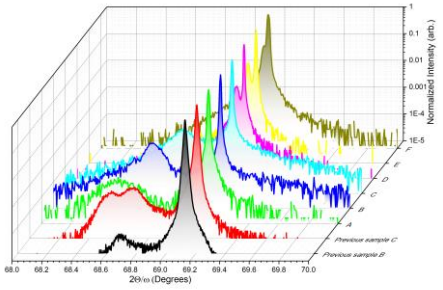

Figure 1: Normalized XRD 2θ/ω scans along the (004) plane. Previous growths are compared with recent growths.

1. M. A. Alher, A. Mosleh, L. Cousar, W. Dou, P. Grant, S. A. Ghetmiri, S. Al-Kabi, W. Du, M. Benamara, and B. Li, “CMOS Compatible Growth of High Quality Ge, SiGe and SiGeSn for Photonic Device Applications,” ECS Trans. **69**(5), 269–278 (2015).
2. J. Tolle, A. Chizmeshya, Y. Fang, J. Kouvetakis, V. D’Costa, C. Hu, J. Menendez, and I. Tsong, “Low temperature chemical vapor deposition of Si-based compounds via SiHSiHSiH: Metastable SiSn/ GeSn/ Si (100) heteroepitaxial structures,” Appl. Phys. Lett. **89**(23), 231924 (2006).
3. Seyedeh Fahimeh Banihashemian, Joshua M. Grant, Abbas Sabbar, Huong Tran, Oluwatobi Olorunsola, Solomon Ojo, Sylvester Amoah, Mehrshad Mehboudi, Shui-Qing Yu, Aboozar Mosleh, and Hameed A. Naseem, "Growth and characterization of low-temperature $Si_{1-x}Sn_x$ on Si using plasma enhanced chemical vapor deposition," Opt. Mater. Express 10, 2242-2253 (2020).

+ Author for Correspondence: syu@uark.edu

Long wavelength distributed feedback tapered quantum cascade lasers

Davide Pinto[1,2], Kumar Kinjalk[2], Ariane Meguekam[2], Michael Bahriz[2], Bernhard Lendl[1] and Alexei N. Baranov[2]

[1] *Institute of Chemical Technologies and Analytics, Technische Universität Wien, Getreidemarkt 9/164, 1060 Vienna, Austria*

[2] *Institute of Electronics and Systems, UMR 5214 CNRS – Université de Montpellier, 34095 Montpellier, France*

We present an investigation of tapered QCLs with taper angles between 0° and 3°. Tapered cavities benefit from bigger active zone volume, preserving the beam quality of the fundamental transverse mode [1]. The QCL was based on the InAs/AlSb material system emitting around 14-15 µm [2], where BTEX compounds exhibit strong absorption, making such laser source interesting for sensing applications. The active zone is composed of an InAs/AlSb superlattice sandwiched between undoped InAs spacers and highly-doped InAs cladding layers. The wafer grown by MBE on an InAs substrate was processed into deep mesa ridge lasers using optical photolithography and wet chemical etching. E-beam lithography and dry etching were employed to pattern Bragg gratings on top of the ridge waveguide, for single longitudinal mode operation. A gold layer was deposited to provide electrical contact.

In Fig. 1(a) a scanning-electron microscope image of the tapered devices is shown. The devices were tested and compared in terms of electrical and optical properties, and in terms of spectral purity. Single-longitudinal mode operation was obtained, with a side-mode suppression ratio (SMSR) greater than 15 dB. In Fig. 1(b), emission spectra of a straight QCL, measured at different temperatures in CW operation, are portrayed. In Fig. 1(c) voltage-light-current characteristics of the tapered devices are shown. Tapers with wider angles provide a greater power output. The different improvement of the slope efficiency is observed, which can be justified by the higher collection efficiency of the system towards higher taper angle devices. The larger front facet of tapered lasers reduces the divergence angle along the slow axis, allowing to collect more light. The far-field intensity profiles were measured in order to determine the beam divergence and estimate the devices brightness.

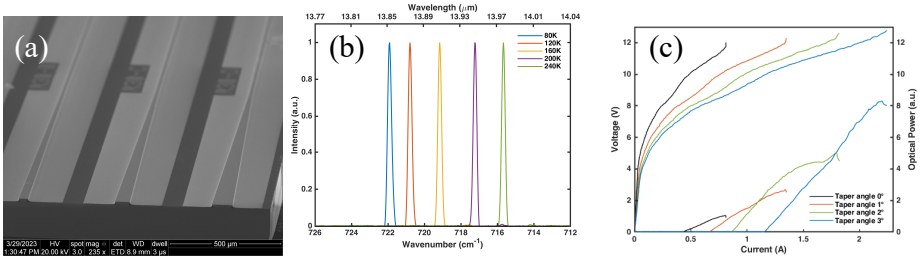

Figure 1. (a) Electron microscope image of the DFB - tapered QCLs. (b) Representative straight single mode DFB CW-spectra, with a SMSR greater than 15 dB. (c) Voltage-Light-Current curves for tapered devices, from 0° to 3° taper angles.

[1] L. Nähle, J. Semmel, W. Kaiser, S. Höfling, and A. Forchel, Applied Physics Letters 91, 181122 (2007).
[2] K. Kinjalk, D. A. Díaz-Thomas, Z. Loghmari, M. Bahriz, R. Teissier, and A. N. Baranov, Photonics 9, 747 (2022).

+ Author for correspondence: davide.pinto@tuwien.ac.at

Low-Loss Plasmonic Resonances in Heavily Doped InAs for Infrared Optoelectronic Integration

E.D. Caudill,[1] C.G. Cailide,[1] M.A. Lloyd,[2] J.P. Murphy,[2] K.E. Arledge,[1] T.D. Mishima,[1] J.A. Nolde,[2] J.A. Frantz,[2] C.T. Ellis,[2] P. Weerasinghe,[3] T.D. Golding,[3] M.B. Santos,[1] J.G. Tischler [1]

[1] The University of Oklahoma, 660 Parrington Oval, Norman, OK, 73019
[2] U.S. Naval Research Laboratory, 4555 Overlook Ave SW, Washington, DC, 20375
[3] Amethyst Research Incorporated, 5738 Huettner Court, Norman, OK, 73069

Plasmonic resonances supported by traditional metals (e.g., gold, silver, and aluminum) have been used to enhance optoelectronic devices such as emitters and detectors.[1] However, these materials are very lossy in the infrared region, hindering their use in actual devices that operate in the infrared.[2] To overcome this issue, we use doped III-V semiconductors as a low-loss plasmonic material that can be easily integrated with traditional III-V infrared optoelectronic devices. Here we show that an InAs epilayer, when highly-doped with Tellurium (up to 10^{20} cm^{-3}), exhibits a plasma frequency corresponding to light at a free-space wavelength of 4.5 μm. When a 1D grating with a period shorter than 5 μm is formed in the epilayer via dry etching, resonances at longer wavelengths (5.5 to 14 μm) are observed with quality factors around 7 and absorption as high as 95%. Finite element electromagnetic models of the resonances show good agreement with our experimental results. This material is based upon work supported by the Office of the Undersecretary of Defense for Research and Engineering Basic Research Office STTR under Contract No. W911NF-21-P-0024. Disclaimer: The content of the information does not necessarily reflect the position or the policy of the Government, and no official endorsement should be inferred.

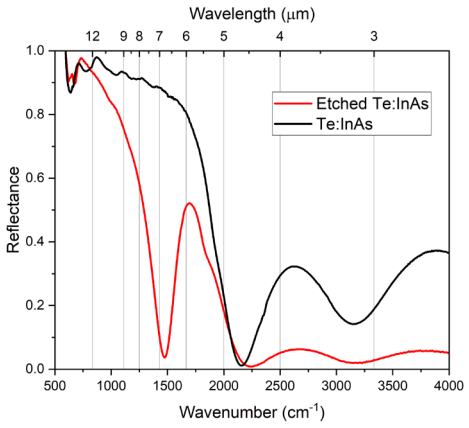

Figure 1: Plasmon Creation

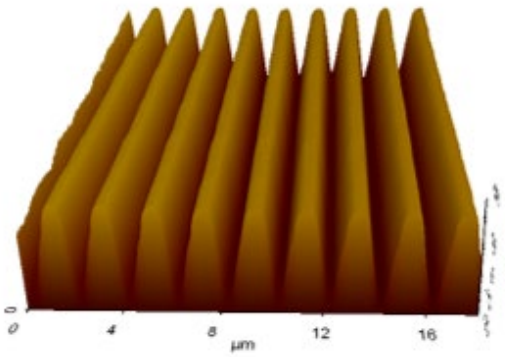

Figure 2: AFM Images

[1] J.A. Nolde et al., "Resonant quantum efficiency enhancement of midwave infrared nBn photodetectors using one-dimensional plasmonic gratings", Appl. Phys. Lett. **106**, (2015) 261109

[2] N. Kinsey et al., "Near-Zero-Index Materials for Photonics", Nature Materials **4** (2019) 742

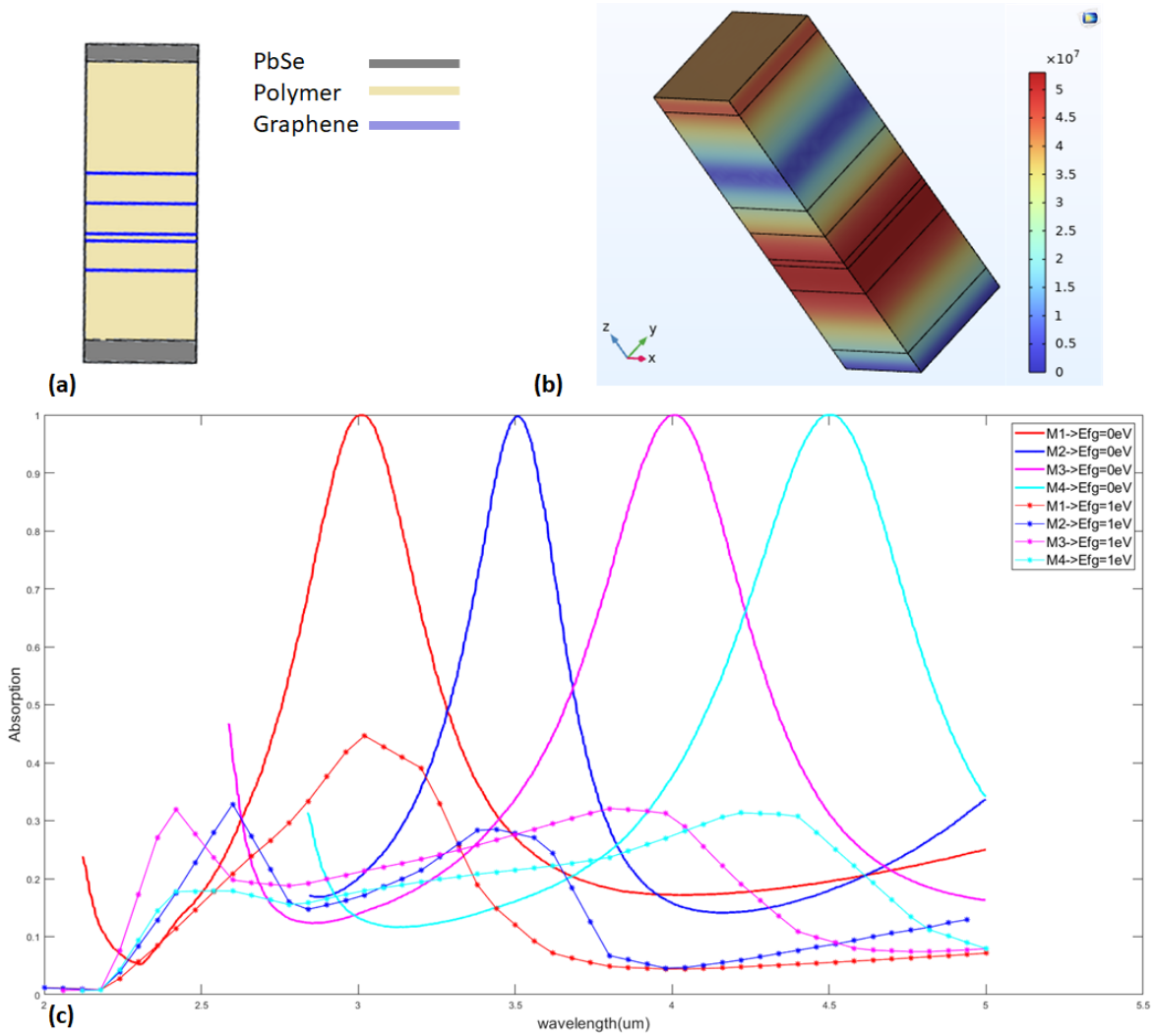

Figure 1(a) schematic of the proposed nanophotonic multilayer structure with emphasize of the material and thickness. (b) electromagnetic wave of the structure at wavelength 3 um and zero electric field at graphene layers. (c) shows the switchability of four different optimized structure with narrowband absorption at 3(um), 3.5 (um), 4 (um) and 4.5(um) at zero electric field and 1 (ev) electric field at graphene layers.

Reference:

[1] A. K. Chowdhary, V. A. Reddy, and D. Sikdar, "Nanophotonics-enabled high-efficiency selective solar absorbers for waste heat management," *IEEE Transactions on Nanotechnology,* vol. 21, pp. 131-136, 2022.

[2] M. S. Asad, "Planar Multilayer Thin Film Coatings for Passive Winter Thermal Management," Queen's University (Canada), 2021.

[3] H. Chen, C. Wang, H. Ouyang, Y. Song, and T. Jiang, "All-optical modulation with 2D layered materials: status and prospects," *Nanophotonics,* vol. 9, no. 8, pp. 2107-2124, 2020.

[4] S. Sharifi, Y. M. Banadaki, V. Nezhad, G. Veronis, and J. Dowling, "Aperiodic multilayer graphene based tunable and switchable thermal emitter at mid-infrared frequencies," *Journal of Applied Physics,* vol. 124, no. 23, 2018.

[5] L. Falkovsky and S. Pershoguba, "Optical far-infrared properties of a graphene monolayer and multilayer," *Physical Review B,* vol. 76, no. 15, p. 153410, 2007.

[6] P.-Y. Chen and A. Alu, "Atomically thin surface cloak using graphene monolayers," *ACS nano,* vol. 5, no. 7, pp. 5855-5863, 2011.

Coherent control of Quantum Cascade Laser Frequency Combs via Optical- and RF-injection

Gerard Wysocki
Electrical and Computer Engineering Department, Princeton University, Princeton, NJ, 08544, USA

Quantum cascade laser (QCL) frequency combs are compact, all-electrically driven, broadband semiconductor laser sources operating in the mid-infrared spectral region that give access to fundamental vibrational bands of many molecular species of environmental and industrial importance. These lasers are being extensively used to perform dual-comb spectroscopy (DCS) and sensitive molecular sensing with high temporal resolution. However, unlike the metrological-grade frequency combs based on mode-locked lasers, free-running QCL-combs are susceptible to intrinsic phase and intensity noise, which makes applications to high-resolution spectroscopy relatively difficult. In this talk I will discuss techniques utilizing external cavity optical feedback injection as well radio-frequency (RF) electrical signal injection to achieve improved comb coherence for dual-com spectroscopy, as well as generate higher-order harmonic QCL comb-states with improved coherence and broader optical bandwidth. Experimental results demonstrating independent control of primary comb parameters (offset frequency , f_0, and repetition rate frequency, f_{rep}) via optical- and RF-injection, resulting in MHz-level frequency control and gapless DCS tuning, will be discussed in details.

[+] Author for correspondence: gwysocki@princeton.edu

Compact QCL-based coherent LiDAR in the mid-infrared

B. Martin[1, 2], Patrick Feneyrou[3], Nicolas Berthou[1], Djamal Gacemi[2], Aude Martin[3], Carlo Sirtori[2]

[1] Thales SIX France,4 av.des Louvresses, Gennevilliers, France
[2]Laboratoire de physique de l'Ecole normale supérieure, 24 rue Lhommond, Paris, France.
[3]Thales research and technology, 1 avenue Augustin Fresnel, Palaiseau, France

Frequency-modulated continuous-wave light detection and ranging (FMCW LiDAR) is a technique for fast and precise measurements of distances and speeds of hard and diffuse targets [1]. Moreover, the effects of feedback reinjection on the laser parameters, such as the optical power, wavelength or voltage can be utilized for numerous sensing applications [2]. We show the first experimental demonstration of a FMCW LiDAR in the mid-infrared, based on a novel self-mixing interferometry technique and compare it with a conventional mid-infrared FMCW system. Thanks to an injection current predistortion technique, high-speed and precise linear optical frequency modulation (LFM) up to 8 GHz in 1µs with less than 1% error to linearity is achieved, allowing a greater FMCW signal-to-noise ratio.

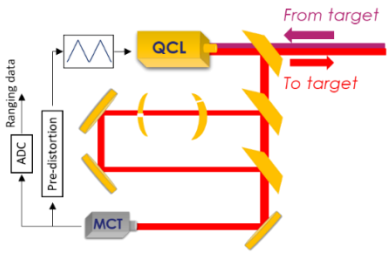

Figure 1 – Experimental setup of the Self-mixing interferometry LiDAR

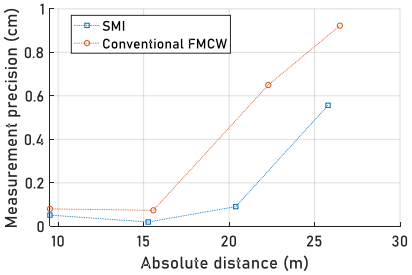

Figure 2 – Absolute distance measurements precision results

One part of the beam (> 90%) is sent to a target in order to perform distance & speed measurement. In the absence of optical isolation, a part of the reflected light will come back inside the laser cavity, interfering with the intracavity field. The changes induced simultaneously on the optical power and frequency are monitored on a photodiode at the output of the interferometer. More specifically, the measurement of the periodic perturbation on the LFM allows for speed and distance measurement, without adding any new components to the LFM system. Taking advantages of intrinsic high-speed dynamics of mid-infrared unipolar sources and detectors, we achieved kHz-rate sub-cm precision measurement of low-reflective targets at distances up to 25 m. Such results pave the way to systems more robust against meteorological perturbations and with an improved discreetness. Moreover, the overall compactness and robustness of the optical setup constitute a leap toward the development of mid-infrared quantum optoelectronic devices and their integration into components.

[1] Feneyrou, P., et al. "Frequency-modulated multifunction lidar for anemometry, range finding, and velocimetry–1. Theory and signal processing." Applied optics 56.35 (2017): 9663-9675 [2] P. R. Wallace, Phys. Rev. **71**, 622(1947).
[2] Rakić, A. D., et al. "Sensing and imaging using laser feedback interferometry with quantum cascade lasers." Applied Physics Reviews 6.2 (2019): 021320

Method

Measurement of absolute distance by swept-frequency self-mixing interferometry has been previously demonstrated with quantum cascade lasers in the THz and short-infrared ranges [3]. The method usually consist in sweeping the frequency of the laser by modulating the injection current with a triangle-shaped waveform, and measuring the changes in the QCL voltage. However, the intrinsic inertia of the thermal effects behind the optical frequency modulation induce a non-linear optical frequency waveform, reducing the signal-to-noise ratio (SNR) or giving rise to intricate compensation algorithms. Furthermore, the measurement technique is only sensitive to the laser diode voltage variations. In this paper, we use a predistortion algorithm to linearly sweep the frequency of the laser, enhancing the FMCW SNR [1]. Moreover, we sense the speed and distance of the target by directly measuring the periodic perturbations induced simultaneously on the optical power and frequency by means of an intensity measurement at the output of an interferometer. Therefore, one single signal is used both to monitor/correct the optical frequency chirps and to measure the effect of the feedback from the target on the laser. This way, we benefit from the stability and high signal-to-noise ratio of the coherent interferometric measurement without adding any complexity to the setup. The technique is illustrated in Fig. 3 & 4, where the blue signal correspond to the voltage on the photodiode at the output of the interferometer when no light is reinjected. In this case, the linear frequency chirps are monitored and adequately corrected. The orange curves correspond to the signal when light reflected from the target is reinjected into the laser. The frequencies of the perturbations on the optical frequency chirps, highlighted in Fig. 4, can be directly utilized to measure the speed and distance of the target.

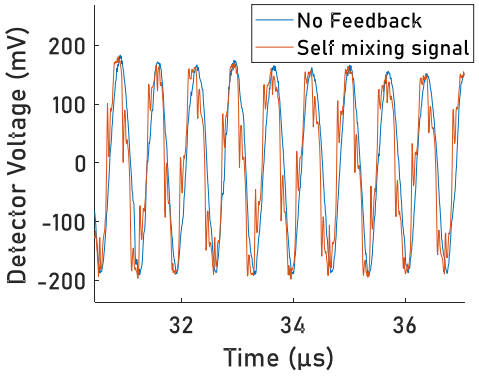

Figure 3 – Time signal of the interference fringes at the output of the interferometer

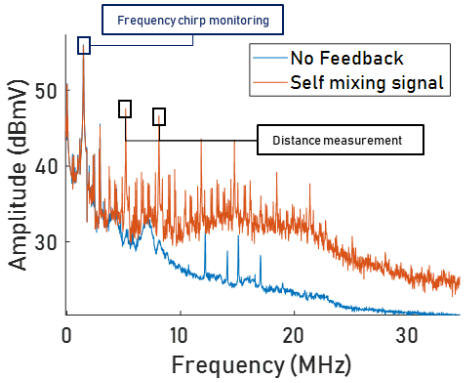

Figure 4 – Spectrum of the interferometer output

Finally, this technique rely on the physical self-mixing model both for high and low feedback ratio. In this way, the system is relevant for distance and speed measurement of low reflective and long distance targets, as shown within the experimental demonstration developed in the next section.

[3] J. Keeley., et al, "Three-dimensional terahertz imaging using swept-frequency feedback interferometry with a quantum cascade laser," Opt. Lett. 40, 994-997 (2015)

A Markov Chain Approach for Modeling Polarized Infrared Radiative Transfer in Optically Anisotropic Media

Feng Xu[1], W. Reed Espinosa[2], Olga V. Kalashnikova[3], Anthony B. Davis[3], David J. Diner[3], Michael J. Garay[3], Jie Gong[2], Benting Chen[1], Lan Gao[1], Jens Redemann[1], and Zhao-Cheng Zeng[4]

[1] School of Meteorology, The University of Oklahoma, Norman, USA
[2] NASA Goddard Space Flight Center, Greenbelt, MD, United States, USA
[3] Jet Propulsion Laboratory, California Institute of Technology, Pasadena, USA
[4] Division of Geological and Planetary Sciences, California Institute of Technology, Pasadena, USA

The polarization state of atmospheric radiation contains abundant information about aerosol and cloud particle properties. To assist in the combined use of reflected and emitted radiation for dust and cloud remote sensing, we developed a Markov chain approach to model polarized infrared radiative transfer in an optically isotropic or anisotropic medium (e.g. Earth atmosphere). A multi-steam scheme is adopted to resolve the angular dependence of total radiance and polarized radiance. Our model accounts for atmospheric emission, scattering, and absorption, as well as directional surface emission and reflection. Non-spherical particles with random and preferred orientations are considered. Simulation is performed for three reference Earth atmospheres (mid-latitude summer, sub-arctic winter, and tropical) which contains dust particles, water droplets, and ice particles of preferred or random orientations. These reference atmospheres overly an ocean or a land surface which contributes both surface emission and reflection. The numerical simulation shows a) remarkable impact of particle orientations, non-sphericities, and the linear and circular polarization components of infrared extinction matrix on the infrared polarimetric signals. By contrast, the infrared radiances are much less impacted.

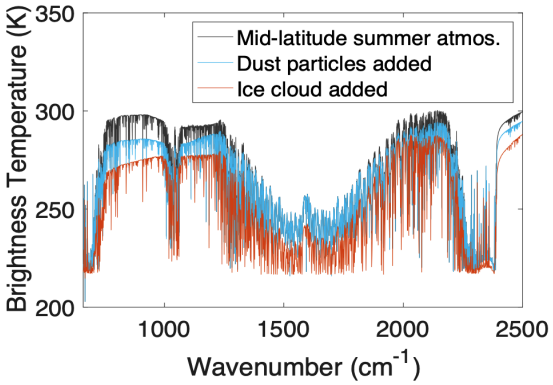

Figure 1 Sensitivity of Infrared Brightness Temperature to Dust and Ice Cloud

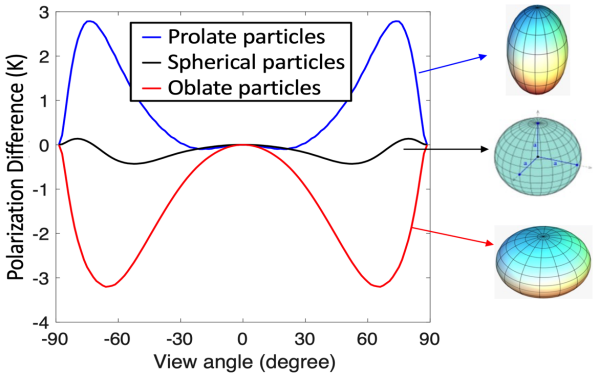

Figure 2 Sensitivity of Polarization Difference to Atmospheric Dust Particle Shape (1000cm^{-1})

+Author for correspondence: fengxu@ou.edu

Mid-infrared trace gas detection enhanced by tuning fork, optical cavity and hollow-core fiber

Wei Ren

[1] *Department of Mechanical and Automation Engineering, The Chinese University of Hong Kong, Shatin, N.T., Hong Kong*

Mid-infrared trace gas detection plays a significant role in many sectors such as energy systems, transportation, environmental monitoring, agriculture, safety, and security. With quantum cascade laser (QCL) and interband cascade laser (ICL) used as the light source, it is promising to develop high-resolution mid-infrared laser-based spectrometers with a portable size and low power consumption. Photoacoustic spectroscopy (PAS) and photothermal spectroscopy (PTS) are two highly sensitive methods for chemical analysis by detecting the absorption-induced acoustic wave and refractive index change, respectively. However, there is still room for improvement compared to the most sensitive spectroscopic techniques such as cavity ring-down spectroscopy (CRDS) or noise-immune cavity-enhanced optical-heterodyne molecular spectroscopy (NICE-OHMS).

In this talk I will discuss recent advances in the development of ultra-sensitive PAS enhanced by tuning fork and optical cavity, as well as PTS enhanced by hollow-core fiber and phase-sensitive interferometry. PAS signal is proportional to the overall incident laser power (W). The most recent innovation of PAS with a double opto-acoustic resonance enables ultra-sensitive and wide-dynamic-range gas detection [1]. The merging of a high-Q-factor acoustic resonator (i.e., quartz tuning fork) with a high-finesse optical resonator leverages on a double standing wave effect. By using a mW-level QCL, the doubly resonant QEPAS sensor demonstrates ppt-level CO detection in the mid-infrared. In comparison, PTS signal is proportional to the light power density (W/m^2), which can be readily achieved in a hollow-core fiber [2]. By taking advantage of mid-infrared fiber technology, I will present our recent innovation of mid-infrared-pump near-infrared-probe PTS for trace gas sensing [3-5]. The variation of refractive index caused by the pump-laser can be sensitively detected by agile interferometric methods such as the Mach-Zehnder interferometer, heterodyne interferometer, Fabry-Pérot interferometer, and fiber mode interferometer.

[1] Z. Wang, Q. Wang, H. Zhang, S. Borri, I. Galli, A. Sampaolo, P. Patimisco, V. L. Spagnolo, P. D. Natale, and W. Ren, Photoacoustics **27**, 100387 (2022).
[2] W. Jin, Y. Cao, F. Yang, and H. L. Ho, Nat. Commun. **6**, 6767 (2015).
[3] Z. Li, Z. Wang, F. Yang, W. Jin, and W. Ren, Opt. Lett. **42**, 3718 (2017).
[4] C. Yao, S. Gao, Y. Wang, W. Jin, and W. Ren, Sens. Actuators B Chem. **346**, 130528 (2021).
[5] M. Hu, A. Ventura, J. Hayashi, F. Poletti, and W. Ren, J. Light. Technol. **40**, 6568 (2022).

[+] Author for correspondence: renwei@cuhk.edu.hk

Highly Selective Toluene Detection using Quartz Enhanced Photoacoustic Spectroscopy at λ = 13.71 µm

Kumar Kinjalk[1,2], Giansergio Menduni[2], Andrea Zifarelli[2], Marilena Giglio[2], Roland Teissier[3], Alexei N. Baranov[1], Angelo Sampaolo[2]

[1]IES, University of Montpellier, CNRS, 34095 Montpellier, France

[2]PolySense Lab, Dipartimento Interateneo di Fisica, University and Politecnico of Bari, Bari, Italy

[3]MirSense, 34095 Montpellier, France

Among anthropogenic and natural volatile organic compounds (VOCs), benzene, toluene, ethylbenzene, and xylene isomers (commonly called BTEX) are the main sources of air pollution. The World Health Organization has classified BTEX compounds as highly aggressive cancer-causing agents, and therefore there is a high interest in developing efficient techniques for their detection.

Although optical sensors proved high performances in terms of sensitivity and selectivity, there is a lack of suitable sources emitting in the 13-15 µm wavelength range, where BTEX exhibits strong absorption features. This work demonstrates a custom-built InAs-based QCL operating at 13.71 µm and its employment in a quartz enhanced photoacoustic spectroscopy (QEPAS) sensor for detecting toluene. The fabricated QCL allowed the excitation of the absorption lines of toluene at 729.39 cm^{-1} (see Fig 1). The QEPAS sensor employs a quartz tuning fork (QTF) excited by sound waves generated via a photoacoustic effect to detect gas traces. The QTF has a fundamental resonance frequency of $f_0 = 12.457\ kHz$ and a quality factor $Q = 22{,}197$ at $200\ Torr$. A 2f-wavelength modulation detection scheme is implemented by modulating the QCL current with a frequency of $f_0/2$ and acquiring the f_0 component of the QTF using a lock-in amplifier [1]. Starting from the obtained calibration curve and the measured noise level, a minimum detection limit of 592 ppb at 0.1s of integration time is achieved. Using the Allan deviation analysis, a detection limit of 150 ppb can be obtained at 10 s of integration time (see Fig 2). Furthermore, the study of gas mixtures revealed no spectral interference from benzene or ethylbenzene (see Fig 3).

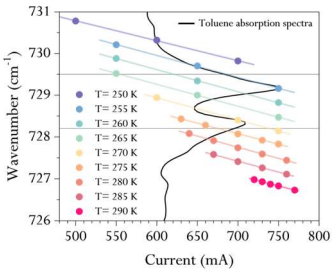

Fig. 1 Wavenumber as a function of current at different temperatures.

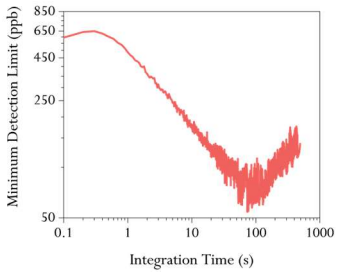

Fig. 2 Minimum detection limit as a function of Integration time.

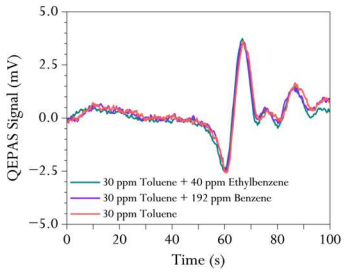

Fig. 3 QEPAS signal of toluene in different gas mixtures.

[1] A. Sampaolo et al., "Quartz-enhanced photoacoustic spectroscopy for multi-gas detection: A review," Anal Chim Acta, vol. 1202, p. 338894, Apr. 2022, doi: 10.1016/j.aca.2021.338894

+ Author for correspondence: kumar.kinjalk@umontpellier.fr

Quartz enhanced photoacoustic spectroscopy exploiting beat frequency approach for environmental monitoring of pollutants

G. Menduni,[1+] B. Li, [1,2,3] A. Zifarelli, [1] M. Giglio,[1] A. Sampaolo,[1] P. Patimisco, [1] H. Wu,[1,2,3] T. Wei, [1,2] L. Dong,[1,2,3] V. Spagnolo[1]

[1] *PolySense Lab - Dipartimento Interateneo di Fisica, University and Politecnico of Bari, Bari 70125, Italy*

[2] *State Key Laboratory of Quantum Optics and Quantum Optics Devices, Institute of Laser Spectroscopy, Shanxi University, Taiyuan 030006, China*

[3] *Collaborative Innovation Center of Extreme Optics, Shanxi University, Taiyuan 030006, China*

Fast and accurate monitoring of pollutant gases in the environment is critical to safeguard public health. Among different sensing solutions, quartz enhanced photoacoustic spectroscopy (QEPAS) is a highly sensitive optical technique, implementing quartz tuning forks (QTFs) to convert sound waves, produced by gas molecules when modulated light is absorbed, into an electric signal. The slow signal acquisition speed depends on the long scan time of the gas absorption feature, requiring few minutes. Furthermore, the real-time monitoring of the QTF resonance frequency (f_0) and quality factor (Q) cannot be carried out during the laser tuning range scan. In this work, the beat frequency-QEPAS (BF-QEPAS) approach [1] was employed to both overcome these limitations and detect NO, using an interband cascaded laser emitting at a central wavelength of 5.263 μm and a 12.4 kHz custom QTF. In BF-QEPAS, a staircase ramp with a rising time of ~1s and a sinewave detuned with respect to f_0 allow exciting the QTF with an acoustic pulse. Considering the BF-QEPAS signal shown in Figure 1 [1], i) the gas concentration is retrieved from the value of P1, ii) f_0 is measured from the time difference between the five peaks, and iii) Q is determined by the decay time, evaluated with an exponential fit of the five peaks. We achieved a minimum detection limit and a normalized noise equivalent absorption of 180 ppb at 5 ms of the lock-in time constant and $2.5 \cdot 10^{-9}$ $cm^{-1}WHz^{-1/2}$, respectively. Furthermore, the BF-QEPAS signal allows determining the f_0 with an accuracy of 0.1 Hz and the Q with a relative error of ~1%.

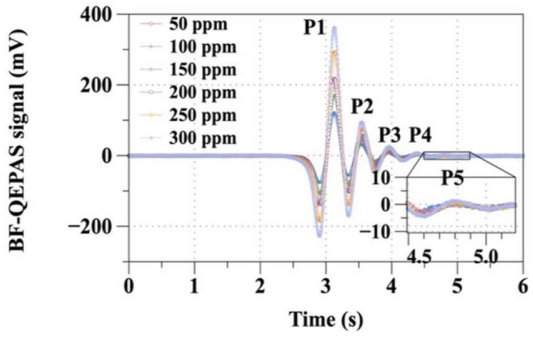

Figure 1 BF-QEPAS spectral scans measured for different NO concentrations in standard air [1].

[1] B. Li, G. Menduni, M. Giglio, et al., Photoacoustics, 100479 (2023), In press.

[+] Author for correspondence: giansergio.menduni@poliba.it

Progress in Antimonide Unipolar Barrier Infrared Detectors

D. Z. Ting, S. B. Rafol, C. J. Hill, A. Khoshakhlagh, B. J. Pepper,
A. Soibel, A. M. Fisher, S. A. Keo, Y. Maruyama, T. Wenger, S. D. Gunapala
NASA Jet Propulsion Laboratory, California Institute of Technology, Pasadena, California

The unipolar barrier device architecture introduced by the nBn [1] and XBn [2] has led to significantly improved performance in III-V semiconductor infrared detectors. In particular, the combination of the unipolar barrier device architecture and antimonide absorbers, including the InAsSb and the GaInAsSb bulk alloys, the InAs/GaSb type-II superlattice (T2SL), and the InAs/InAsSb type-II strained-layer superlattice (T2SLS), has enabled a new generation of high-performance infrared detectors that can provide continuous cutoff wavelengths coverage in the short-, mid-, and long-wavelength range. Notably, focal plane arrays (FPAs) based on the mid-wavelength Ga-free InAs/InAsSb T2SLS unipolar barrier infrared detector have demonstrated a 40 – 50 K higher operating temperature than the InSb FPA, while retaining the same III-V semiconductor manufacturability and affordability benefits [3]. We will provide an overview of the progress and challenges [4] in the development of antimonide unipolar barrier infrared detectors, as well as some of their applications for NASA infrared spectral imaging needs.

This research was carried out at the Jet Propulsion Laboratory, California Institute of Technology, under a contract with the National Aeronautics and Space Administration.

[1] S. Maimon and G. W. Wicks, *Appl. Phys. Lett.* **89**(15), 151109 (2006).

[2] P. C. Klipstein, *Proc. SPIE* **6940**, 6940–2U (2008).

[3] D. Z. Ting, A. Soibel, A. Khoshakhlagh, S. B. Rafol, S. A. Keo, L. Höglund, A. M. Fisher, E. M. Luong, and S. D. Gunapala, *Appl. Phys. Lett.* **113**, 021101 (2018).

[4] D. Z. Ting, A. Khoshakhlagh, A. Soibel, and S. D. Gunapala, *J. Elec Materi* **49**, 6936 (2020).

[+] Author for correspondence: David.Z.Ting@jpl.nasa.gov

MWIR Resonant Cavity Infrared Detectors (RCIDs) with High Quantum Efficiency and High Frequency Response

C. L. Canedy,[1] E. M. Jackson,[1] R. L. Espinola,[1] C. S. Kim,[1] E. H. Aifer,[1] I. Vurgaftman,[1] V. Jayaraman,[2] B. Kolasa,[2] R. Marsland,[3] B. Knipfer,[3] M. Turville-Heitz,[4] J. Ryu,[4] L. J. Mawst,[4] D. Botez,[4] and J. R. Meyer[1]

[1] Naval Research Laboratory, Washington DC 20375
[2] Praevium Research, 601 Pine Avenue, Suite C, Goleta CA 93117
[3] Intraband, LLC, 505 S. Rosa Road, Suite 34, Madison WI 53719
[4] Department of Electrical and Computer Engineering, U. Wisconsin, Madison WI 53706

NRL recently demonstrated the first MWIR resonant cavity IR detectors (RCIDs) to exhibit high performance [1]. At resonance wavelength λ_{res} = 4.0 μm, devices with a grown GaSb/AlAsSb bottom mirror, dielectric top mirror, and absorber thickness of only 50 nm attained external quantum efficiency EQE = 34%, with linewidth 46 nm. U. Lancaster subsequently reported RCIDs with InAs absorber displaying $\lambda_{res} \approx 3.3$ μm and 52% EQE [2].

Here we report devices for which an *nBn* detector chip with 20 InAs/InAsSb active quantum wells and total absorber thickness 103 nm was bonded to a GaAs/AlGaAs mirror with reflectivity > 99%. The GaSb substrate was then removed, and mesas processed from the back side of the as-grown detector epitaxy. The RCID's very thin absorber allows rapid extraction of the photoexcited carriers for high frequency response. For a device with small diameter (d = 21 μm) for reduced capacitance, the optical heterodyne data illustrated in Fig. 1 (taken before the top dielectric mirror was deposited) confirm a 3dB response of 5.9 GHz. The EQE spectrum for a larger RCID (d = 105 μm) was measured with an FTIR by fitting the ratio of photocurrent to measured blackbody flux through a calibrated narrowband filter (blue curve in Fig. 2). This yielded peak EQE = 57% at λ_{res} = 4.618 μm, with FWHM = 31 nm. EQEs for the same device were also characterized from the photocurrent induced by excitation from a quantum cascade laser (QCL) with calibrated incident power, in independent measurements at NRL (blue points) and Intraband, LLC (red points).

Figure 1 – Frequency response of an RCID with d = 21 μm.

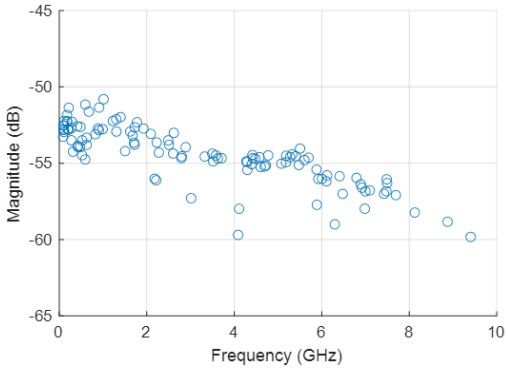

Figure 2 – EQE *vs.* wavelength for an RCID with d = 105 μm, as measured by three experiments.

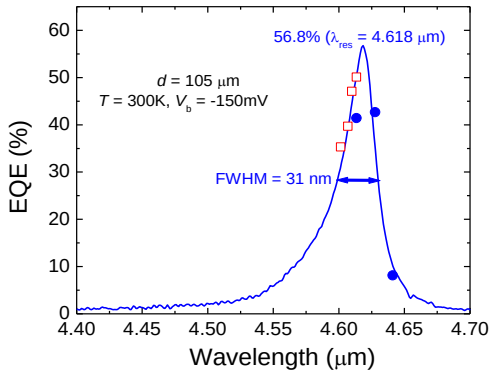

[1] C. L. Canedy *et al.*, *Opt. Expr.* 27, 3771 (2019).
[2] A. Bainbridge *et al.*, *phys. stat. sol. (a)* **218**, 2100056 (2021).
+ Author for correspondence: jerry.meyer@nrl.navy.mil

Growth and development of antimony-based III-V detector materials for the regime from eSWIR to LWIR

V. Daumer[+], L. Kirste, R. Müller, J. Niemasz, M. Wobrock, A. Wörl, Q. Yang, and R. Rehm

Fraunhofer Institute for Applied Solid State Physics IAF,
Tullastraße 72, 79108 Freiburg, Germany

The family of the 6.1 Å-materials (InAs, GaSb, AlSb), their ternary and quaternary alloys, and the corresponding type-II superlattices (T2SLs) permit wavelength tuning over a wide spectral range in the infrared (IR). The flexibility in detector design that these materials provide, allows for sophisticated device concepts and high-performance bandgap-engineered IR technology for various applications. Grown lattice matched on GaSb substrate by molecular beam epitaxy (MBE), these materials can be combined to address the requested requirements. At Fraunhofer IAF, we utilize these materials to develop IR detectors and arrays for the extended shortwave infrared (eSWIR), the mid-wavelength infrared (MWIR), the long-wavelength infrared (LWIR) and combinations thereof.
For the eSWIR region from 1.7 up to 3.0 µm, where InGaAs on InP substrates suffers from a high dislocation density resulting in limited performance, InGaAsSb on GaSb is currently under investigation for room temperature operation employing a heterojunction approach. This talk will report on fundamental material study as well as electro-optical characterization results of heterojunction diodes.
For the thermal infrared in the range from 3 up to 12 µm covering MWIR to LWIR, T2SLs based on InAs/GaSb and InAs/InAsSb are developed. The activities range from basic studies up to pilot line production with detectors at TRL9. Recent advances aiming at high operating temperatures (HOT) for MWIR, enhanced quantum efficiency for LWIR and extended sensitivity combining MWIR and LWIR diodes will be presented.

[+] Author for correspondence: volker.daumer@iaf.fraunhofer.de

Optically-Addressed Monolithically-Integrated Triple-Band Photodetectors Using Type-II Superlattice Materials

Z. Ju[1,2], A. McMinn[1+], X. Qi[1], S. Schaefer[1,3], T. McCarthy[1], Y.-H. Zhang[1]
[1] School of Electrical, Computer, and Energy Engineering, [2] Department of Physics
Arizona State University, Tempe, AZ, USA
[3] National Renewable Energy Laboratory, Golden, CO, USA

Multiband photodetectors are desired in various applications, including thermal imaging, environmental resources surveying, and chemical sensing. When implementing multiband photodetectors into an FPA, reducing the number of terminals on the photodetector is necessary since an increase in terminal count reduces the detector's active area and complicates ROIC and FPA layout and device processing [1]. This talk reports the demonstration of two-terminal multiband monolithically integrated optically addressed photodetectors using InAs/InAsSb type-II superlattice (T2SL) to cover SWIR, MWIR, and LWIR, as shown by the device structure in Figure 1.

The operating principle of the optical-addressing design is to use multiple optical biases on a stack of photodiodes (PDs) connected in series to switch detection bands, as shown in Figure 1 schematically. The detecting PD becomes the current-limiting device and determines the spectral response. Our preliminary results show that the MBE-grown InAs/InAsSb T2SLs as MWIR and LWIR photodetectors are nearly perfectly strain-balanced onto GaSb, showing distinct satellite peaks and a perfect overlap of the 0 order SL peak with the substrate peak, as plotted in Figure 2. Additionally, an analytical model has been established to analyze the noise characteristics and cross-talk between bands of the optically-addressed multiband detectors.

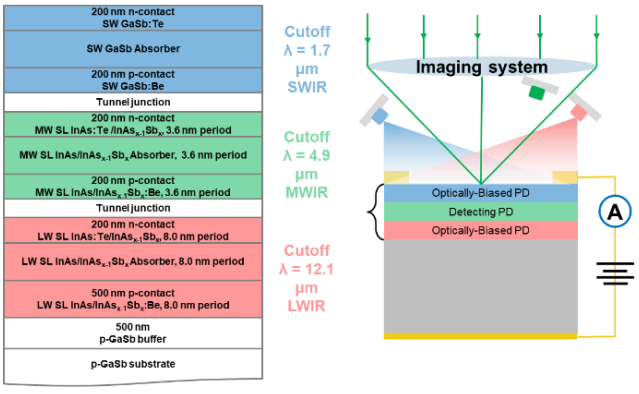

Figure 1: (Left) Triple-band PD layer structure, (right) and its operating principle under optical addressing.

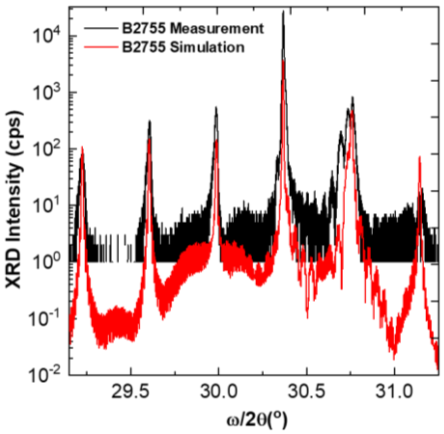

Figure 2: ω/2θ scan of a strain-balanced T2SL on a GaSb substrate.

[1] E. H. Steenbergen, Appl. Phys. Lett. **97**, 161111-161114 (2010).

[+] Author for correspondence: amcminn1@asu.edu

Supplementary Pages (Optional)

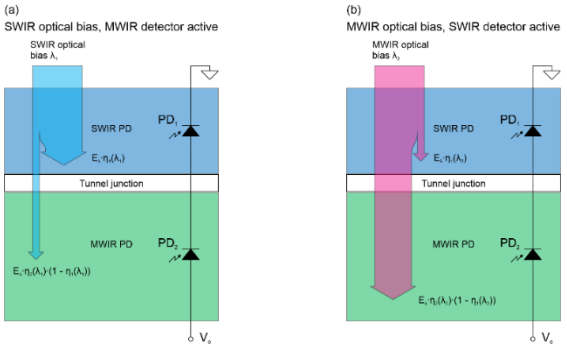

Figure 3: Schematics illustrating (a) incomplete absorption in the SWIR optically biased PD, whereas (b) parasitic absorption occurs in the SWIR PD while under MWIR optical bias. Incomplete absorption in the SWIR PD creates spectral cross-talk, directly contributing to the shot noise current in the MWIR device.

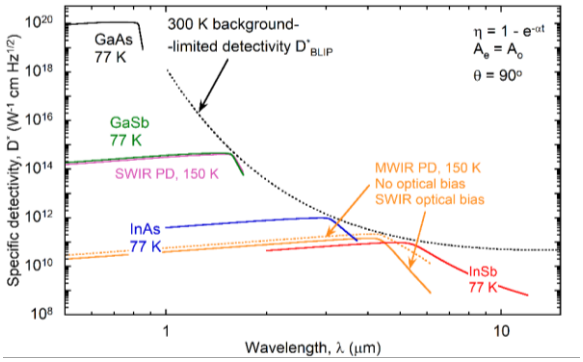

Figure 4: Specific detectivity D^* as a function of wavelength at zero output current for optically-addressed SW/MWIR multiband photodetector showing the degradation in the MWIR detectivity under SWIR optical bias.

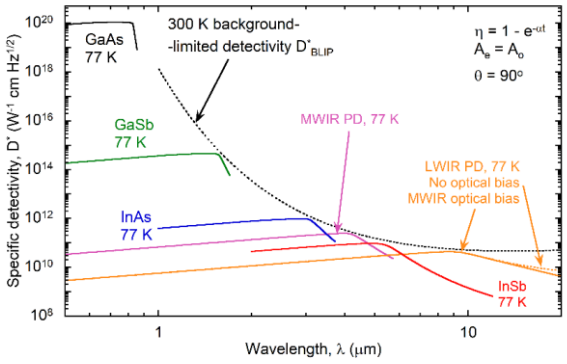

Figure 5: Specific detectivity D^* as a function of wavelength at zero output current for optically-addressed MW/LWIR multiband photodetector showing minimal degradation in the LWIR detectivity under MWIR optical bias.

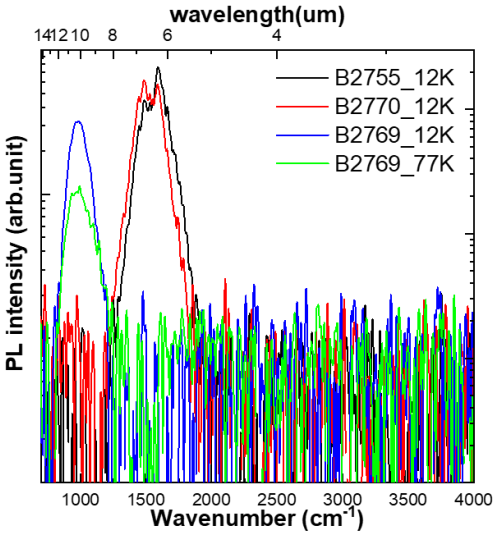

Figure 6: PL spectra of MWIR and LWIR T2SL measured by FTIR showed peaks at 6 μm for the MWIR sample and 10 μm for the LWIR sample.

Optimizing the design of type-II InAs/InAsSb superlattices for the incorporation of unintentional Sb in the tensile electron well

M. S. Milosavljevic,[1,2,3] P. T. Webster,[2] S. R. Johnson[1]

[1] Center for Photonics Innovation & Electrical, Computer, and Energy Engineering, Arizona State University, Tempe, Arizona 85287, USA

[2] Air Force Research Laboratory, Space Vehicles Directorate, Kirtland Air Force Base, New Mexico 87117, USA

[3] A-Tech, LLC, a BlueHalo company (ATA BlueHalo), Albuquerque, New Mexico 87123, USA

Several strain-balanced 5.3 μm midwave and 12.0 μm longwave InAs/InAsSb superlattices are grown on (100) GaSb substrates by molecular beam epitaxy and examined using X-ray diffraction and temperature-dependent photoluminescence. A significant amount of surface Sb incorporates into the tensile InAs layer that subsequently affects the design and performance. For a given wavelength design the presence of unintentional Sb in the InAs layer i) increases the tensile electron well thickness, thereby increasing electron confinement and decreasing electron wavefunction intensity, ii) decreases hole well depth, thereby decreasing hole well width and hole confinement, and as a result iii) decreases the absorption coefficient by 8% for midwave and 11% for longwave. This is presented in Figure 1 in terms of total wavefunction overlap and that within the tensile and compressive layers for structures with and without unintentional Sb as a function of the compressive layer Sb mole fraction. The solid curves show the case with unintentional Sb and the dashed curves show the case without unintentional Sb, with the compressive layer in red, the tensile layer in black, and the total (sum of red and black) in blue. The values for the grown superlattices are shown as open circles. The measurements and calculations are for an operating temperature of 77 K. The grown superlattice tetragonal distortion ranges from -0.019% to 0.020% with a -0.001% average for midwave and from 0.021% to 0.039% with a 0.027% average for longwave. A combination of X-ray diffraction and photoluminescence is utilized to determine that the unintentional Sb mole fraction in tensile layer is 1.9% for midwave and 1.2% for longwave.

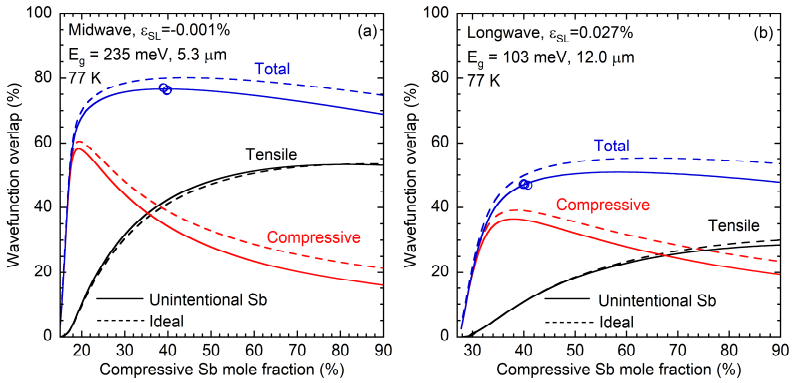

Figure 1. Electron-hole wavefunction overlap in 5.3 μm midwave (a) and 12.0 μm longwave (b) InAs/InAsSb superlattices.

[+] Author for correspondence: shane.johnson@asu.edu

Top-Illuminated Mid-IR HgTe Colloidal Quantum Dot Photodiodes

J. C. Peterson,[1] **P. Guyot-Sionnest**[1]

[1] *The James Franck Institute, 929 E. 57th St., The University of Chicago, Chicago, IL, 60627, USA.*

Colloidal quantum dots offer an inexpensive, solution-processed alternative to conventional, crystalline material devices for mid-infrared photodetection. pn-junction devices using HgTe quantum dots previously reached the background limit at cryogenic temperatures. These devices have since shown increased effective operating temperatures. [1] [2] For use in thermal imaging arrays, devices must be developed which are illuminated from the top.

The focus of this work is to understand and improve the performance of top-illuminated HgTe quantum dot photodiodes. Signal collection is a function of series resistance, diffusion length, and thin film absorption, and all can be improved separately for higher operating temperatures. We show results with a bottom n-type reflector contact, varying thicknesses of HgTe films of different mobility and doping profile and a semi-transparent metallic top electrode, made in a process compatible with integration into silicon readout chips. We also show an analysis of the temperature and photon flux dependence of the diode current, to gain insight into the dominant recombination mechanisms present in the device and the nature of the shunt resistance.

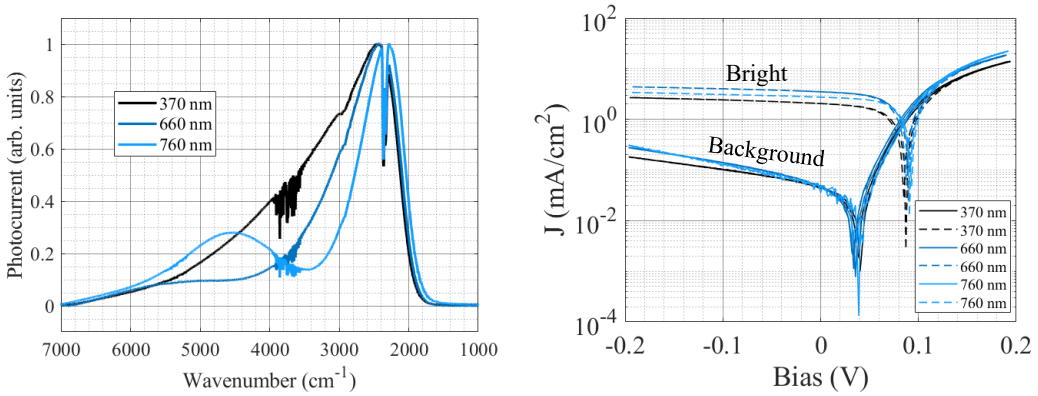

Figure 1: Photocurrent spectra of top-illuminated devices of varying thickness (left) and JV curves (right).

[1] J. C. Peterson, P. Guyot-Sionnest, Room-Temperature 15% Efficient Mid-Infrared HgTe Colloidal Quantum Dot Photodiodes. ACS Applied Materials & Interfaces. Article ASAP, (2023).

[2] X. Xue, M. Chen., Y. Luo, T. Qin, X. Tang, Light: Science and Applications **12**, 2(2023).

+ Author for correspondence: jcpeterson@uchicago.edu

Synthesis of HgTe Colloidal Quantum Dots and Processing of Films to Maximize Photodetector Performance.

P. Guyot-Sionnest,[+] J. Peterson, H. Zhang, A. Caillas
James Franck Institute, The University of Chicago, 929 East 57th Street, Chicago, IL 60637

Since 2011, HgTe colloidal quantum dots have been researched for infrared photodetection in the MWIR,[1] but also in the SWIR and LWIR. They are readily tunable in the MWIR by controlling the size around 12 nm as shown in Fig. (a). The detector performances are still below those of single crystal and epitaxial materials, but the solution processing promises high throughput and low-cost fabrication of simple detectors and imagers. Our goal is to raise the performance of 4.5 microns HgTe quantum dot at 300K to match polycrystalline PbSe ($D^*=10^{10}$Jones), for fair and fast thermal imaging at room temperature, and another related goal is to raise the BLIP temperature to thermolelectric temperatures.

This presentation focuses on the measurements of optical absorption, carrier mobility, and carrier lifetime of MWIR HgTe colloidal quantum dots, and how these properties inform the best possible performance achievable. Simple experimental methods based on photoconductors, as shown in Fig. (b), allow to obtain these properties.[2] Then we distinguish film preparations that use non-polar inks or polar inks of quantum dots. While both can give similar carrier mobility after mild annealing, the carrier lifetime is retained in one instance, while the carrier lifetime is shortened by trapping in the other. Such a study indicates clearly which is the better process, and leads to improved device performances as shown in Fig (c).

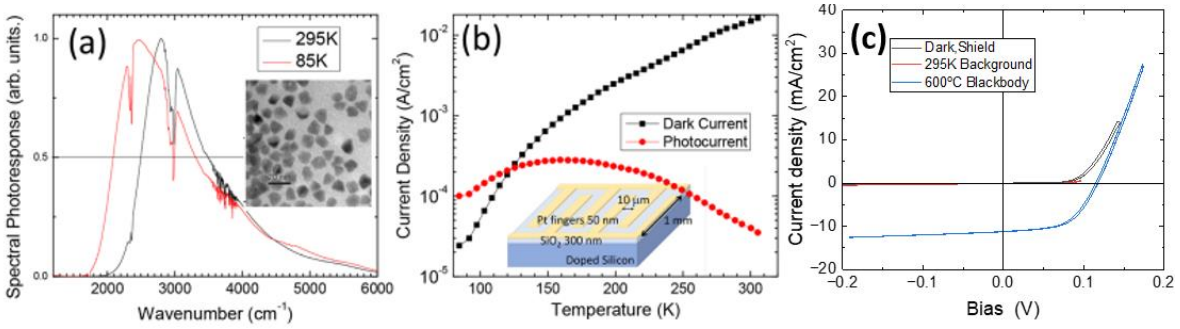

Figure . (a) Photoresponse spectra of a photoconductor of MWIR HgTe quantum dots. The inset is a TEM picture of the quantum dots. (b) Dark current and photocurrent temperature dependence. (c) JV curves of a MWIR PV device with 50% EQE and 10^{12} Jones at 85K without bias.

[1] S Keuleyan, E Lhuillier, V Brajuskovic, P Guyot-Sionnest, Mid-infrared HgTe colloidal quantum dot photodetectors, Nature Photonics 5 (8), 489-493 (2011)
[2] P Guyot-Sionnest, JC Peterson, C Melnychuk, Extracting Bulk-like Semiconductor Parameters from the Characterization of Colloidal Quantum Dot Film Photoconductors, The Journal of Physical Chemistry C 126 (40), 17196-17203 (2022)

[+] Author for correspondence: pgs@uchicago.edu

Exploring Quantum Dots/Graphene van der Waals Heterostructures for Uncooled SWIR-MWIR Detection

J. Wu[1]
[1]*Department of Physics and Astronomy, University of Kansas, Lawrence, KS 66045, USA*

Semiconductor quantum dots/graphene (QD/Gr) heterostructures provide a quantum sensor scheme for photodetection and have witnessed remarkable progress in broadband photodetection. The QD/Gr photodetectors take advantages of the quantum confinement in QDs for spectral tunability and that in graphene for superior charge mobility to enable a high photoconductive gains or high photoresponsivity. A key question on whether high detectivity (D*) may be achieved in uncooled QD/Gr photodetectors in infrared (IR) spectrum is whether thermal noise in narrow bandgap semiconductor QDs in the QD/Gr photodetectors would degrade the detector performance in a similar way to conventional IR detectors based on semiconductor films and therefore demand cryogenic cooling to reduce the thermal noise. In order to answer this question, this talk presents our recent investigation on the noise origin of the QD/Gr heterostructures in the short-wave to middle-wave (SWIR-MWIR) spectra. Interestingly, it is found to be dominated by the noise in graphene either in dark or illuminated by SWIR-MWIR illumination. Furthermore, it has been found that the narrow-bandgap semiconductor QDs may be designed to reduce the noise towards the intrinsic limit in graphene by shifting its Fermi energy towards the Dirac point. Through development of atomic-scale surface and interface engineering approaches for optimize QD/Gr interface, uncooled $D^* > 10^{11}$ Jones at wavelengths of 2.25-3.25 μm has been achieved. This result reveals a different noise origin in the QD/Gr heterostructures, which is not directly affected by the thermal noise in narrow-bandgap semiconductor QDs. Therefore, QD/Gr heterostructures may provide a promising low-cost, scalable scheme for uncooled SWIR-MWIR detection.

Core-Shell PbSe/CdSe Quantum Dot Mid-Infrared Photoconductor

M. Rastkar Mirzaei,[1] Z. Shi,[1]
[1] *The School of Electrical and Computer Engineering, University of Oklahoma, Norman, OK 73019, USA*

Reducing Size, Weight, Power consumption, and Cost (SWaP+C) while maintaining good range and resolution has been the key goal for focal plane array (FPA) imagers. In mid-wave infrared (MWIR), a low SWaP+C imager with fast response time is highly desirable for many applications such as small unmanned aerial vehicles, smart munitions, and missile defense. Elimination of bulky and expensive cryogenic cooling systems and monolithic integration on Si readout integrated circuitry (ROIC) to reduce fabrication cost and to increase yield become two essential requirements for low SWaP+C MWIR imagers. Polycrystalline IV-VI semiconductor PbSe photoconductor (PC) meets both requirements and thus has been used by for years. However, one key challenge for the current PbSe PC FPA is the inhomogeneity of polycrystalline film which requires ROIC to perform non-uniformity correction on pixels and thus increases the power consumption and cost.

In this study, we report a novel threading core-shell PbSe/CdSe quantum dots (QDs) (QD Shish Kebab) room-temperature MWIR detector with much-improved homogeneity. The detector is grown on a SiO_2/Si substrate which enables monolithic integration of FPA on Si ROIC. We have optimized the QDPC's layer thickness, Core to shell ratio, and the total number of layers to improve its performance. The cutoff wavelengths can be tuned with different QD sizes.

To evaluate the performance of the QDPC, we have performed various characterization measurements, including current-voltage (IV) measurements, and blackbody radiometric measurements. The charge separation model is used to explain the QD 3-dimensional (3D) Shish Kebab detector structure.

The successful demonstration of our 3D network Core-Shell PbSe/CdSe nano-structured Photoconductor with improved homogeneity will have significant implications for many applications including large-format FPA monolithically integrated on Si ROIC with small pixel size.

[+] Author for correspondence: rastkarmilad@ou.edu, Shi@ou.edu

Tensile-strained InGaAs quantum dots with interband emission in the mid-infrared

K. D. Vallejo,[1] T. A. Garrett,[2] C. I. Cabrera-Perdomo,[3] M. D. Drake,[2]
B. Liang,[4] K. A. Grossklaus,[5] and Paul J. Simmonds[2,6,+]
[1]Condensed Matter and Materials Physics, Idaho National Laboratory, ID, USA
[2]Micron School of Materials Science & Engineering, Boise State University, ID, USA.
[3]Unidad Académica de Ciencia y Tecnología de la Luz y la Materia, Universidad Autónoma de Zacatecas, 98160, Zacatecas, Zac., Mexico.
[4]California NanoSystems Institute, University of California Los Angeles, CA, USA.
[5]Department of Electrical and Computer Engineering, Tufts University, MA, USA.
[6]Department of Physics, Boise State University, ID, USA.

Novel tunable light sources operating in the mid-infrared are desirable for a wide range of applications. Quantum cascade approaches produce devices with excellent performance but these structures are complex and time consuming to create. An alternative could be to use tensile strain as a way to reduce the band gap energy of semiconductors such as InGaAs, and push their emission deeper into the IR. We will discuss our efforts to use tensile-strain to drive the self-assembly of $In_{1-x}Ga_xAs$ quantum dot (QD) nanostructures on GaSb(111)A surfaces. The highly localized tensile strain stored in these QDs modifies the InGaAs band structure to red-shift the photon emission wavelength by ~2000 nm. We have determined a robust set of growth conditions for the self-assembly of the tensile-strained InGaAs QDs. During molecular beam epitaxy (MBE), InGaAs QDs form spontaneously on GaSb(111)A with less than 1 ML deposited, indicating a Volmer-Weber growth mode. We characterized these nanostructures using atomic force microscopy (AFM), transmission electron microscopy (TEM) and energy-dispersive X-ray spectroscopy (EDS) to understand InGaAs/GaSb(111)A QD structure as a function of the MBE growth conditions. A combination of photoluminescence (PL) spectroscopy and computational modeling shows that residual tensile strain in the QDs reduces the InGaAs band gap energy, to produce band-to-band light emission at 3.2–3.9 µm (Figure 1). When coupled with quantum size effects, the use of tensile strain to red-shift QD emission offers an attractive way to create highly tunable mid-IR light sources. This work is supported by the National Science Foundation under NSF CAREER Grant No. 1555270.

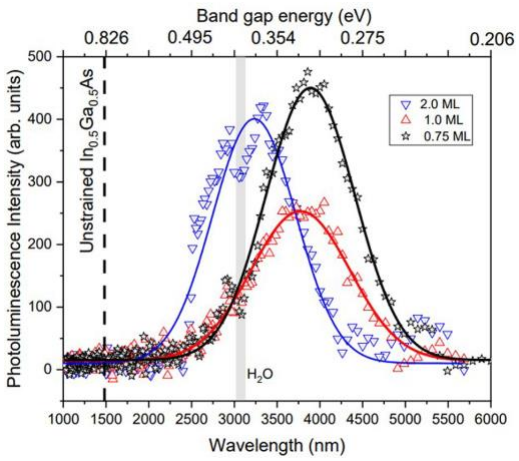

Figure 1. PL spectra at 77 K from InGaAs/GaSb(111)A samples containing a single layer of 0.75, 1.0, and 2.0 ML QDs. The continuous lines are Gaussian fits to each spectrum. The gray line highlights the position of a water absorption feature present in all three spectra at ~3000 nm.[1]

[1] Vallejo *et al.*, ACS Nano **17**, 2318 (2023).

[+] Author for correspondence: paulsimmonds@boisestate.edu

Supplementary Pages

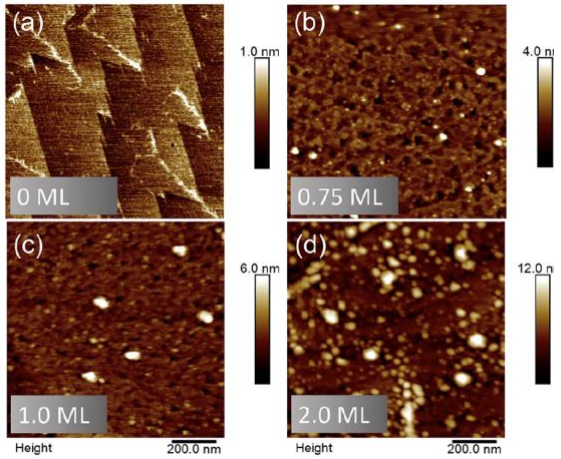

Figure S1. (a–d) 1 × 1 μm^2 atomic force microscope images showing the surface morphology of 0–2 ML InGaAs deposited on GaSb(111)A at 450 ºC, at 0.4 ML/s.

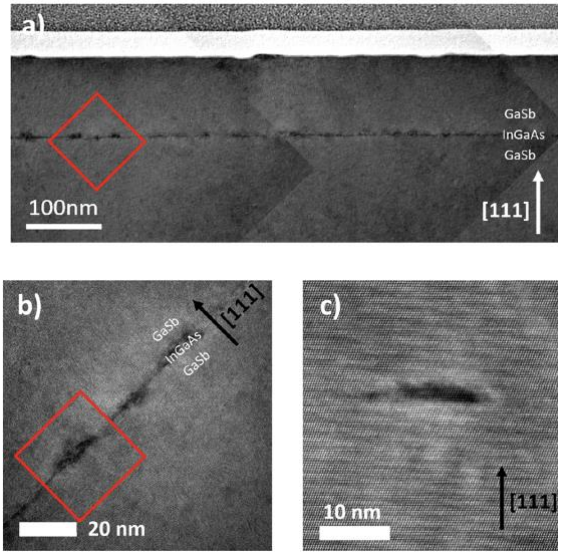

Figure S2. (a) Bright-field transmission electron microscope (BF TEM) image montage of a 1 ML InGaAs QD layer surrounded by GaSb(111)A barriers, with a second layer of identical InGaAs QDs at the surface. (b) BF TEM image of several buried 1 ML InGaAs QDs corresponding to the red square in (a). (c) High-angle annular dark-field scanning TEM image of the buried 1 ML InGaAs QD enclosed by the red square in (b).

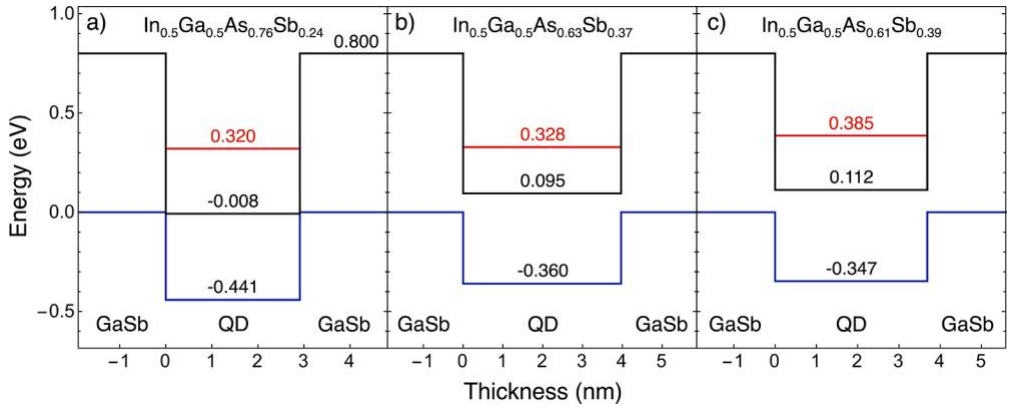

Figure S3. Calculated band alignments at 77 K for (a) 0.75 ML, (b) 1.0 ML, and (c) 2.0 ML InGaAs/GaSb(111)A QDs. A type-III band alignment exists for the 0.75 ML QDs, with a type-II alignment for the 1.0 and 2.0 ML QDs. The conduction band minimum is shown in black and the valence band maximum in blue. Red lines indicate the electron ground state energies. Comparison between this model and our experimental PL data reveals the unintentional incorporation of Sb into the InGaAs QDs from the surrounding GaSb barriers.

Broadband Room-Temperature Mid-infrared Detection with Nanoparticles

Chongwu Wang[1], Liangliang Liang[2], Jiaye Chen[2], Xiaogang Liu[2], Qi Jie Wang[1,3,*]

1. Centre for OptoElectronics and Biophotonics, School of Electrical and Electronic Engineering, Nanyang Technological University, Singapore, Singapore.
2. Department of Chemistry, National University of Singapore, Singapore, Singapore
3. Centre for Disruptive Photonic Technologies, School of Physical and Mathematical Sciences, Nanyang Technological University, Singapore, Singapore.

Email: qjwang@ntu.edu.sg

Abstract: By utilizing ratiometric luminescence, which can be modulated at MIR radiation under ambient conditions, a novel lanthanoid nanocrystal-based transducers for broadband mid-infrared (MIR) sensing is created. The high photostability and simplicity of processing provide opportunities for developing low-cost, scalable MIR imaging and spectroscopy techniques with unprecedented sensitivity.

MIR spectroscopy is widely used in life sciences, remote sensing, security, industrial imaging, and environmental monitoring. Despite significant attempts, the development of simple, low-cost, low-noise systems for MIR detection and imaging at room temperature remains a challenge. Converting MIR radiation to visible and near-infrared regions is an ideal approach, which can be easily detected and imaged with silicon photodetectors due to their high sensitivity, low cost, and CMOS compatible. Current MIR conversion technology is limited to nonlinear optics with bulky crystals [1] or resonant nanocavities [2], which suffer from low efficiency and phase match requirement.

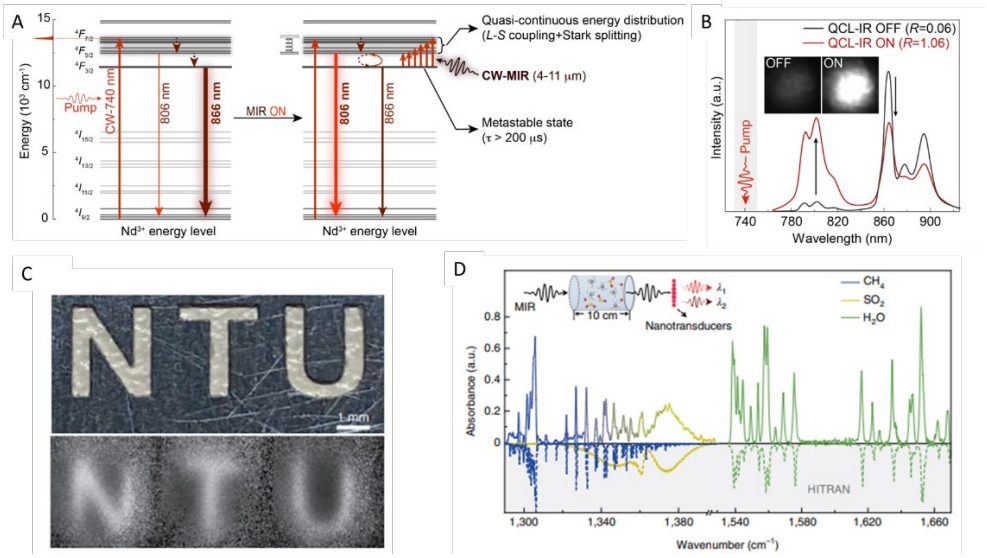

Fig. 1 (A) Working principle of broadband MIR sensing using Nd^{3+} nanotransducers. (B) Change in ratiometric luminescence nanotransducers with and without MIR radiation. (C) MIR imaging (7.3 μm) using lanthanide film captured by a CMOS camera. (D) Gas sensing for a mixture of CH_4, SO_2 and water using Nd nanotransducers. [3]

Here, we report a transducer using lanthanide nanocrystals that realize broadband MIR detection under ambient conditions. The Nd doped NaYF4 has two emission bands around 806 nm (4F5/2 → 4I9/2) and 866 nm (4F3/2 → 4I9/2), The 806 nm emission band is much weaker than that at 866 nm due to a nonradiative multiphonon-assisted depopulation process. Thanks to the ultralong luminescence lifetime of the metastable 4F3/2 state, efficient MIR back-pumping from 4F3/2 to higher energy levels (4F5/2, 4F7/2) is possible. Consequently, the emission at 806 nm enhances drastically while that at 866 nm decrease significantly. With the improved sensitivity, stability, and fast response, we further performed proof-of-principle measurements for room-temperature MIR imaging using a low-cost CMOS camera. The broadband wavelength response ensures its application for MIR spectroscopy. The absorption spectra are recorded for gas mixture of CH_4, SO_2 and water from 1290 to 1670 cm^{-1} using lanthanide transducer.

Acknowledgements, This research was also supported partially by National Research Foundation Singapore programme (NRF-CRP22-2019-0007) and A*STAR grant number A18A7b0058 and A2090b0144, and National Medical Research Council (NMRC) (MOH-000927).

References

[1] K. Huang, J. Fang, M. Fan, E. Wu, H. Zeng, "Wide-field mid-infrared single-photon upconversion imaging" Nat. Commun. 13, 1077, 2022.

[2] A. Xomalis, X. Zheng, R. Chikkaraddy, Z. Koczor-Benda, E. Miele, E. Rosta, G. A. E. Vandenbosch, A. Martinez, J. J. Baumberg. "Detecting mid-infrared light by molecular frequency upconversion in dual-wavelength nanoantennas", Science, 374, 1268, 2021.

[3] L. Liang, C. Wang, J. Chen, Q. J. Wang, X. Liu, "Incoherent broadband mid-infrared detection with lanthanide nanotransducers", Nat. Photon. 16, 712, 2022.

Bi-layered silicon with strain-induced tunable optical properties for IR applications

K. Vishal,[1] Y. Zhuang[1]

[1] *Department of electrical engineering, Wright State University, Dayton, Ohio, 45435*

The compatibility with the main-stream silicon technology makes silicene and a few layers of silicon very promising for VLSI beyond 3nm technology node. Similar as its carbon counterpart graphene, energy bandgap (EB) opening presents the most critical demand for potential applications in digital electronics. Based on density function theory, EB opening in bi-layer silicon structures (BLSi) has been obtained under biaxial in-plane strain in our previous works [1, 2]. In this work, we performed a theoretical study of the optical properties of the strained BLSi in mid-IR. It turns out that by applying the in-plane tensile strain, the optical properties of the BLSi can be tuned in a wide range over the entire mid-IR bandwidth.

Our previous works show that buckle-free bilayer silicon structure (Fig.1) can be obtained once the biaxial in-plan tensile strain exceeds 11.2% [1, 2]. As the in-plane strain continuously increases to 16.4%, a direct EB (E_{g_D}) is formed at Γ point in addition to the in-direct EBs (E_{g_ID}) (Fig.2), which promotes direct band transition at IR. To verify it, various optical properties including permittivity, refraction index, and optical conductivity of the BLSi have been calculated versus photonic energy at different strain levels. Figure 3 plots the complex in-plane permittivity of the BLSi under an in-plane strain of 14.8%. The observed absorption (P1 marked in Fig. 3) evidences the direct-band transition. By varying the applied strain, such featured absorptions can be tuned in the range between 0.154-1.056 eV, which covers the entire mid-IR (See supplementary pages). In addition to the featured absorptions, its real part of the permittivity in Mid-IR (<0.2 eV) is of a factor 3 greater than the fully relaxed BLSi, leading to two times enhancement of reflectance. We believe that the buckle-free planar BLSI might open new opportunities of applications at IR.

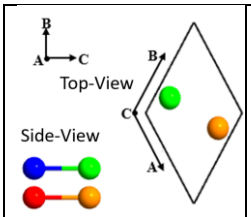

Figure 1. Atomic structure of BLSi

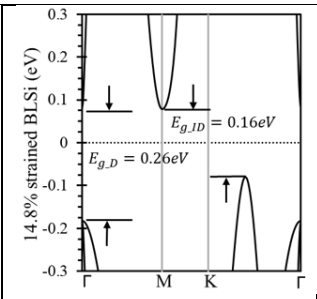

Figure 2. Energy band diagram of strained BLSi

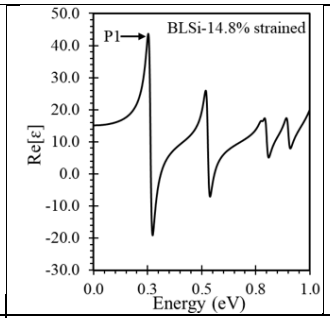

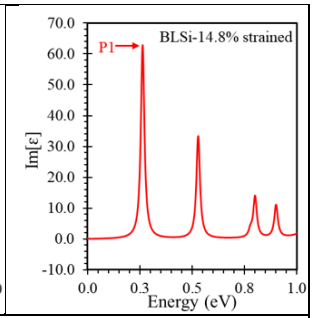

Figure 3. Real (Left) and imaginary (Right) parts of permittivity of BLSi VS photon energy.

[1] Z. Ji, et al, IEEE J. Elec. Mat, 45, 5040 (2016).
[2] K. Vishal, et al, J. Vac. S & T A 41, 022201(2023)

+ Author for correspondence: yan.zhuang@wright.edu

Supplementary Pages (Optional)

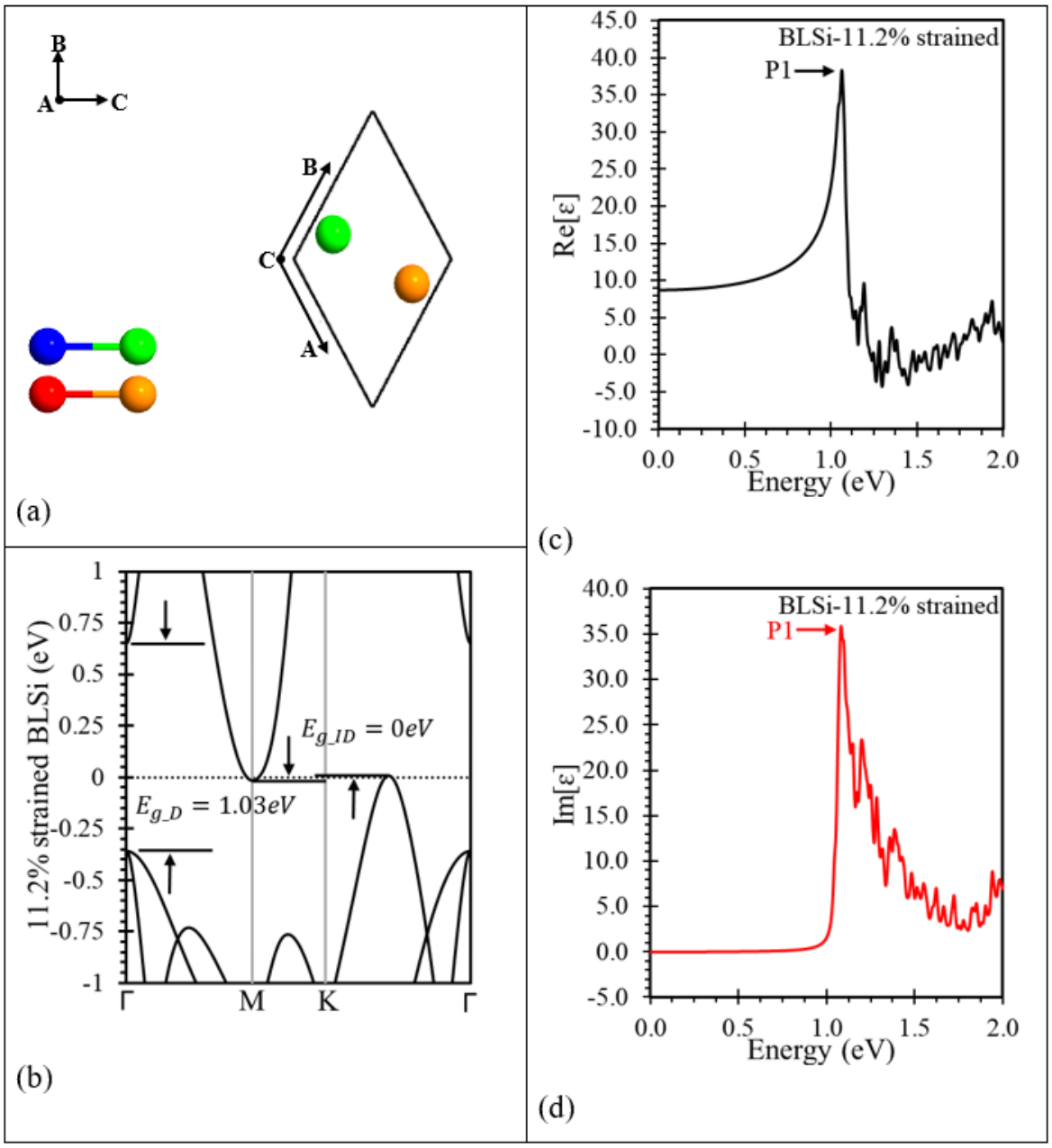

Figure S1. Structural (a), energy band diagram (b), real (c) and imaginary (d) parts of the complex permittivity of a strained BLSi under bi-axial in-plane strain 11.2%. The absorption P1 occurs at 1.056 eV. The buckle height of the strained BLSi is close to zero, resulting in a planar BLSi.

Growth and Optical Properties of InGaAs QW on c-plane Sapphire for Laser Development

Subhashis Das[1,2], Rajesh Kumar[1,3], Fernando Maia de Oliveira[1], Yuriy I. Mazur[1], Wei Du[1,3], Shui-Qing Yu[1,3], Gregory Salamo[1,2]

[1] *Institute for Nanoscience and Engineering, University of Arkansas, Fayetteville, AR, 72701, USA.*

[2] *Department of Physics, University of Arkansas, Fayetteville, AR, 72701, USA.*

[3] *Department of Electrical Engineering, University of Arkansas, Fayetteville, AR, 72701, USA.*

Epitaxial growth of III-V semiconductors on c-plane sapphire would potentially allow the integration of microwave photonics on a single sapphire chip [1]. We will report on the growth of high-quality crystalline InGaAs quantum well on a trigonal c-plane sapphire substrate by molecular beam epitaxy (MBE). For fabrication on sapphire, an AlAs nucleation layer was followed by a two-step GaAs growth method including an early-stage low temperature (LT) GaAs layer and a high-temperature GaAs growth layer. The high temperature GaAs buffer growth incorporates two annealing steps during the growth. An InGaAs quantum well (QW) with GaAs cap layer was epitaxially grown on the 70 nm GaAs buffer [1]. We will discuss the surface morphology, structure quality, and the optical properties of the MBE grown samples. Two structures with 20 nm wide quantum well (QW), S1 and S2, were grown with indium molar fraction of 0.15 and 0.10, respectively. The QW energy transitions were observed at 1.46 eV and 1.48 eV from low temperature (10 K) photoluminescence spectra (Figure 1). Excitingly, the optical results were comparable with the same structure grown on a GaAs substrate. Overall, these observations exhibit potential to achieve an integrated microwave photonic chip on a sapphire platform.

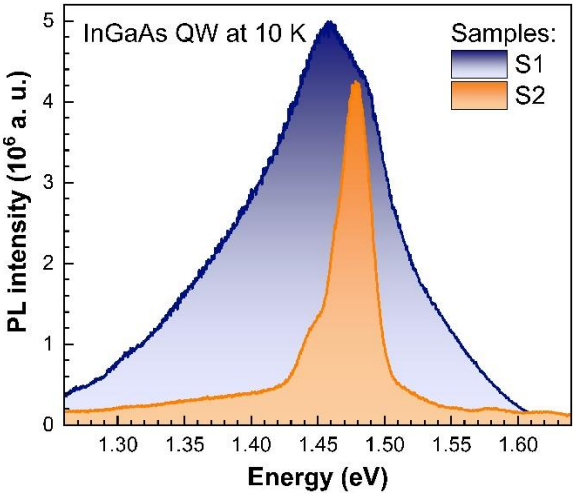

Fig. 1. Low Temperature (10 K) Photoluminescence of InGaAs QW.

[1] R. Kumar, S. K. Saha, A. Kuchuk, Y. Maidaniuk, F. M. de Oliveira, Q. Yan, M. Benamara, Y. I. Mazur, S.-Q. Yu, G. Salamo, Applied Surface Science, **542**, 148554(2021).

[+] Author for correspondence: subhashis.ds@gmail.com

Supplementary Page

Figure 2 depicts the nominal structure of the InGaAs QW. A 5 nm AlAs nucleation layer was grown at 700 °C whereas, the buffer GaAs layer consists of 200 nm GaAs grown at 600 °C and 500 nm GaAs grown at 700 °C. Samples were annealed at 800 °C for 45 seconds after every 200 nm of high temperature GaAs growth. A 20 nm $In_xGa_{(1-x)}As$ QW was grown at 600 °C on top this GaAs buffer, followed by a 50 nm GaAs cap layer. The values for x are 0.15 and 0.10, respectively. The thickness and composition values are nominal. The cap layer comprises of 5 nm GaAs grown at 600 °C and 45 nm GaAs grown at 700 °C. All the growth temperatures were measured by the thermocouple. However, the actual substrate temperature may be 30 to 100 °C less than the thermocouple temperature since the thermocouple is not touching the substrate. Figure 4 illustrates the reflection high energy electron diffraction (RHEED) images at different stages during the growth. Prominent streaky RHEED images are evident from for the GaAs buffer just before the growth of the QW (figure 3(a) and 3(d)), after the InGaAs QW figure 3(b) and 3(e) and final cap layer figure 3(c) and 3(f). From fig. 4, the root mean square (RMS) surface roughness of the samples, S1 and S2, on the scan area of 5 µm x 5 µm are 1.44 nm and 1.15 nm, respectively.

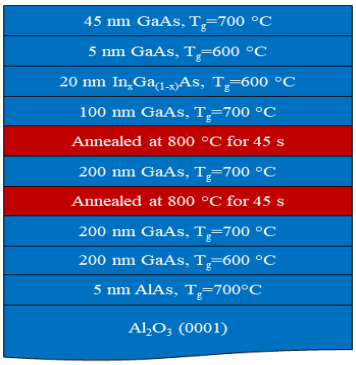

Fig. 2. Schematic structure of InGaAs/GaAs QW.

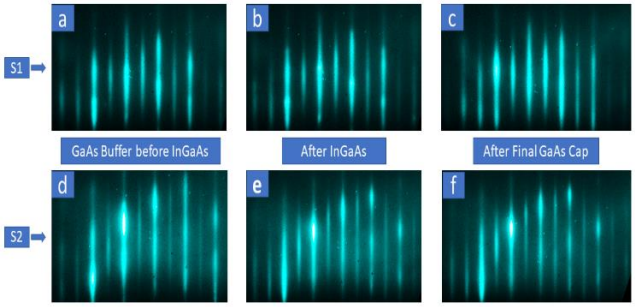

Fig. 3. RHEED images at different stages of growth.

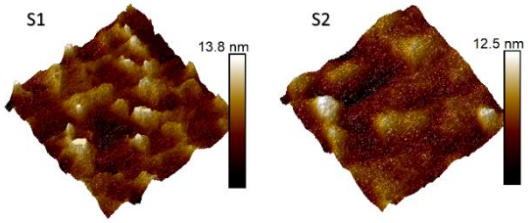

Fig. 4. AFM image (5 µm x 5 µm) of InGaAs/GaAs QW structure.

Low-Loss Infrared Ultrawide Type II Hyperbolic Metamaterials based on III-V Semiconductors

P. Weerasinghe,[1] E.D. Caudill,[2] C.G. Cailide,[2] M.A. Lloyd,[3] J.P. Murphy,[3] K.E. Arledge,[2] T.D. Mishima,[2] J.A. Nolde,[3] J.A. Frantz,[3] C.T. Ellis,[3] T.D. Golding,[1] M.B. Santos,[2] J.G. Tischler [2]

[1] Amethyst Research Incorporated, 5738 Huettner Court, Norman, OK, 73069

[2] The University of Oklahoma, 660 Parrington Oval, Norman, OK, 73019

[3] U.S. Naval Research Laboratory, 4555 Overlook Ave SW, Washington, DC, 20375

While polar dielectric materials provide natural low-loss infrared hyperbolic resonances through the excitation of phonon polaritons, the operational bandwidth of these materials is limited to a few hundred wavenumbers (cm^{-1}) or tenths of electronvolts. Also, integrating these materials with large-scale infrared optoelectronic devices presents many challenges. In this work, we implemented an ultrawide low-loss Type I hyperbolic metamaterial covering a spectral bandwidth of 2000 cm^{-1} for wavelengths above 4.7 µm. We produced the hyperbolic metamaterial with a stack of intercalated heavily-doped InAs and undoped InAs epilayers grown by molecular beam epitaxy. The InAs epilayer was heavily doped with Tellurium to obtain electron concentrations of ~8×10^{19} cm^{-3}. The Type II hyperbolicity of these stacks was determined through infrared ellipsometry obtaining effective optical constants for the stacks. These materials were then dry etched to form one-dimensional (1D) square gratings with periods and linewidths ranging from 1 to 5 µm. The measured effective optical constants measured through ellipsometry were used to model the grating's optical response by finite element electromagnetic calculations (COMSOL). The models agree with measurements, showing the formation of hyperbolic plasmon polaritons at the same frequencies where experimental features were observed. This work demonstrates that high subdiffractional light confinement can be achieved with a III-V metamaterial that can be integrated with III-V semiconductor infrared devices such as photodetectors and emitters at a large scale.

This material is based upon work supported by the Office of the Undersecretary of Defense for Research and Engineering Basic Research Office STTR under Contract No. W911NF-21-P-0024. Disclaimer: The content of the information does not necessarily reflect the position or the policy of the Government, and no official endorsement should be inferred.

A 231 GHz Generation in High-Power Long-Wavelength Quantum Cascade laser Operating at Room Temperature

S. Hayashi, A. Ito, T. Dougakiuchi, M. Hitaka, A. Nakanishi, and K. Fujita
[1] *Hamamatsu Photonics K.K., Central Research Laboratory*
5000 Hirakuchi, Hamakita-ku, Hamamatsu City, Shizuoka, 434-8601 Japan

Terahertz quantum cascade laser sources (THz nonlinear QCLs) based on nonlinear optical difference frequency generation (DFG) in the mid-infrared QCL are currently the only monolithic semiconductor laser sources that can operate at room temperature, covering the sub-THz to 6 THz range. Recently, the performance of THz nonlinear QCLs has been significantly improved by optimizing active regions and waveguide structures. Our group has demonstrated room-temperature operation at a frequency of ~0.42 THz by employing anti-crossed dual-upper-state (DAU) design in the active region of THz nonlinear QCL source to achieve a watt-class MIR pump power with long wavelength (λ~14 μm) [1].

In this paper, we report on the extension of the operating range on the low-frequency side down to <300 GHz in a terahertz nonlinear quantum cascade laser source adopting a long-wavelength and high-power DAU active region. All epilayers of the device were grown on semi-insulating InP substrates by metal-organic chemical vapor deposition (MOCVD). Figure 1 shows a schematic of the device structure. For the optical confinement of the mid-infrared pumps, dielectric waveguides were formed. Additionally, the front facet of the semi-insulating InP substrate was polished at an angle of about 10 degrees to extract the DFG emitted by the Cherenkov radiation. Two-section distributed feedback gratings (DFB) were set to produce the difference frequency ($\omega_{THz}=\omega_{DFB1}-\omega_{DFB2}$) of each pump light is 7.7 cm-1 (~231 GHz) and fabricated in the laser cavity. Figure 2 and its inset show the THz and MIR current-optical output characteristics and spectral measurements for a device with a ridge width of 14 μm and a cavity length of 3 mm during pulsed operation. THz spectra were measured by Fourier transform infrared (FTIR) using a Si bolometer as a detector. The THz spectrum of the device matched the difference frequency of the MIR spectrum, indicating single-mode operation at about 231 GHz. This is the lowest operating frequency for a semiconductor laser source operating at room temperature with current injection.

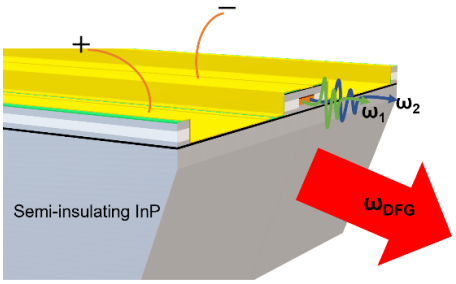

Figure 1 The schematic image of the nonlinear QCL source.

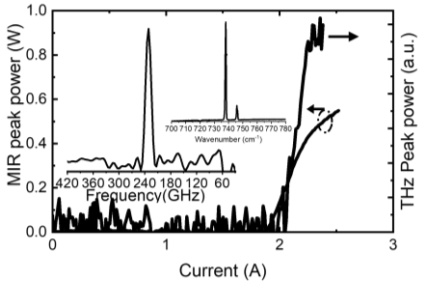

Figure 2 The current-voltage-light output characteristics of the device for THz and MIR peak power. The inset shows the MIR and THz emission spectra of the device.

[1] K. Fujita, S. Hayashi, A. Ito, T. Dougakiuchi, M. Hitaka, and A. Nakanishi, Photon. Res., **10**, 703(2022).

+ Author for correspondence: kfujita@crl.hpk.co.jp, shohei.hayashi@crl.hpk.co.jp

Supplementary Pages

Figure S1(a) displays the current-voltage-MIR output (I-V-L) characteristic of a 14 μm wide and 3 mm cavity length of the device without the grating operating in pulsed mode (pulse width 200 ns; duty cycle 1 %). The emission spectra at various currents are shown in Figure S1(b). This Febri-Perot device produces a threshold current density of 3.5 kA/cm^2 at 293 K and a maximum power of 1.1W (from a single facet) with a slope efficiency is 0.95 W/A, which is one of the highest peak powers in long wavelength (> 13 μm) QCLs reported to date.

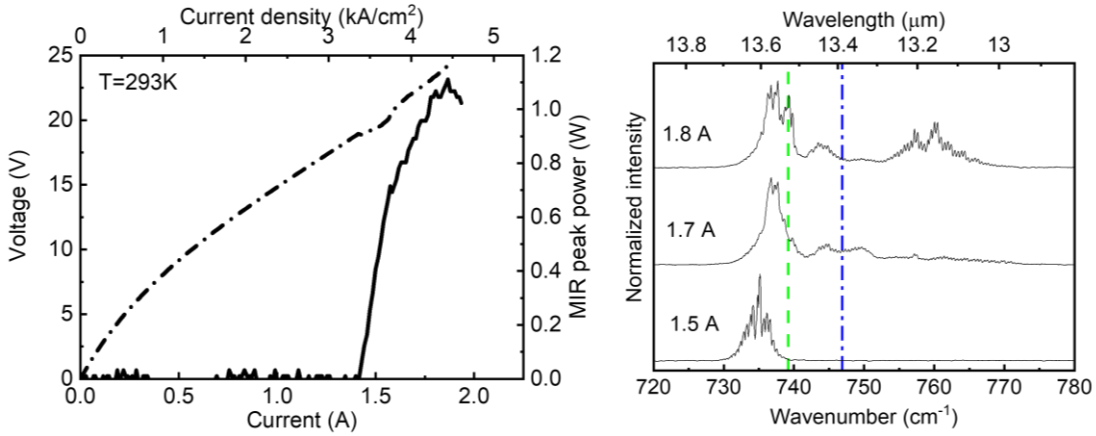

Figure S1 (a)The current-voltage-light output characteristics of the Fabre-Perot device for MIR peak power. (b) MIR emission spectra of the device

Suplementary Pages (Optional)

Surface phonon polaritons (SPhPs) are electromagnetic surface waves that emerge when photons couple with optical phonons in a polar dielectric material[1]. SPhPs are mid- to far-infrared (IR) analogs of surface plasmon polaritons (SPPs) which emerge when photons couple with the free carrier plasma in a metal. Although SPPs and SPhPs are both resonant surface modes which can remarkably enhance the near-field electromagnetic density[2, 3], SPhPs suffer from lower losses due to the relatively long-lifetime of optical phonons.4–6 The ability of SPhPs to mediate light-matter interactions is usually manipulated by nanostructuring the material interface in order to modify the near-field electromagnetic density of states (EMDOS). Nanostructuring polar dielectrics to design SPhP modes is thus a promising approach to engineer near-field optical phenomena. In particular, SPhPs enable the confinement of electromagnetic fields below the Abbe diffraction limit, providing a way to realize high quality-factor resonances. Sub-diffraction light confinement has already facilitated the development of the field of nanophotonics and promises further advances in applications such as surface-enhanced spectroscopy techniques (such as SEIRA and SERS), free-space IR communications, and superlensing[4].

In this work, we demonstrate 3D Raman mapping of surface electromagnetic modes in InP nanopillars and 1D gratings of 4H-SiC, using a standard confocal Raman microscopy setup. We further demonstrate that the polarizability associated with SPhP modes investigated is consistent with the Raman polarizability selection rules. Finally, we illustrate the ability of Raman mapping to investigate electron-phonon coupling via the longitudinal optical plasmon coupled (LOPC) effect.

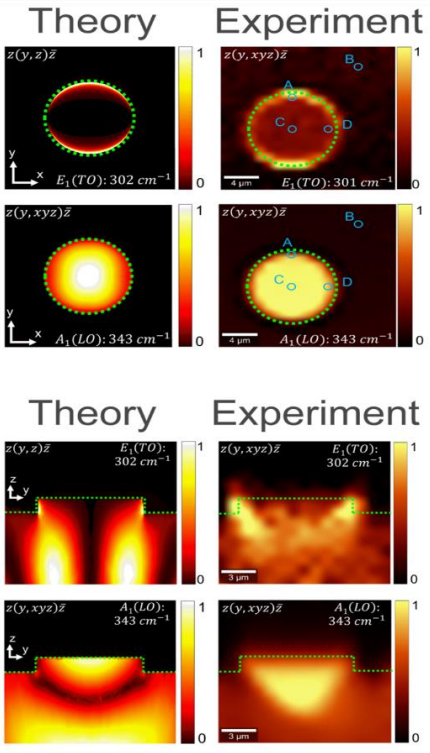

Supplementary Figure 1:
Top Panel: (Left) Theoretical and (right) experimental maps of the LO and TO phonon modes for a xy cross-sectional view. The edge of the nanopillar is denoted by dotted green lines.

Bottom Panel: Same as top for a yz cross-sectional view.

Surface Phonon Polariton Coupling to 4H SiC Triangular Gratings Produced by Two-Photon Polymerization

N. Rasouli Sarabi,[1] V.R. Whiteside,[1] E. Seabron,[2] E.R. Cleveland,[2,4] C.T. Ellis,[2] J.G. Tischler[1]

1. *University of Oklahoma*
2. *Naval Research Laboratory*
3. *Laboratory for Physical Sciences*

Surface phonon polaritons (SPhPs) are a promising alternative to plasmon polaritons for localizing mid-IR to terahertz light in the nanoscale with low optical loss and higher quality factor. However, to excite SPhPs modes on the crystal surface, additional in-plane momentum needs to be added with methods such as grating coupling or evanescent fields from prism internal reflections. Previous work on square gratings has been limited by unwanted spatial frequencies and difficulty adding desired spatial frequencies, limiting their functionality [1]. Here, we propose using sinusoidal gratings as a Fourier surface to couple input light to surface modes and design the diffractive properties of the surface accordingly. Two-photon polymerization enables the creation of 2.5D metasurfaces of arbitrary shape on various materials.

In this work, we demonstrate the ability to produce metallic-like triangular one-dimensional gratings using a Photonic Professional GT2 Nanoscribe. We produced 4H SiC triangular gratings that support surface phonon polariton resonances within the Reststrahlen band of SiC between 797 cm^{-1} and 972 cm^{-1}. Gratings were produced by etching a grayscale mask into the SiC substrate, resulting in triangular gratings with periods varying from 1 to 6.2 μm and heights varying from 0.3 to 2 μm. The Q factors of the resonances within the Reststrahlen band were in the range of 50-110, as expected from a low-loss phonon polar dielectric. To understand the origin of these surface phonon polariton resonances, we performed finite element calculations using COMSOL showing good agreement between theory and experiment.

[1] Caglayan, Humeyra, et al. "Near-infrared metatronic nanocircuits by design." *Physical review letters* 111.7 (2013): 073904.

+ Author for correspondence: nazli.r@ou.edu

Dielectric Resonances in Hexagonal Boron Nitride Nanodisks

Authors: M. Nourbakhsh,[1] H. Ling,[2] V. R. Whiteside,[1]A.R. Davoyan,[2] J. G. Tischler[1]

[1] University of Oklahoma,Norman, OK 73072 USA
[2] Samueli School of Engineering, UCLA, Los Angeles, CA 90095 USA

High-index nanomaterials play a substantial role in the enhancement of optical effects based on electric and magnetic Mie resonances. While hexagonal boron nitride (hBN) has been heavily explored within the Reststrahlen bands (RB) as a natural hyperbolic phonon polariton material [1], close to the transversal optical modes outside the RB the dielectric constant has extremely high positive values. The latter provides the opportunity of producing dielectric resonators with very large dielectric constants. We report infrared Mie resonances of hBN nanodisks (NDs). Reflection and transmission spectra of hBN NDs of different sizes have been investigated to understand Mie resonances within the infrared range. We show the presence of a strong magnetic dipole resonance which energy and strength depends on the size and geometry of the hBN NDs as well as the substrate properties. Finite element modeling of the electromagnetic fields has been performed and is in excellent agreement with our experimental results. Numerical and experimental data have indicated that by selecting the proper substrate thickness and hBN NDs radius, much more prominent Mie resonances are achieved. Mie resonances provide an opportunity to easily manipulate light confinement for the design of optical devices such as nanoresonators, nanolasers, highly efficient metasurfaces and ultrafast metadevices.

[1] Caldwell, Joshua D., et al. "Sub-diffractional volume-confined polaritons in the natural hyperbolic material hexagonal boron nitride." *Nature communications* 5.1 (2014): 5221.

[+] Author for correspondence: Milad.Nourbakhsh-1@ou.edu

Supplemental Document Author Index

Bold page numbers indicate presenter

Supplemental Document Author Index

Supplemental Document Author Index

— Z —